Environment

Submitted to:
Wyoming Department of
Environmental Quality
Air Quality Division

Submitted by:
AECOM
Fort Collins, Colorado
60237725
April 2014

Ozone Modeling Results and Analyses for Winter in Sublette County, Sweetwater County, and Lincoln County, Wyoming – Interim Report

Environment

Submitted to:
Wyoming Department of
Environmental Quality
Air Quality Division

Submitted by:
AECOM
Fort Collins, Colorado
60237725
April 2014

Ozone Modeling Results and Analyses for Winter in Sublette County, Sweetwater County, and Lincoln County, Wyoming – Interim Report

Prepared for:
Josh Nall
Wyoming Department of Environmental Quality
122 West 25th Street
Cheyenne, WY 82002

Prepared by:
Dr. Marco Rodriguez, Jason Reed, Dr. Chao-Jung Chien, Courtney Taylor
AECOM Environment
1601 Prospect Parkway
Fort Collins, CO 80525

Stephen Reid, Kenneth Craig
Sonoma Technology, Inc.
1455 N. McDowell Blvd.
Petaluma, CA 94954

List of Acronyms

ACM2	Asymmetric Convective Model version 2
AECOM	AECOM Technical Services, Inc.
AERO6	sixth-generation CMAQ aerosol module
AGL	above ground level
AHO	albedo, haze, and column ozone
BC	boundary condition
CAMx	Comprehensive Air Quality Model with extensions
CB6	Carbon Bond chemical mechanism version 6
CCTM	CMAQ Chemistry-Transport Model
CEM	continuous emissions monitoring
CMAQ	Community Multi-Scale Air Quality Model
CMAQ2CAMx	CMAQ to CAMx Processor
CMAS	Community Modeling and Analysis System
CO	carbon monoxide
DDM	Decoupled Direct Method
DIAG	WRFCAMX diagnosis approach
FEM	Federal Equivalent Method
GEOS-Chem	Goddard Earth Observing System – Chemical Model
HONO	nitrous acid
IC/BC	initial conditions and boundary conditions
IOP	Intensive Operation Periods
ISORROPIA	Inorganic Aerosol Thermodynamics/Partitioning Scheme
km	kilometers
Kv	vertical eddy diffusivity
LCC	Lambert Conformal Conic
m	meter
m^2/s	meters squared per second
MCIP	Meteorological-Chemistry Interface Processor
MEGAN	Model of Emissions of Gases and Aerosols from Nature
MOVES	Motor Vehicle Emission Simulator
MST	Mountain Standard Time
MYJ	Mellor, Yamda, and Janjic
NAAQS	National Ambient Air Quality Standards
NAM	North American Model
NEI	National Emissions Inventory
NH_3	ammonia
NO	nitric oxide

NO_3	nitrate
NOAA	National Oceanographic and Atmospheric Administration
NONE	WRFCAMX no diagnosis of sub-grid clouds
NO_X	nitrogen oxide
OH	Hydroxyl radical
OSAT	Ozone Source Apportionment Technology
PA	Process Analysis
PBL	planetary boundary layer
PGM	photochemical grid model
PM	particulate matter
PM_{10}	particulate matter with an aerodynamic diameter of 10 microns or less
$PM_{2.5}$	particulate matter with an aerodynamic diameter of 2.5 microns or less
ppb	parts per billion
PPM	Piecewise Parabolic Method
ppm	parts per million
RADM	Regional Acid Deposition Model
RPO	Regional Planning Organization
SMOKE	Sparse Matrix Operator Kernel Emissions
SO_2	sulfur dioxide
SO_4	sulfate
SOAP	Secondary Organic Aerosol Formation/Partitioning
SODAR	Sonic Detection and Ranging
STI	Sonoma Technology, Inc.
TAG	Technical Advisory Group
tpd	tons per day
TUV	total ultraviolet
U.S.	United States
UGRB	Upper Green River Basin
UGWOS	Upper Green River Winter Ozone Study
USEPA	U.S. Environmental Protection Agency
UTC	Universal Time Coordinate
VMT	vehicle miles traveled
VOC	volatile organic compound
WDEQ	Wyoming Department of Environmental Quality
WRAP	Western Regional Air Partnership
WRF	Weather Research and Forecasting
WRFCAMx	WRF to CAMx Processor
YAMO	Yamartino scheme

Contents

1.0 Introduction 1-1

1.1 Background 1-1

1.2 Conceptual Model for Ozone formation during the Winter 1-2

1.3 Summary of Findings 1-2

1.4 Report Purpose and Content 1-3

2.0 Modeling Approach 2-1

2.1 Episode Selection 2-1

2.2 Model Selection 2-2

2.2.1 CMAQ 2-2

2.2.2 CAMx 2-3

2.3 Modeling Domains 2-4

2.3.1 Horizontal Domain 2-4

2.3.2 Vertical Domain 2-8

2.4 Meteorological Inputs 2-10

2.4.1 Meteorological Processing 2-10

2.5 Emissions Inputs 2-12

2.5.1 Emissions Inventory Overview 2-12

2.5.2 Oil and Gas Sources 2-13

2.5.3 Point and Nonpoint Sources 2-14

2.5.4 Mobile Sources 2-15

2.5.5 Other Sources 2-15

2.5.6 Emissions Processing 2-15

2.6 Ancillary Data 2-16

2.6.1 Initial and Boundary Conditions 2-16

2.6.2 Photolysis Rates 2-17

2.6.3 Snow Cover Fields 2-17

2.7 Model Settings 2-17

3.0 Boundary Condition Test and Base Case Modeling Results 3-1

3.1 Introduction 3-1

3.2 Boundary Condition Test 3-1

3.2.1 Boundary Condition Test Background 3-1

3.2.2 Boundary Condition Test Analyses 3-2

3.2.3 Boundary Condition Test Findings 3-5

3.3 36-km Base Case Ozone Modeling 3-9

3.3.1 36-km Ozone Analyses 3-9

3.3.2 36-km Ozone Findings 3-12

3.4 1.33-km Base Case Ozone Modeling 3-12
3.4.1 1.33-km Ozone Time series 3-12
3.4.2 1.33-km Ozone Spatial Plots 3-17
3.4.3 1.33-km Ozone Findings 3-19
3.5 Base Case Surface Layer Analyses 3-19
3.5.1 Surface Layer Time Series Comparisons 3-20
3.5.2 Surface Layer Spatial plots 3-21
3.5.3 Surface Layer Emissions Density Plots 3-23
3.5.4 Surface Layer Analyses Findings 3-24
3.6 Base Case Vertical Analyses 3-24
3.6.1 Vertical Emissions Distribution 3-25
3.6.2 Vertical Profiles 3-26
3.6.3 Vertical Cross-Sections 3-26
3.6.4 Vertical Spatial Plots 3-29
3.6.5 Vertical Analyses Findings 3-33

4.0 Sensitivity Runs 4-1
4.1 Introduction 4-1
4.2 CMAQ Albedo Test 4-1
4.2.1 Albedo Test Background 4-1
4.2.2 Albedo Test Analyses 4-1
4.2.3 Albedo Test Findings 4-4
4.3 HONO Test 4-4
4.3.1 HONO Test Background 4-4
4.3.2 HONO Emissions Preparation 4-5
4.3.3 HONO Test Analyses 4-8
4.3.4 HONO Tests Comparison 4-11
4.3.5 HONO Test Findings 4-11
4.4 Area Source Test 4-15
4.4.1 Area Source Test Background 4-15
4.4.2 Area Source Test Emissions Preparation 4-16
4.4.3 Area Source Analyses 4-16
4.4.4 Area Source Test Findings 4-17

5.0 Summary of Findings 5-1

6.0 References 6-1

List of Tables

Table 2-1	RPO Unified Grid Definition	2-8
Table 2-2	Modeling Domain Dimensions	2-8
Table 2-3	WRF and PGM Vertical Layers	2-9
Table 2-4	MCIP Configuration	2-11
Table 2-5	WRFCAMx Configuration	2-11
Table 2-6	Data Sources for the Base Year 2008 Emissions Inventory	2-12
Table 2-7	Emissions (tons) Summary for the 1.33-km Domain for February-March 2008	2-13
Table 2-8	Oil and Gas Emissions (tons) by Source Category for Sublette County, February-March 2008	2-14
Table 2-9	CMAQ and CAMx Air Quality Model Configurations for Base Case	2-19
Table 3-1	Vertical Layering Scheme Used to Tag Boundary Ozone Contributions by Vertical Level of Origin	3-2
Table 3-2	Height of Model Vertical Layer Interfaces up to 1100-m AGL	3-24
Table 4-1	Stack Parameters Used for all Oil and Gas-related Emissions Sources in the Area Source Test	4-16

List of Figures

Figure 2-1 Modeling domains 36-km, 12-km, 4-km, and 1.33-km 2-6

Figure 2-2 Modeling Domains Relative to the Ozone Nonattainment Area 2-7

Figure 2-3 NO Emissions From All Sources for February 20, 2008, at 1200 MST for the 36-km (Upper Left), 12-km (Upper Right), 4-km (Lower Left), and 1.33-km (Lower Right) Domains. Note the Different Scales Between the Panels 2-16

Figure 3-1 Comparison between Observed Ozone Concentrations and 36-km Domain Modeling Results. Total Tracer Concentrations are the Sum of all 24 Tagged Boundary Ozone Species 3-3

Figure 3-2 Spatial Plots Differences of Daily-Averaged 36-km CMAQ and CAMx Ozone Tracer Concentrations for February 10 and 28, 2008 3-4

Figure 3-3 Inter-domain Comparison of CMAQ Ozone Tracer Concentrations at Boulder 3-4

Figure 3-4 CMAQ and CAMx 1.33-km Domain Boundary Ozone Contributions from the 4 Lateral Boundary Directions at Boulder during February and March of 2008 3-6

Figure 3-5 Time Series Comparison between CMAQ and CAMx 1.33-km Domain Boundary Ozone Contributions from the 6 Tagged Vertical Level at Boulder during February and March of 2008 3-7

Figure 3-6 Bar Chart Comparison between CMAQ and CAMx 1.33-km Tracer Concentrations by Each of the Source Regions used to Tag Boundary Conditions. O3W03 Means Western Boundary, Level 3, etc. 3-8

Figure 3-7 CAMx (left) and CMAQ (right) 36-km Domain Surface Layer Ozone Concentration Predicted on February 23, 2008 at 0000 UTC. The CAMx Simulation Used the Default WRFCAMx Snow Cover Conversion Algorithm and a Snow Albedo of 0.8 3-9

Figure 3-8 CAMx (left) and CMAQ (right) 36-km Domain Surface Layer Ozone Concentration Predicted on February 23, 2008 at 0000 UTC. The CAMx Simulation Used the Default WRFCAMx Snow Cover Algorithm and a Snow Albedo of 0.5 3-10

Figure 3-9 Observed (left) and WRF-predicted (right) Snow Cover Fields on February 23, 2008. Observed Snow Cover Fields Obtained from NOAA Snow Cover Maps Website 3-11

Figure 3-10 CAMx-ready Snow Cover Field for February 23, 2008 Generated from the Default (left) and Modified (right) WRFCAMx Algorithm for Determining CAMx Snow Cover from WRF Fractional Snow Cover 3-11

Figure 3-11 CAMx (left) and CMAQ (right) 36-km Domain Surface Layer Ozone Concentration Predicted on February 23, 2008 at 0000 UTC. The CAMx Simulation Used the Revised WRFCAMx Snow Cover Algorithm and a Snow Albedo of 0.5 3-12

Figure 3-12 Time Series of Observed (black), CAMx (red) and CMAQ (blue) Ozone Concentrations at Boulder During the Three IOPs 3-13

Figure 3-13 Time Series of Observed (black), CAMx (red) and CMAQ (blue) Ozone Concentrations at Jonah During the Three IOPs 3-14

Figure 3-14 Time Series of Observed (black), CAMx (red) and CMAQ (blue) Ozone Concentrations at Daniel During the Three IOPs 3-14

Figure 3-15 Time Series of Observed (black), CAMx (red) and CMAQ (blue) Ozone Concentrations at Warbonnet During the Three IOPs 3-15

Figure 3-16 Time Series of Observed (black), CAMx (red) and CMAQ (blue) Ozone Concentrations at La Barge During the Three IOPs 3-15

Figure 3-17 Time Series of Observed (black), CAMx (red) and CMAQ (blue) Ozone Concentrations at Haystack Butte During the Three IOPs 3-16

Figure 3-18 Time Series of Observed (black), CAMx (red) and CMAQ (blue) Ozone Concentrations at Simpson Gulch During the Three IOPs 3-16

Figure 3-19 Spatial Plots of CMAQ (left) and CAMx (right) Near-Surface Ozone Concentration from the 1.33-km Domain at 1400 MST on February 22, February 28, and March 11, 2008. The observed ozone concentrations for multiple sites are shown in circles overlaid on model results 3-18

Figure 3-20 Time Series Comparison of Modeled (green) and Observed (red) Near-Surface NO_x Concentrations During Each IOP at Daniel and Jonah. 3-20

Figure 3-21 Time Series Comparisons of Modeled (green) and Observed (red) Paraffin Concentrations During Each IOP at Boulder, Jonah and Daniel Plotted on a Log Scale 3-21

Figure 3-22 CAMx Spatial Plot of Modeled Surface Layer Ozone Concentrations Overlaid with Wind Vectors (left), and Modeled NO_x Concentrations Overlaid with Ambient Data (right) on February 22, 2008 at 1500 MST. 3-22

Figure 3-23 CAMx Spatial Plot of Modeled Surface Layer Paraffin VOC (left) and Xylene (right) Overlaid with Ambient Data on February 21, 2008 at 0900 MST 3-23

Figure 3-24 CAMx Layer 1 Emission Density Plots for NO_x (left) and Paraffins (right) on March 11, 2008 at 1500 MST 3-23

Figure 3-25 Spatial Plot of NO_x Emissions in Layer 3 (left) and Layer 10 (right) on February 19, 2008 at 1600 MST 3-25

Figure 3-26 Spatial Plot of Paraffin VOC Emissions in Layer 3 (left) and Layer 10 (right) on February 19, 2008 at 1600 MST 3-26

Figure 3-27 CAMx Modeled (black dots) and Observed Ozone Profiles (blue lines) at Pinedale Airport on February 20, 2008 at 1:00 PM (left) and 4:00 PM (right) MST 3-27

Figure 3-28 CAMx Modeled (black dots) and Observed (blue lines) Ozone Profiles at Pinedale Airport on February 29, 2008 at 1:00 PM (left) and 4:00 PM (right), MST 3-27

Figure 3-29 CAMx Vertical Cross-Sections of NO_x, CO, Xylene and O_3 on February 20, 2008 at 1600 MST Along a West-East Transect Taken Across the 1.33-km Modeling Domain Through Jonah. Black Reference Lines Indicate the Position of 250-m and 1,300-m AGL. 3-28

Figure 3-30 Mixing Heights Predicted by CAMx on the 1.33-km Domain on February 20, 2013 at 13:00 MST. 3-29

Figure 3-31 CAMx NO_x Concentrations at 100-m AGL (left) and 250-m AGL (right) Overlaid with Modeled Wind Vectors on February 20, 2008 at 1600 MST 3-30

Figure 3-32 Ozone Concentrations from Aircraft Observations (left) and CAMx Predictions at Layer 7 (right) During the Afternoon of February 20, 2008. Modeled Wind Vectors at Layer 7 are Overlaid on the CAMx Ozone Plot. Note the Different Spatial Scales Between the Plots 3-31

Figure 3-33 Ozone Concentrations from Aircraft Observations (left) and CAMx Predictions at Layer 7 (right) During the Afternoon of March 11, 2008. Modeled Wind Vectors at

Layer 7 are Overlaid on the CAMx Ozone Plot. Note the Different Spatial Scales Between the Plots 3-32

Figure 3-34 CAMx NO_x Concentrations at the Surface (left) and 100-m AGL (right) Overlaid with Modeled Wind Vectors on March 11, 2008 at 0800 MST 3-32

Figure 4-1 Time Series Comparison of Ozone Concentrations Between Original CMAQ Version 5.0 (blue), the Updated in-line Photolysis Module CMAQ (black) and observations (red). 4-2

Figure 4-2 Time Series Comparison of NO_x Concentrations Between Original CMAQ Version 5.0 (blue) and the Updated in-line Photolysis Module CMAQ (black). 4-3

Figure 4-3 Spatial Plots of CMAQ Near-Surface Ozone Concentration from the 1.33-km Domain at 0800 and 1600 MST on February 21 2008. From Left to Right: Base Case with Updated Photolysis Module, Default Version Without Updated Photolysis, Difference Between Both Cases (Default Case Minus Base Case) 4-6

Figure 4-4 Time Series Plot of 10-minute HONO Data for January 11 – March 31, 2011 (ENVIRON et al. 2011) 4-7

Figure 4-5 Diurnal Profile Developed for HONO Emissions from the Snowpack 4-8

Figure 4-6 Time Series Comparison of CMAQ Ozone Concentrations Between the Base Case (black) ,the HONO Emissions Test Simulations (orange) and Observations (red). 4-9

Figure 4-7 Time Series Comparison of CMAQ HONO Concentrations Between the Base Case (black) and the HONO Emissions Test Simulations (orange). 4-10

Figure 4-8 CMAQ HONO Diurnal Concentration with Mean and 95% Confidence Interval Between the Base Case (black) and the HONO Emissions Test Simulations (orange). 4-12

Figure 4-9 Spatial Plots of CMAQ Near Surface Ozone Concentrations from the 1.33-km domain at 0800 and 1600 MST on February 21 2008. From Left to Right: Base case with Updated Photolysis Module, HONO Test and Difference Between Both Cases (HONO Test minus Base Case) 4-13

Figure 4-10 Spatial Difference Plots of CMAQ Surface Ozone Concentrations from the 1.33-km domain at 0100 and 1500 MST for selected days during the first IOP. In all cases, the difference is between the results for the test with HONO at a source strength of 50 times higher at night and 20 times higher during the day and the HONO test with a source strength of 20 times higher during the day and night. 4-14

Figure 4-11 Vertical Distribution of CO, NO_x, and VOC Emissions from Oil and Gas Sources in the 1.33-km Domain for February 19, 2008. 4-15

Figure 4-12 Layer 1 NO_x Emissions from Oil and Gas-Related Sources for the Base Case Modeling (left) and the Area Source Test (right). 4-17

Figure 4-13 Time Series Comparison of CMAQ Ozone Concentrations Between the Base Case (black), Area Source Test Simulations (blue) and Observations (red). 4-18

Figure 4-14 Time Series Comparison of CMAQ NO_x Concentrations Between the Base Case (black) and Area Source Test Simulations (blue). 4-19

Figure 4-15 Spatial Plots of CMAQ Near Surface Ozone Concentrations from the 1.33-km domain at 0800 and 1600 MST on February 21 2008. From left to right: Base Case, Area Source Test, and the Difference Between Both Cases (Areas Test minus Base Case). 4-20

1.0 Introduction

1.1 Background

Modeling ozone formation in the Upper Green River Basin (UGRB) in southwest Wyoming during the winter has been performed by AECOM Technical Services, Inc. (AECOM) in collaboration with Sonoma Technology, Inc. (STI) for the Wyoming Department of Environmental Quality, Air Quality Division (WDEQ or the Division). The following interim report provides a detailed summary of the methodology, analysis, and findings of the photochemical grid modeling performed with the Community Multi-Scale Air Quality Model (CMAQ) and the Comprehensive Air Quality Model with extensions (CAMx).

Several episodes of elevated 8-hour ozone concentrations in the UGRB have been measured in southwest Wyoming since monitoring began in 2005. These episodes typically occur in the late winter and early spring. The Federal Equivalent Method (FEM)[1] Jonah and Boulder ozone monitors measured exceedances of the 8-hour ozone National Ambient Air Quality Standards (NAAQS) during several episodes in February and March 2008 and in February and March 2011. As a result of the 2008 exceedances, the State of Wyoming recommended a nonattainment designation for ozone for all of Sublette County, and portions of Sweetwater and Lincoln counties (State of Wyoming 2009). In 2011, the United States Environmental Protection Agency (USEPA) issued a letter to the Governor of Wyoming indicating their support of the recommendation. An official designation of marginal nonattainment status was issued by the USEPA on July 20, 2012.

The State of Wyoming has been proactive in its attempt to understand the observed occurrences of ozone in rural areas during the winter. Multiple studies have been commissioned by the Division to further understand and analyze the meteorological, chemical, and environmental factors that combine to form ozone in the UGRB during the winter. These include box modeling studies (Argonne 2007; ENVIRON 2008), a 3 dimensional photochemical grid modeling study (TRC 2010), field studies (Upper Green Winter Ozone Studies [UGWOS] 2011, 2010, 2009, 2008, 2007), monitoring network assessments (STI 2010) and a conceptual model (ENVIRON 2010a) along with recent studies of snow climatology (McVehil-Monnett 2011) and chemical reactivity in winter (Carter and Seinfeld 2011). All of these studies have been essential to the overall understanding of the issues; however, it is important to note that the exact processes involved in the ozone formation during winter conditions in the UGRB have not been fully identified or replicated with a 3-dimensional photochemical grid model (PGM).

In consideration of the complexities raised by the above studies, the Division established the ozone Technical Advisory Group (TAG) to provide recommendations to the Division on the most prudent path forward. The consensus of the TAG was that the Division should concentrate on two state-of-the-science PGMs in an attempt to replicate the 2008 ozone events and facilitate future air quality management strategies in the UGRB. The two PGMs recommended for evaluation are: 1) the CMAQ modeling system, and 2) CAMx. It was recommended that both CMAQ and CAMx be run and evaluated to determine which model is more appropriate for the specific conditions and processes found in the UGRB that lead to ozone formation during the winter. If at least one of the models shows adequate performance relative to ozone observations, then the selected model will be used for air quality management purposes such as the assessment of control strategies and future compliance with the ozone NAAQS.

[1] Monitoring ambient air quality to determine compliance with the NAAQS requires use of either Federal Reference Methods (FRMs) or Federal Equivalent Methods (FEMs), as specified in Section 2.1 of Appendix C to 40 CFR Part 58. FEMs are based on different technologies than FRMs, but have passed rigorous equivalency testing as outlined in 40 CFR Part 53.

In order to select an ozone model suitable for air quality management decisions, the ideal model should replicate both ozone formation processes and previously observed ozone episodes during wintertime. To this end, three study objectives have been identified:

- To design a study to optimize model performance for ozone formation during the wintertime in the UGRB;
- To identify the model that best replicates the key ozone formation processes occurring during winter in the UGRB; and
- To apply the model to support and inform the Division's management of air quality.

The following report provides interim results related to the first and second objectives: model simulations with both CMAQ and CAMx and the corresponding model evaluation with available observations to determine the best-performing model. Additional sensitivity scenarios have also been explored with the goal to replicate the observed ozone formation during wintertime periods.

1.2 Conceptual Model for Ozone formation during the Winter

The conceptual model (ENVIRON 2010a) was developed based on field studies and observations of high ozone concentrations in the UGRB during the winter. The conceptual model summarized the key environmental characteristics of ozone episodes in the UGRB as:

- Strong and persistent surface-based temperature inversion;
- Increased albedo due to extensive snow cover;
- Lack of ozone transport from upwind sources as evidenced by background levels of ozone above the inversion and outside of the UGRB;
- Diurnal wind recirculation patterns that keep the ozone precursors in the UGRB; and
- High concentrations of precursor emissions from oil and gas development within the UGRB.

Recent ozone events in the winter of 2011 had many of the same characteristics as in 2008, including extensive snow cover and strong temperature inversions (Meteorological Solutions 2011). The conceptual model has been used extensively in the evaluation of modeling studies and for forecasting high ozone events during the winter so that field campaigns can be deployed. It also served as the framework for the ozone nonattainment recommendation (State of Wyoming 2009) and will continue to serve as the basis of comparison for new modeling analyses and field studies.

1.3 Summary of Findings

A detailed analysis was conducted with the surface and aloft base case modeling results. Several of the environmental characteristics that lead to ozone episodes during wintertime conditions were verified to be present in both models used in this study. During episodes it was confirmed that transport (recirculation) within the mixed layer and the amounts of vertical mixing in the models confine pollutants within the boundary layer and the UGRB. It was also verified that enhanced albedo/photolysis occurs during periods with sufficient snow cover. While both models perform well at the LaBarge site, they perform poorly at and around the Boulder, Jonah and Daniel sites when evaluated for ozone and precursor concentrations. The addition of an explicit nitrous acid (HONO) source for snow pack chemistry did not significantly improve the model performance for ozone at Jonah or Boulder; however it did systematically increase ozone concentration over large areas of the 1.33-km domain.

Previous versions of CMAQ relied on look-up tables for estimation of photolysis rates. The version of CMAQ used in this study has a more accurate treatment of photolysis rates. One of the benefits of CMAQ's new photolysis rate calculation method is that the surface albedo, and its associated photolysis rate, varies throughout the model simulation. This improvement is particularly relevant to this study due

to variations in the snow cover surface that occur during the winter in the UGRB. The CMAQ model, as applied for this study, had systematical higher ozone concentrations and a better diurnal response (most notably in southwest Sublette County) than CAMx version 5.4.[2] This version of CAMx, unlike CMAQ, relied on look-up tables for estimates of the photolysis rates over snow covered areas.

1.4 Report Purpose and Content

The purpose of this interim report is to provide an overview of the base case and various sensitivity results performed with both CAMx and/or CMAQ thus far. Chapter 2.0 provides a summary of the model inputs, configurations and methodology. Chapter 3.0 provides an overview of a boundary condition test along with a detailed analysis of the base case model results for both CMAQ and CAMx. Chapter 4.0 provides a detailed analysis of several sensitivity analyses conducted in an effort to better replicate observations. Chapter 5.0 provides a comprehensive summary of findings and conclusions.

[2] A more recent version of CAMx has an updated photolysis rate calculation method; however, this version of CAMx was not available at the time this study was initiated.

2.0 Modeling Approach

2.1 Episode Selection

Several episodes of elevated 8-hour ozone concentrations have been measured in the UGRB in southwest Wyoming since monitoring began in 2005. These episodes are found to typically occur in the late winter and early spring. In order to better understand the unique situations that led to formation of ozone in southwest Wyoming, field studies (UGWOS) have been conducted each winter since 2007. During these studies, the maximum 8-hour average ozone concentration exceeded the NAAQS several different times. There were two monitored 8-hour values in excess of 75 parts per billion (ppb) in 2005 and three in 2006 with several prolonged high ozone periods monitored in both 2008 and 2011. The episodes that occurred in 2008 were selected for this modeling analysis based on several factors including: number of episodes, peak observed ozone concentrations, availability and type of monitoring data during the episodes, and availability of data required for the modeling analysis.

During late winter and early spring 2008 in the UGRB, several ozone episodes with 8-hour average concentrations exceeding 75 ppb were monitored at the Jonah and/or Boulder sites. Both the Jonah and Boulder sites monitor ozone concentrations using a FEM, thus direct comparison to the NAAQS is appropriate. Based on ambient monitored data collected during the 2008 UGWOS campaign and submitted to the USEPA (USEPA 2012), the 2008 ozone episodes occurred on:

- February 15, 8-hour average ozone concentrations reached 82 ppb at Jonah and 95 ppb at Boulder;
- February 19 through 24, peak 8-hour average ozone concentrations reached 102 ppb at Jonah and 122 ppb at Boulder;
- February 29 through March 1, peak 8-hour average ozone concentrations reached 77 ppb at Jonah and 82 ppb at Boulder;
- March 7, 8-hour average ozone concentrations reached 76 ppb at Boulder; and
- March 9 through 11, peak 8-hour average ozone concentrations reached 98 ppb at Jonah and 102 ppb at Boulder.

As part of the UGWOS campaign, ozone forecasts were prepared daily based on the conceptual model of ozone formation for the area in order to preemptively launch special monitoring studies (Intensive Operation Periods [IOPs]) during high ozone events. During 2008, three IOPs were launched for a total of 10 intensive sampling days. Each of these IOPs had similar characteristics in terms of measured high ozone, meteorology, snow cover, and dispersion potential in line with the conceptual model. The 2008 IOPs were conducted during:

- February 18 through 22;
- February 27 through 29; and
- March 10 through 12.

These IOP days are critical to this modeling analysis since the monitored data during these events provide detailed air quality information useful to assess model performance for specific pollutants.

PGMs are initialized with constant concentrations for all modeled species. These are usually values that are representative of background atmospheric concentrations or very small values depending on the species. Then the model predicts numerical estimates of pollutant concentrations for the entire simulation. However, modeling results are not considered valid for an initial period known as “spin-up”

since models require a transitional time before they reach a state in which they fully represent atmospheric concentrations that are the result of emissions, boundary conditions and all other processes, such as chemistry. The PGMs were run for the period starting February 1, 2008, through March 31, 2008. Different scenarios were simulated but in all cases model results were evaluated once the spin-up period (February 1 through 7, 2008) was completed. All detailed model performance evaluations have been limited only to the IOP days.

2.2 Model Selection

Given the technical complexities of successfully modeling ozone, the Division has engaged multiple stakeholders in the analysis and discussion of work performed to-date through the TAG. Based on an understanding of the issues particular to ozone formation in the UGRB during the winter, the TAG recommended a model evaluation of the two state-of-science photochemical grid models: USEPA's CMAQ (Byun and Ching 1999) and ENVIRON Corporation's CAMx (ENVIRON 2010b).

Both CAMx and CMAQ have been used in conjunction with a meteorological model and an emissions processor system. The following meteorological and emissions models have been selected for this study:

- The Weather Research and Forecasting (WRF) model is a state-of-science mesoscale numerical weather prediction system capable of supporting urban- and regional-scale photochemical modeling studies. It was run for the February 1 through March 31, 2008 period of interest (ENVIRON and Alpine Geophysics 2011).
- The Sparse Matrix Operator Kernel Emissions (SMOKE) modeling system is an emissions modeling system that generates hourly, gridded, and speciated emissions inputs of mobile, non-road, area, point, fire, and biogenic emissions sources for photochemical grid models. It was run for the emissions inventory described in Section 2.5.

Although many of the same science options generally are available in both CMAQ and CAMx, the models do have appreciable differences. In conjunction with the first study objective – to design a study to optimize model performance for ozone formation during the wintertime in the UGRB – the models have been configured to maximize each model's unique capabilities and obtain the best possible performance.

2.2.1 CMAQ

The CMAQ modeling system is a publicly available, state-of-the-science, three-dimensional Eulerian[2] model system capable of modeling multiple air quality issues including tropospheric ozone, fine particulates, toxics, acid deposition, and visibility change. CMAQ is designed to be a "one atmosphere" model capable of addressing multiple issues simultaneously across varying temporal and spatial scales. The temporal scales may range from short term (days to weeks) to longer term (seasonal to multi-year) and spatial scales from urban and regional scale to hemispheric.

The CMAQ development and maintenance is performed by the Community Modeling and Analysis System (CMAS) established by the Center for Environmental Modeling for Policy Development at the University of North Carolina under funding from the USEPA. The goal of CMAS is to standardize model development in a consistent and modular approach so as to efficiently implement the latest science and

[2] Eulerian models simulate changes in the chemical composition of air pollutants by describing their concentrations in an array of computational cells fixed in space. In an Eulerian modeling framework, species enter and leave each cell though its walls, and the model simulates the species concentrations at all locations as a function of time (Seinfeld and Pandis 1998).

modeling tools. The CMAQ modeling system includes diagnostic tools such as Process Analysis (PA), Decoupled Direct Method (DDM), sulfur tracking, primary carbon apportionment, and other source apportionment technologies. The CMAQ modeling system has been used by a variety of agencies at national, state, and local levels for the regulatory decision making process to meet NAAQS for ozone and particulate matter (PM).

A number of features in CMAQ's theoretical formulation and technical implementation allow the model to be well-suited for episodic ozone modeling. This study used the release of CMAQ version 5.0 (CMAS 2012). CMAQ version 5.0 includes:

- Updated Carbon Bond V (CB05) chemical mechanism with toluene chemistry (CB05-TU), Whitten et al. 2010;
- Revised rate constants for dinitrogen pentoxide (N_2O_5) hydrolysis;
- Dynamic representation of the PM size distribution with three log-normal modes (2 fine and 1 coarse mode);
- Equilibrium mass balance between the aerosol and gas phases and all secondary aerosols are assumed to be in the fine size modes;
- Addition of an new "in-line" photolysis algorithm to dynamically calculate surface albedo from seasonal land use categories, zenith angle, seasonal vegetation, snow and sea ice coverage; and
- Updated PM species, aging of primary organic aerosol, Inorganic Aerosol Thermodynamics/Partitioning (ISORROPIA2.1), aqueous chemistry, and windblown dust.

During the course of the project, version 5.0 of the CMAQ model code was revised (or patched) by USEPA Region 8 in an effort to enhance the photolysis over snow covered surfaces due to an identified issue (G. Tonnesen, personal communication, April 24, 2013) in the publicly released version. The revised version of the model was tested against the default version (described in Chapter 4.0) and used in the base case modeling (described in Chapter 3.0).

The CMAQ model requires the following inputs:

- Hourly meteorological fields, topographic information, and land use categories generated by the Meteorological-Chemistry Interface Processor (MCIP) processer;
- Three-dimensional hourly emissions generated by SMOKE; and
- Initial conditions and boundary conditions (IC/BC).

2.2.2 CAMx

Similar to CMAQ, the CAMx modeling system is a publicly available, state-of-the-science, three-dimensional Eulerian "one atmosphere" model capable of modeling multiple air quality issues including tropospheric ozone, fine particulates, toxics, acid deposition, and visibility degradation. It is capable of addressing multiple issues simultaneously across varying temporal and spatial scales.

The CAMx modeling system is a publicly available multi-scale photochemical/aerosol grid modeling system developed and maintained by ENVIRON Corporation. CAMx was developed with new codes during the late 1990s using modern and modular coding practices. This has made the model an ideal platform to treat a variety of air quality issues including ozone, condensable PM, visibility, and acid deposition. The flexible CAMx framework also makes it a convenient and robust host model for the implementation of a variety of mass balance and sensitivity analysis techniques including PA, Decoupled DDM, and the Ozone Source Apportionment Technology (OSAT). Designed originally to address multiscale ozone issues from the urban- to regional-scale, CAMx has been widely used in recent years

by a variety of regulatory agencies for 1-hour and 8-hour ozone State Implementation Plan modeling studies.

Although the models have been developed with similar objectives, some of the notable differences between the models include: one-way (CMAQ) versus two-way[3] (CAMx) nested grid structure; the availability of flexi-nesting in CAMx where the user can arbitrarily introduce and/or remove various nested grids; and the OSAT module in CAMx that identifies the ozone contribution due to geographic source regions and source categories.

The CAMx model version 5.40 (ENVIRON 2010b) available at the time of project initiation includes:

- Improvements to the vertical advection solver to more closely approximate the CMAQ vertical advection approach;
- Changes to the top boundary condition to a "zero-gradient" approach, alleviating the need for a top boundary condition input file;
- Addition of the Zhang deposition method to compute deposition velocities;
- Addition of a new in-line version of total ultraviolet (TUV) module to adjust clear-sky photolysis rates for the presence of clouds and aerosols;
- Incorporation of Carbon Bond VI (CB6); and
- Updated plume rise algorithm to calculate plume depth at final rise and distribute point source emissions throughout all model layers within the plume depth.

The CAMx model requires the following inputs:

- Three-dimensional hourly meteorological fields generated by the WRFCAMx processor;
- Two-dimensional low-level (surface layer) emissions and elevated point source emissions generated either by SMOKE or by the CMAQ2CAMx emissions processor tool;
- IC/BC inputs generated by the CAMx IC/BC processors;
- Photolysis rates look up table;
- Albedo/haze/ozone column input file; and
- Land use and topography.

2.3 Modeling Domains

2.3.1 Horizontal Domain

For regional photochemical modeling, it is beneficial to develop several nested modeling domains with finer grid spacing around the areas of primary interest (USEPA 2007). Four nested domains have been developed for this study during the WRF modeling (ENVIRON and Alpine Geophysics 2011):

- A 36-kilometers (km) grid covering the continental U.S., as defined by the Western Regional Air Partnership (WRAP) for the WestJump modeling project;
- A 12-km grid covering the northwestern U.S.;

[3] Two-way grid nesting means that information about changes in pollutant concentrations propagates into and out of all grid nests during model simulations. In one-way grid nesting, information can only propagate from the outermost to the innermost computational domains.

- A high resolution (4-km) grid covering much of western Wyoming and portions of neighboring states; and
- A very high resolution (1.33-km) grid covering the nonattainment area and surrounding terrain.

The PGM modeling domains are contained within the WRF domains to ensure edge-effects are not introduced into the simulation. The PGM modeling domains are illustrated in **Figure 2-1**. A detailed view of the PGM domains relative to: the UGRB; monitors included in the analysis of model performance; and the nonattainment area is shown in **Figure 2-2**.

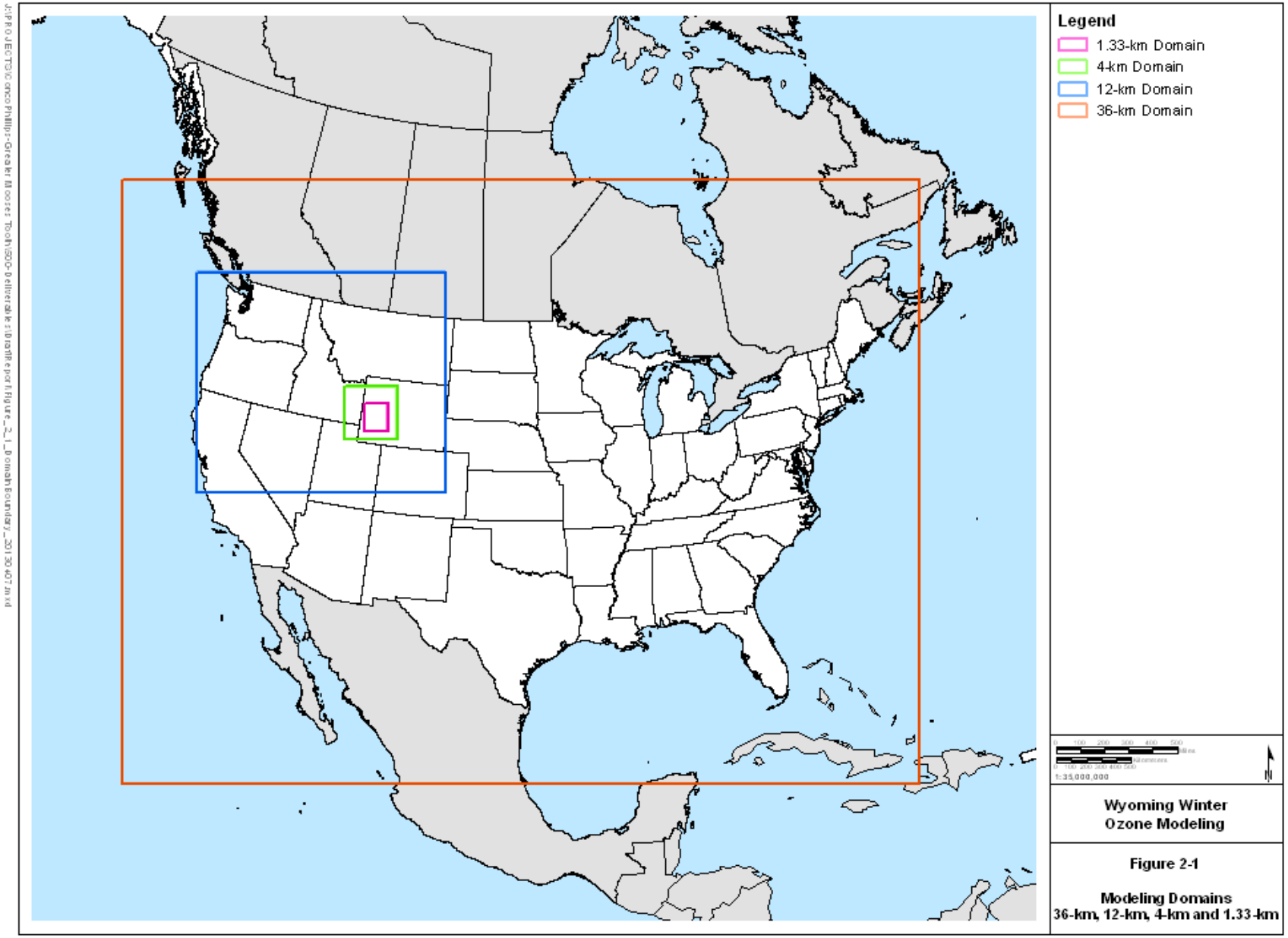
Legend
1.33-km Domain
4-km Domain
12-km Domain
36-km Domain
1:35,000,000
Wyoming Winter
Ozone Modeling
Figure 2-1
Modeling Domains
36-km, 12-km, 4-km and 1.33-km

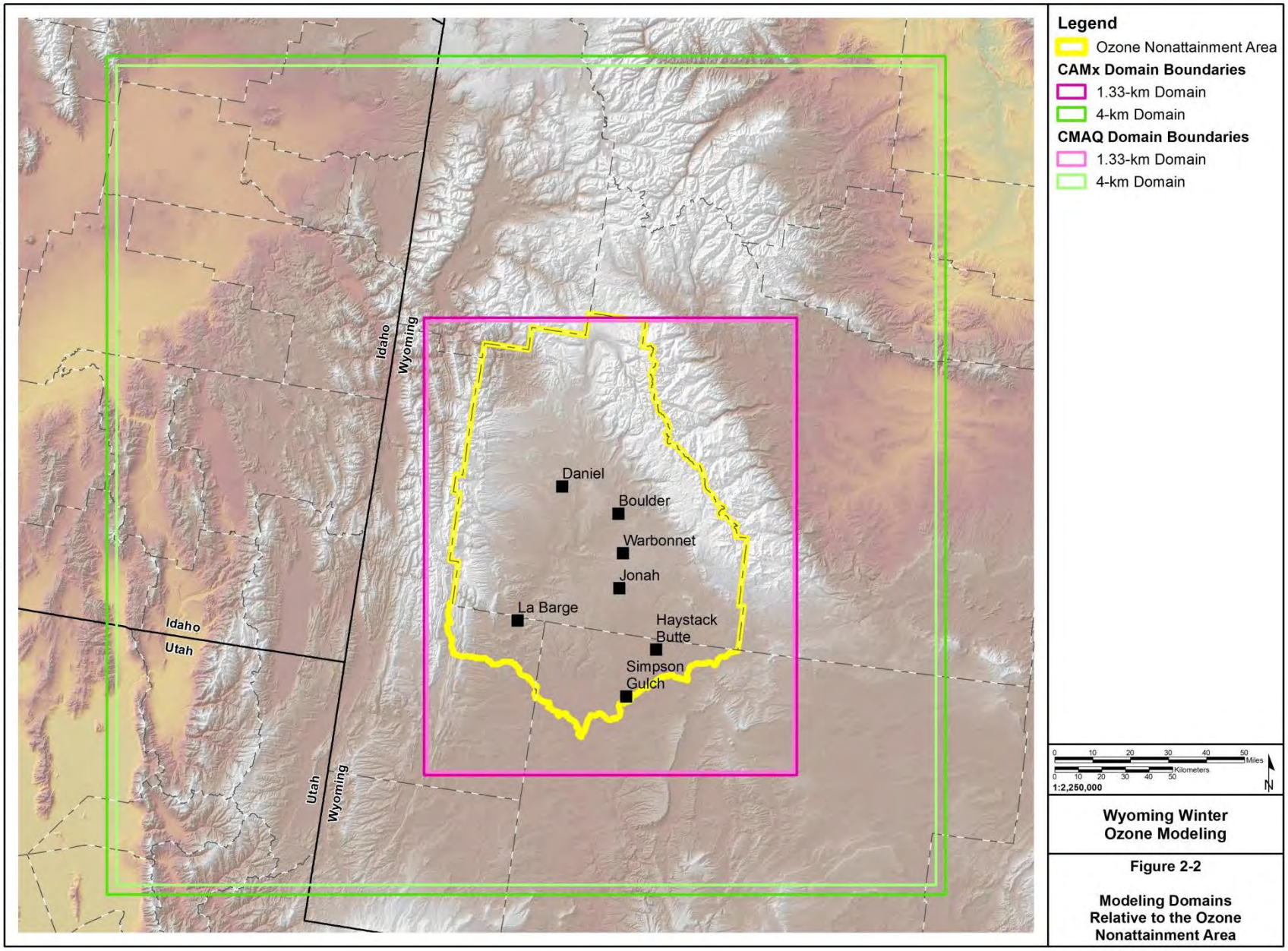

Wyoming Winter Ozone Modeling

Figure 2-2

Modeling Domains Relative to the Ozone Nonattainment Area

X:\0Projects\WDEQ_PGM_60237725\FIGs\DOC\WinterOzoneModelProtocol\Figure_2_2_DomainBoundary_20140402.mxd

All modeling domains are based on the standard map projection from the Regional Planning Organization (RPO) unified grid, which was used by the RPOs in prior regional modeling analyses. This unified grid consists of a Lambert Conformal Conic (LCC) map projection using the map projection parameters listed in **Table 2-1**. Additional information for the domains is provided in **Table 2-2**.

Table 2-1 RPO Unified Grid Definition

Parameter	Value
projection	LCC
datum	World Geodetic System 1984
alpha	33 degrees (°) latitude
beta	45° latitude
x center	97° longitude
y center	40° latitude

Table 2-2 Modeling Domain Dimensions

Model	Domain	Number of Grid Cells in X and Y Direction	Coordinates of southwestern corner of grid (km)
WRF	36-km	165 x 129	-2952,-2304
	12-km	151 x 136	-2304,-216
	4-km	100 x 100	-1272,192
	1.33-km	136 x 160	-1132,252
PGM (CMAQ and CAMx)	36-km	148 x 112	-2736, -2088
	12-km	138 x 123	-2232, -144
	4-km	87 x 87	-1248, 216
	1.33-km	117 x 144	-1116, 264

The modeled PGM domains were modified slightly from the original WRF output domains so that all nesting requirements could be met. In order to meet CAMx nesting domains requirements, and to minimize substantial changes to the domains, the following changes were made: the 1.33-km domain was trimmed by 3 cells in the x-direction and 6 cells in the y-direction. In addition, the 36-km domain was run as a stand-alone domain and used as input via boundary conditions to the 12-km domain. These two changes satisfied the CAMx nesting requirements for the 12-, 4-, and 1.33-km domains. These changes were also made to the CMAQ domain since SMOKE was run for CMAQ and its outputs converted for input into CAMx.

2.3.2 Vertical Domain

The WRF vertical grid is composed of 35 layers intervening between the ground and the top of the domain with more layers in the planetary boundary layer (PBL) than aloft. The layers used in the WRF modeling were used directly in the PGM modeling. The WRF and PGM layer structure is shown in **Table 2-3**.

Table 2-3 WRF and PGM Vertical Layers

Model Layer	(Eta)[1]	Height (meters)	Depth (meters)
1	1.0	0.0	
2	0.9985	12.0	12.0
3	0.997	24.1	12.1
4	0.995	40.1	16.0
5	0.993	56.2	16.1
6	0.991	72.4	16.2
7	0.988	96.6	24.2
8	0.985	120.9	24.3
9	0.98	161.5	40.6
10	0.97	243.2	81.7
11	0.96	325.6	82.4
12	0.95	408.6	83.0
13	0.94	492.3	83.7
14	0.93	576.6	84.3
15	0.91	747.5	170.9
16	0.89	921.2	173.7
17	0.87	1098.0	176.8
18	0.84	1369.1	271.1
19	0.8	1742.2	373.1
20	0.76	2129.7	387.5
21	0.72	2533.1	403.4
22	0.68	2953.7	420.6
23	0.64	3393.4	439.7
24	0.6	3854.1	460.7
25	0.55	4463.3	609.2
26	0.5	5114.9	651.6
27	0.45	5816.1	701.2
28	0.4	6576.3	760.2
29	0.35	7407.9	831.6
30	0.3	8327.8	919.9
31	0.25	9360.1	1032.3
32	0.2	10541.2	1181.1
33	0.15	11929.7	1388.5
34	0.1	13630.3	1700.6
35	0.06	15355.1	1724.8
36	0.027	17204.9	1849.8
37	0.0	top	top

[1] The WRF model uses a terrain following vertical coordinate system (Eta). The coordinate is defined as a function of pressure at the model top and the standard atmosphere mean sea level pressure. It varies from a value of 0 at the ground level to 1.0 at the top of the model domain (National Center for Atmospheric Research 2009).

2.4 Meteorological Inputs

The meteorological fields required for the PGM simulations have been developed using the WRF model and documented by ENVIRON and Alpine Geophysics (2011). As discussed in the 2011 WRF report, extensive testing was conducted on high ozone days to maximize model performance for the 1.33-km domain during high ozone events. As a result of this testing, the following pertinent model input and options were selected for the final WRF runs:

- Initialization data from the 12-km North American Model (NAM);
- Nudging with the Meteorological Assimilation Data Ingest System (MADIS) observational data, UGWOS observational data and NAM analysis fields;
- WRF Single-Moment 3-class microphysics;
- Mellor-Yamada-Janjic planetary boundary layer scheme;
- Rapid Radiative Transfer Model for Global Climate Models (RRTMG) longwave and shortwave radiation;
- Kain-Fritch cumulus physics for 36- and 12-km domains; and
- NOAH land surface model with Monin-Obukhov similarity surface layer.

These final model options were selected because they were able to produce the best model performance among vertical profiles of temperature, moisture, and inversion strength. Temperature profiles verified well against observations, and most importantly surface-based inversions (cold pools) were well replicated (ENVIRON and Alpine Geophysics 2011).

2.4.1 Meteorological Processing

The WRF outputs were post-processed to prepare air quality model-ready meteorological data files using MCIP for CMAQ and the WRFCAMx processor for CAMx. The functions of these meteorological processors include:

- Reading the WRF meteorological model output files;
- Extracting and formatting the WRF output for the PGM;
- Diagnosing the PBL characteristics and cloud parameters;
- Computation of species-specific dry deposition velocities;
- Conversion of coordinate-dependent meteorological output to the generalized coordinate system used in the air quality simulation; and
- Reduction of the WRF output to match the PGM modeling domain.

The MCIP (version 4.0) was executed with the above functions to pre-process the WRF meteorological output into the CMAQ-ready format. The MCIP diagnosed additional meteorological parameters required by the PGM such as cloud and moisture parameters for each horizontal grid cell, Monin-Obukhov length, PBL height, convective velocity scale, temperature, wind at specific heights (used for plume rise calculations when vertically distributing the emissions in the SMOKE model), and dry deposition velocities. Since the WRF data was developed with the Mellor-Yamada-Janjic PBL scheme, the deposition velocities were not calculated in MCIP; but instead they were computed exclusively within CMAQ by treating the deposition process as the loss of mass due to a net flux at the bottom of the model (in-line method). This treatment of dry deposition (CMAQ's bidirectional flux algorithm) characterizes more accurately the surface emissions and deposition of ammonia (NH_3). **Table 2-4** provides the configuration that was used in MCIP for the CMAQ model simulations.

Table 2-4 MCIP Configuration

Module or Option	Values or Setting	Additional Information
LPV	1	Potential vorticity was not calculated or output in MCIP.
LWOUT	1	Produce outputs of vertical velocity in MCIP files.[1]
LUVCOUT	1	Produce outputs of u- and v-components of the wind speed.
LSAT	0	No satellite data was used for MCIP outputs.

[1] Note that vertical velocity is not used in CMAQ; however, review of this parameter may provide additional insights in the analyses.

The WRFCAMx (version 3.3) was used to pre-process the WRF meteorological output into the CAMx-ready format. Meteorological parameters necessary for CAMx but not available from the WRF model were estimated with appropriate diagnostic algorithms in the WRFCAMx program, as listed in **Table 2-5** and summarized here. The Mellor, Yamada, and Janjic (MYJ) turbulent kinetic energy approach was used to diagnose vertical eddy diffusivity (Kv) values, and the minimum Kv threshold value was set to 0.01 meters squared per second (m^2/s). WRF output variables required for the Grell cumulus scheme for sub-grid cloud processing in WRFCAMx were not available; therefore, the WRFCAMx diagnosis approach (DIAG) was used for the master CAMx modeling grids (36-km and 12-km domains). No diagnosis of sub-grid clouds (NONE) was used for the nested grids (4-km and 1.33-km domains). Additionally, the Zhang dry deposition scheme was used to generate fractional distribution of 26 landuse categories.

Table 2-5 WRFCAMx Configuration

Module or Option	Values or Setting	Additional Information
Kv method	MYJ	Available methods include the O'Brien 1970 Method; Byun et al. 1999 integration methodology (CMAQ); Pleim 2007 Asymmetric Convective Model version 2 (ACM2) methodology; Mellor, Yamada, and Janjic 1994 Level 2.5 turbulent kinetic energy approach (MYJ); and Hong and Noh, Yonsei University 2006 approach
Minimum Kv	0.01	Unit is m^2/s
Projection	LCC	Same map projection as in WRF
Process snow cover	True	
Sub-grid cloud method	DIAG (master grids); NONE (nested grids)	Approaches include diagnosing sub-grid clouds from gridded meteorology fields (DIAG); passing cloud fields from the Grell cumulus scheme; and no diagnosis of sub-grid clouds (NONE)
Grid time zone	0	Using Universal Time Coordinate (UTC)

As discussed in Chapter 3.0, after review of the 36-km base case results, the WRFCAMx code was modified to treat a grid cell as snow covered if coverage is greater than or equal to 0.5.

2.5 Emissions Inputs

Emissions data were prepared for use in CMAQ and CAMx using the latest release (version 3.0) of the Sparse Matrix Operator Kernel Emissions (SMOKE) modeling system, which uses a collection of interrelated programs to convert "raw" emissions inventory data (i.e., annualized or average day criteria pollutant emissions at the county or facility level) to the resolution required by an air quality model (i.e., hourly emissions of model species apportioned to individual grid cells and vertical layers). This section provides a summary of the data sources and processing steps used to prepare emissions inputs for CMAQ and CAMx using SMOKE. Additional details about the development of air quality model-ready emissions inputs can be found in the emissions report prepared for this project (Reid et al. 2013).

2.5.1 Emissions Inventory Overview

The emissions inventory used for the model inter-comparison was based primarily on detailed 2008 emissions data for oil and gas production sources assembled by WDEQ and USEPA's 2008 National Emissions Inventory (NEI), version 2. For some source sectors, these inventories were supplemented with other data sources, such as the 2006 and 2012 emissions inventories for the oil and gas sector prepared by the WRAP (see **Table 2-6**).

Table 2-6 Data Sources for the Base Year 2008 Emissions Inventory

Source Type	Location	Data Source
Oil and gas sources	Sublette County	2008 winter (Feb-Mar) inventory from WDEQ
	Other Wyoming counties	2008 annual inventory from WDEQ
	WRAP states (other than Wyoming) [1]	2008 inventory developed from 2006 and 2012 WRAP inventories
	Non-WRAP states	2008 NEI data
Non-oil and gas point sources	4-km modeling domain	Annualized 2008 NEI data supplemented with hourly continuous emissions monitoring (CEM) data
	Outside 4-km modeling domain	Annualized emissions from the 2008 NEI
Non-oil and gas nonpoint sources (including ammonia emissions and fugitive dust)	All locations	2008 NEI data
On-road mobile sources	4-km modeling domain	Results from USEPA's Motor Vehicle Emission Simulator (MOVES) model run with vehicle miles traveled (VMT) data from WDEQ
	Outside 4-km modeling domain	2008 NEI data
Non-road mobile sources	All locations	2008 NEI data
Fires	All locations	2008 NEI data
Biogenic sources	All locations	Results from version 2.1 of the Model of Emissions of Gases and Aerosols from Nature (MEGAN)

[1] The WRAP oil and gas inventories included emissions data for Arizona, California, Colorado, Montana, Nevada, New Mexico, North Dakota, Oregon, South Dakota, Utah, and Washington.

During the collection and processing of emissions data, special attention was given to the high-resolution 4-km domain and the very high-resolution 1.33-km domain, since accurate model-ready emissions inputs for those domains will produce the greatest benefits for the air quality modeling simulations. In the 1.33-km modeling domain, which includes Sublette County and portions of neighboring counties, oil and gas sources are responsible for 89 percent of the total volatile organic compound (VOC) emissions and 59 percent of the total nitrogen oxide (NO_X) emissions, as shown in **Table 2-7**.

Table 2-7 Emissions (tons) Summary for the 1.33-km Domain for February-March 2008

Source	CO	NO_x	VOC	NH_3	SO_2	PM_{10}	$PM_{2.5}$
Point	331.5	441.5	227.0	0.0	255.3	25.6	22.7
Nonpoint	136.8	140.7	80.5	201.5	3.1	3,896.1	426.8
On-road Mobile	1,003.7	206.5	72.3	3.1	1.6	12.7	10.1
Non-road Mobile	1,038.4	81.0	354.9	0.1	1.6	13.5	13.5
Fire	132.6	3.9	26.8	2.2	1.6	15.4	13.0
Oil and Gas	763.3	1,268.0	4,753.1	0.0	11.7	29.0	28.9
Total	**3,406.3**	**2,141.6**	**5,514.6**	**206.9**	**274.9**	**3,992.3**	**514.9**

CO = carbon monoxide

NO_x = nitrogen oxides

VOC = volatile organic compounds

NH_3 = ammonia

SO_2 = sulfur dioxide

PM_{10} = particulate matter with an aerodynamic diameter of 10 microns or less

$PM_{2.5}$ = particulate matter with an aerodynamic diameter of 2.5 microns or less

2.5.2 Oil and Gas Sources

The WDEQ provided two detailed oil and gas emissions inventories for sources in Wyoming: 1) a winter 2008 (February-March) inventory for Sublette County; and 2) an annualized 2008 minor source inventory for all oil and gas sources in the state. The data for both inventories were well-specific and include the American Petroleum Institute number, oil and gas production levels, and location coordinates for each well. The winter inventory for Sublette County, which is summarized in **Table 2-8**, also included the following additional details:

- Information on emissions controls (e.g., combustors for flashing emissions);
- Temporal information on episodic activities (e.g., venting/blowdown events);
- Speciated VOC emissions for a subset of sources; and
- Process-specific stack parameters (e.g., stack height, gas exit temperature).

The oil and gas emissions data provided by WDEQ were subjected to numerous quality assurance checks, including verification of location coordinates, comparisons of total VOC emissions with the sum of speciated VOC emissions, and range checks on stack parameters. Scripts were then written to convert these data to SMOKE-ready format. In the SMOKE-ready files, each well was treated as a discrete point source with multiple emissions-producing processes (e.g., engines or flares) that have distinct stack parameters. In addition, to preserve the chemical resolution of the original inventory data,

new SMOKE-ready speciation profiles for the Carbon Bond V [CB05] mechanism[4] were developed from the speciated VOC emissions provided by WDEQ.

Table 2-8 Oil and Gas Emissions (tons) by Source Category for Sublette County, February-March 2008

Source Category	NO_x	CO	HONO	Formaldehyde	PM	SO_2	Total VOC	Speciated VOC
Drill rigs	578.2	315.9	17.3	0.3	12.1	7.8	17.4	
Process heaters	86.8	57.2	2.6	0.0			3.2	
Tanks and pressurized vessels	80.2	18.6	2.4				754.4	✓
Glycol dehydration units	136.2	48.2	4.1				689.0	✓
Pneumatic pumps	14.3	3.5	0.4				565.6	✓
Fugitives							394.9	✓
Truck loading							143.4	✓
Compressor engines	236.8	188.8	7.1	24.1	1.5	0.1	143.2	
Workover engines	36.4	33.9	1.1		1.5	0.5	3.3	
Well vent and blowdown events							30.9	✓
Well completions	1.4	0.3	0.0				5.5	✓
Total	**1,170.3**	**666.4**	**35.0**	**24.4**	**15.1**	**8.4**	**2,750.80**	

HONO = nitrous acid

For oil and gas sources outside Wyoming, 2008 emissions were interpolated from 2006 and 2012 data developed during the WRAP Phase II and Phase III emissions inventory projects[5]. These inventories covered oil and gas production basins in Colorado, New Mexico, Utah, and other western states. For non-WRAP states, oil and gas emissions from version 2 of the 2008 NEI were used (oil and gas emissions for WRAP states were removed from the 2008 NEI data to avoid double-counting).

2.5.3 Point and Nonpoint Sources

For point and nonpoint[6] sources not associated with the oil and gas sector, SMOKE-ready emissions data from version 2 of USEPA's 2008 NEI were used. Since these data represent annualized emissions, the temporal accuracy of major point source emissions was improved by incorporating CEM data from USEPA's Clean Air Markets Division. These data include unit-level, hourly SO_2 and NO_X emissions data in SMOKE-ready format for power plants and other large point sources. The CEM data for facilities that were within 200 km of the 4-km domain and that had NO_X emissions greater than 1,500 tons in February

[4] Note that the updated CB05 mechanism with toluene chemistry (CB05-TU) was used for CMAQ modeling, and the CB6 mechanism was used for CAMx modeling. However, emissions inputs prepared with CB05 speciation profiles are used for both of these mechanisms, as new toluene and CB6 reactions are implemented in the air quality models.

[5] See http://www.wrapair.org/forums/ogwg/PhaseIII_Inventory.html.

[6] Nonpoint sources are stationary sources that are too small, numerous, and/or geographically dispersed to treat as individual point sources.

through March 2008 were used in place of annualized 2008 NEI data. Ten facilities met these criteria, including the Naughton and Jim Bridger power plants in the southern portion of the 4-km domain[7].

2.5.4 Mobile Sources

On-road mobile source emissions estimates for the inner (4-km and 1.33-km) modeling domains were prepared using USEPA's MOVES model, which recently replaced the Vehicle Emission Modeling Software model. The MOVES model has been incorporated into SMOKE via the SMOKE-MOVES Integration Tool, which facilitates large-scale emissions modeling efforts through the use of gridded meteorological data and MOVES-based emission rate lookup tables (Baek and DenBleyker 2010). Day specific on-road mobile source inventories for counties in the 1.33-km and 4-km modeling domains were generated by running the SMOKE-MOVES tool for February-March 2008 using episode-specific meteorology for that period and VMT data derived from Wyoming Department of Transportation traffic counts. For the 12-km and 36-km modeling domains, the project team relied on SMOKE-ready on road emission files from version 2 of the 2008 NEI, which were generated using the SMOKE-MOVES tool run with default county-level data.

For non-road mobile source emissions, the SMOKE-ready data from version 2 of the 2008 NEI were used. These 2008 emissions data were primarily prepared with the USEPA's Nonroad Engines, Equipment, and Vehicles model, which estimates county-level emissions for a wide variety of non-road equipment types, including agricultural equipment, construction equipment, and recreational vehicles.

2.5.5 Other Sources

For all modeling domains, day-specific wildland and prescribed fire emissions estimates for February and March 2008 were developed using the U.S. Department of Agriculture Forest Service's BlueSky Framework (BlueSky), which was also used to prepare fire emissions inventories for the 2008 NEI (Pollard et al. 2011). BlueSky reconciles satellite fire detections with ground-based report and produces hourly fire emissions and plume rise estimates in SMOKE-ready formats (Sullivan et al. 2009), and system outputs were compared with data from WRAP's Fire Emissions Tracking System to ensure that no large fires were missing from the BlueSky inventory.

Similarly, day-specific biogenic emissions estimates for all modeling domains were prepared using Version 2.1 of MEGAN (Guenther et al. 2006). The WRAP recently sponsored improvements to MEGAN that include updates to land cover data inputs for the Western U.S. (Guenther and Sakulyanontvittaya 2011).

2.5.6 Emissions Processing

Once all emissions inventory data were assembled and prepared for processing, these data were converted to CMAQ- and CAMx-ready emissions inputs using SMOKE version 3.0. In general, ancillary input data (e.g., speciation profiles, temporal profiles, and spatial surrogate data) provided with SMOKE v3.0 were used for emissions processing. However, because the SMOKE-ready spatial surrogate data provided by the USEPA were only available at 36-km, 12-km, and 4-km grid resolutions, surrogate data for the 1.33-km grid was generated using the same underlying raw spatial data (e.g., land use and land cover data) that the USEPA used to develop the SMOKE-ready spatial surrogates for coarser-resolution modeling domains. In addition, CB05 speciation profiles for oil and gas sources were developed using the speciated VOC emissions provided with the WDEQ oil and gas emissions inventories.

Figure 2-3 shows the spatial distribution of merged nitric oxide (NO) emissions for each of the four modeling domains. These data shown in these plots include emissions from all sources integrated

[7] Note that because the CEM data for these facilities included hourly emissions for only SO_2 and NO_x, annualized emissions from the 2008 NEI were used for other pollutants.

across all vertical layers, and the locations of oil and gas sources in the 1.33-km modeling domain are apparent.

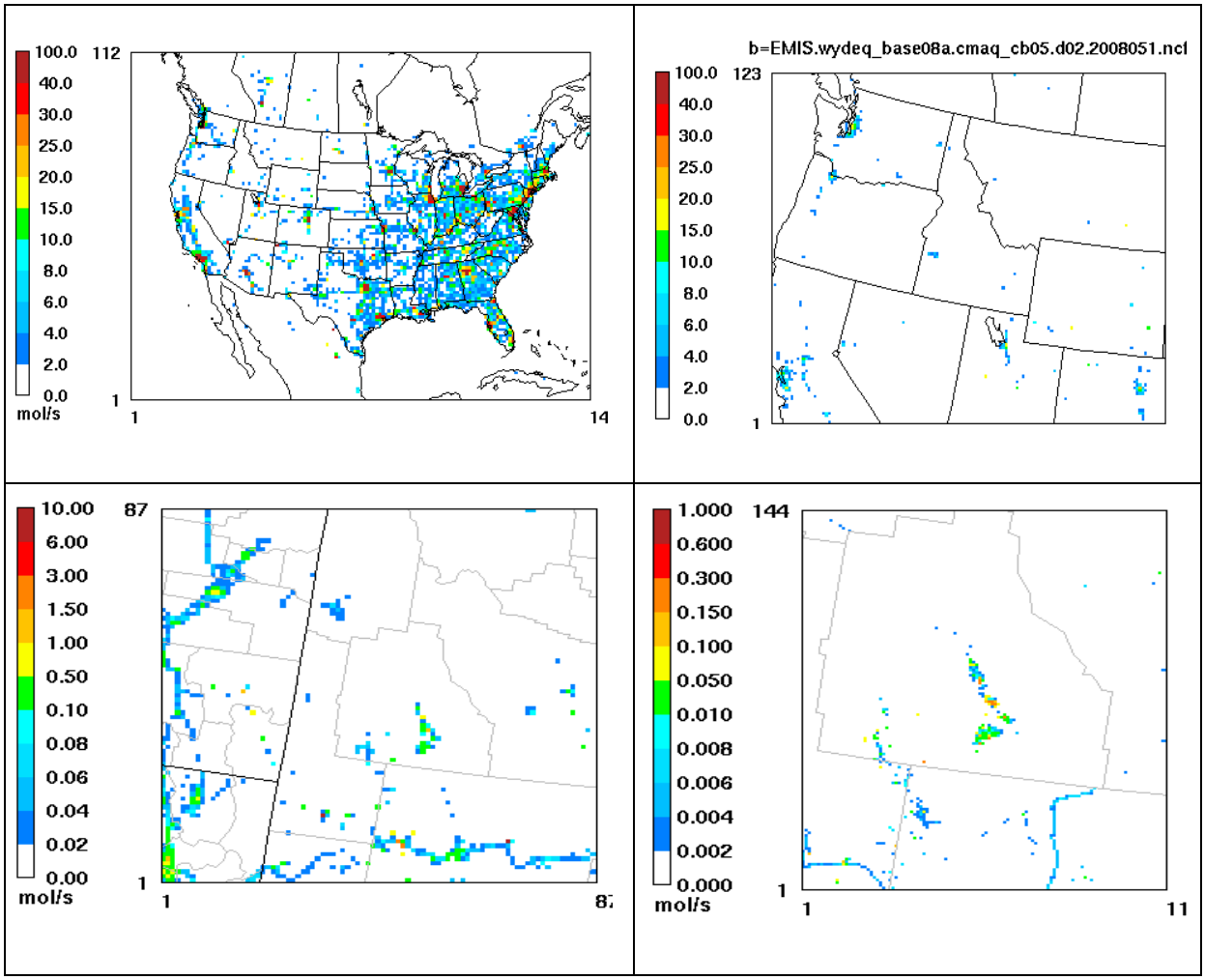

Figure 2-3 NO Emissions From All Sources for February 20, 2008, at 1200 MST for the 36-km (Upper Left), 12-km (Upper Right), 4-km (Lower Left), and 1.33-km (Lower Right) Domains. Note the Different Scales Between the Panels.

2.6 Ancillary Data

2.6.1 Initial and Boundary Conditions

Initial conditions provide an estimate of modeled species concentrations that exist at the beginning of the simulation, and are a required input for both PGMs. Initial conditions generated by a spin-up simulation are considered more representative of actual ambient concentrations than default values from a coarser scale model. For the base case modeling, initial conditions for both PGMs were based on a 7-day spin-up period (February 1 to February 7, 2008) using day-specific emissions inventories for each day.

Boundary conditions, which represent continuous pollution inflow into the lateral sides of the model domain, are also required as input for both PGMs. Boundary conditions for the outermost (36-km) domain for both models were prepared using outputs from a 2008 GEOS-Chem simulation provided by USEPA's Office of Research and Development. For CAMx, boundary condition inputs for the 12-km

domain were obtained by processing the output for the 36-km domain CAMx simulation with the Initial and Boundary Conditions Preparation processor program, while boundary conditions for the 4-km and 1.33-km domains were generated dynamically through the two-way nesting process. For CMAQ, boundary conditions inputs for the 12-km, 4-km, and 1.33-km domains were generated by processing the output from each grid's parent domain simulation using the Boundary Conditions Processor program.

2.6.2 Photolysis Rates

Photolysis rates for all photolytic reactions in CMAQ modeling were calculated for each grid cell at every synchronization time step using the in-line photolysis module available in CMAQ version 5.0. The in-line photolysis module is more computationally efficient than using the Photolysis Rate Processor look-up tables. This module also introduces an algorithm that calculates the surface albedo based on land use categories, cloud cover, zenith angle, seasonal vegetation, and snow cover. As discussed in Section 2.2.1 and Chapter 4.0 in more detail, the photolysis rate for snow covered surfaces was revised by the USEPA Region 8 for use in the analyses.

For the CAMx modeling, day-specific multidimensional look-up tables of clear-sky photolysis rates for 15 vertical levels were calculated using the TUV radiative transfer and photolysis model. The TUV model accounts for environmental parameters that influence photolysis rates, including solar zenith angle, altitude, surface ultraviolet albedo, aerosols (haze), and stratospheric ozone column. In addition, CAMx was configured to use an in-line version of TUV that internally adjusts the clear-sky photolysis rates for the presence of clouds.

Albedo, haze, and column ozone (AHO) inputs for CAMx and TUV processing were prepared using the AHOMAP program. The ozone column data source was the 1° longitude by 1° latitude resolution Ozone Monitoring Instrument data. Landuse data for AHOMAP processing were taken directly from the WRF output files via WRFCAMx. Snow cover fields extracted from the WRF model and output by WRFCAMx were appended to the AHOMAP output files using a custom script. The albedo for snow covered grid cells was initially set 0.8 to account for enhanced photolysis present during the ozone episodes. As discussed in Section 3.3.2, the base case modeling with CAMx was conducted with an albedo value of 0.5 for snow covered grid cells.

2.6.3 Snow Cover Fields

Based on an evaluation of the WRF-predicted snow cover fields from all 4 domains, as compared to National Oceanographic and Atmospheric Administration (NOAA) snow cover observations, it was found that WRF snow cover fields were adequate for use in the PGM simulations. For CMAQ modeling, the WRF fractional snow cover fields from all 4 domains were extracted by MCIP and used directly by each CMAQ domain. For the CAMx modeling, all nested grids receive snow cover input from the master grid. Since the 36-km CAMx simulation was executed separately from the 3-domain nested grid CAMx simulation, the 36-km and 12-km domains serve as master grids for the CAMx simulations. Therefore, snow cover fields only from the 36-km and 12-km domains were extracted from WRF by WRFCAMx. The resulting snow cover fields were appended to the AHO input files using a custom script.

In CAMx, snow cover data for each grid cell is parameterized as a binary value that is assigned by the WRFCAMx processor. By default, when the WRF-predicted snow cover fraction is greater than 0.0, WRFCAMx assigns a "with snow" value, otherwise it assigns a "without snow" value. The WRFCAMx code was modified so that grid cells were assigned a "with snow" binary value when the WRF-predicted snow cover fraction was greater than 0.5. The justification for this change is presented in Chapter 3.0.

2.7 Model Settings

The configuration options used for the base case modeling with CMAQ and CAMx are shown in **Table 2-9**. The table is organized by groups of options for domains and grid-nesting, model input preprocessors, and chemistry and transport mechanisms.

As summarized in the table, one-way grid nesting was used in the CMAQ configuration, since two-way nesting is not available for CMAQ. The CMAQ model options also included the CB05 gas-phase photochemical mechanism with updated toluene chemistry (i.e., CB05-TU), the updated Regional Acid Deposition Model (RADM) aqueous-phase, and the AERO5/ISORROPIA2 aerosol chemistry scheme. The particulate chemistry mechanism utilizes products from the gas phase photochemistry for production of sulfate (SO_4), nitrate (NO_3), condensable organic gases, and chloride, and mineral nitrate was included in the calculation of aerosol nitrate formation. Vertical diffusion in CMAQ was modeled by the Assymetric Convective Model version 2 (ACM2) algorithm, and the Yamartino Scheme (YAMO) advection scheme and multiscale horizontal diffusion options were used.

The CAMx was configured for two-way grid nesting for the 12/4/1.33-km nested grid simulation. Due to limitations imposed by CAMx nested grid specification requirements, a separate single-grid CAMx simulation was performed for the 36-km domain. The CAMx model options used to estimate ozone and PM formation included the CB6 gas-phase chemistry mechanism, RADM aqueous chemistry, ISORROPIA, and Secondary Organic Aerosol Formation/partitioning (SOAP) schemes. The particulate chemistry mechanism utilizes products from the gas phase photochemistry for production of SO_4, NO_3, condensable organic gases, and chloride, and mineral nitrate was included in the calculation of aerosol nitrate formation. Vertical diffusion in CAMx was modeled by the K-theory approach, and the Piecewise Parabolic Method (PPM) advection solver was used along with the spatially varying horizontal diffusion approach.

Table 2-9 CMAQ and CAMx Air Quality Model Configurations for Base Case

Parameter	CMAQ	CAMx	Details
Model Version	CMAQ (v.5.0)	CAMx (v.5.40)	Latest model versions during protocol development phase.
Horizontal grid mesh	36/12/4/1.33-km	36/12/4/1.33-km	Due to CAMx grid nesting requirements, a CAMx simulation for the 36-km grid was performed separately from the nested grid (12/4/1.33-km) CAMx simulation.
Vertical grid mesh	37 layers	37 layers	Using WRF layers with no collapsing.
Grid Interaction	One-way nesting	Two-way nesting for 12/4/1.33-km domains.	CMAQ does not have two-way nesting available.
Initial Conditions	Spin-up	Spin-up	Cold start spin-up.
Boundary Conditions	2008 GEOS-Chem hourly	2008 GEOS-Chem hourly	
Meteorological Processor	MCIP (v.4.0)	WRFCAMx (v3.3)	For processing WRF meteorology.
Emissions Processor	SMOKE (v.3.0)	CMAQ2CAMx processor	CMAQ2CAMx converter tool will convert CMAQ-ready emissions inputs to CAMx-ready format.
Chemistry			
Gas-Phase Chemistry	CB05-TU	CB6	CB05-TU is CB05 with updated toluene chemistry. CB6 is only available in CAMx at this time. Both mechanisms can use the same SMOKE output.
Aerosol Chemistry	AERO5 and ISORROPIA2.1	SOAP and ISORROPIA1.6 with static 2-mode coarse/fine size distribution.	Each mechanism represents the recommended scheme for each model. However, AERO6 is available in CMAQ, but would require additional PM species in the emissions with no benefit to ozone.
Cloud Chemistry	RADM-type aqueous chemistry	RADM-type aqueous chemistry	

Table 2-9 CMAQ and CAMx Air Quality Model Configurations for Base Case

Parameter	CMAQ	CAMx	Details
Numerics			
Gas Phase Chemistry Solver	Euler Backward Iterative (EBI) solver	EBI solver	
Horizontal Advection	YAMO scheme	PPM scheme	The YAMO scheme is the recommended scheme is CMAQ and is currently unavailable in CAMx while PPM is the most accurate horizontal advection scheme available in CAMx. It is noted that the YAMO scheme is based on the PPM scheme with advances in mass conservation.
Vertical Advection	WRF scheme	Implicit scheme with vertical velocity update	The WRF scheme is the recommended scheme for CMAQ 5.0 and is currently unavailable in CAMx while the implicit scheme is the default method in CAMx.
Diffusion			
Horizontal Diffusion	Multiscale	K-theory 1st order closure with K_h grid size dependence	The multiscale option is the default in CMAQ and unavailable in CAMx, which implements the K-theory 1st order closure concept.
Vertical Diffusion	ACM2	K-theory approach	Kzmin was set to 0.01 m^2/s for base case runs per USEPA guidance. It is expected that vertical diffusion under stable conditions will dominate, which is what ACM2 defaults to during stable periods. K-theory by itself is unavailable in CMAQ.
Deposition			
Dry deposition	CCTM in-line	Zhang scheme	Dry deposition velocities are computed exclusively in CMAQ's CCTM while CMAQ's in-line calculation provides bidirectional exchange of NH_3.
Wet Deposition	CMAQ-specific	CAMx-specific	
Integration Time Step	Wind speed dependent	Wind speed dependent	

3.0 Boundary Condition Test and Base Case Modeling Results

3.1 Introduction

This chapter presents the results and analyses of a boundary condition test and base case modeling simulations performed by AECOM and STI with guidance from WDEQ. The CAMx and CMAQ models were setup in accordance with the modeling domains and configurations described in Chapter 2.0. The two modeling simulations were performed for the winter period that included the IOP days in the year 2008. Section 3.2 provides a detailed analysis of the results of the boundary condition test that was an inert tracer simulation that follows the evolution of ozone concentrations from the 36-km lateral boundaries to the inner domains. Sections 3.3 to 3.6 compare the base case results between both models and provide in-depth analysis on surface and aloft modeling results performed with CAMx.

3.2 Boundary Condition Test

3.2.1 Boundary Condition Test Background

The boundary condition (BC) test is a sensitivity simulation performed to understand the influence of the lateral boundary ozone to the total ozone concentrations in Sublette County predicted by CMAQ and CAMx before a full investigation of the base case results was performed. In the models, background ozone is transported into the modeling domains from the boundary conditions provided by the GEOS-Chem global model. To isolate the effects of the boundary conditions in this sensitivity test, the initial conditions, natural emissions, and anthropogenic emissions were set to zero. In addition, the chemistry solvers were turned off, and deposition was deactivated, leaving transport and diffusion as the only physical processes that could affect ozone concentrations in the modeling systems. Both CMAQ and CAMx were provided with an equivalent set of GEOS-Chem ozone boundary conditions for the 36-km domain. Boundary conditions for the inner domains were generated through the nesting process applicable to each model.

As described in Chapter 2.0 the lateral boundary conditions imposed in the 36-km domain have been extracted from the GEOS-Chem global model. Both models prescribe ozone and other pollutants' concentrations from the global model at the lateral boundaries, while there is a zero gradient of pollutant concentrations at the top of the model. The boundary conditions provide a continuous inflow of ozone (and other pollutants) at the outermost domain that gets transported into the inner domains by the input meteorology. Before using the boundary conditions for the BC test, it was verified that these concentrations presented a reasonable spatial profile and that their magnitudes were within an expected range (Reed et. al. 2013).

In previous versions of GEOS-Chem, the tropopause was denoted by a single level. The full chemistry mechanism was then solved for in all grid boxes up to this fixed level. However, using a single level to represent the tropopause significantly underestimated the tropopause height in the tropics. A more recent version of GEOS-Chem improved upon the situation by introducing a dynamic tropopause, i.e., the location of the tropopause is now computed at each dynamic timestep of a GEOS-Chem simulation (GEOS-Chem tropopause 2014). A more detailed analysis of the GEOS-Chem output with this dynamic tropopause capability by USEPA Region 8 suggested a significant influx of stratospheric ozone into the mid/lower troposphere at the northern boundary around the time high ozone levels occurred in Sublette County (G. Tonnesen, personal communication, August 2, 2012). This finding raised concern about the transport of this stratospheric ozone into the refined modeling grids given its close proximity to the area of interest; therefore it was determined that a sensitivity test was necessary to assess what the resulting ozone concentrations would be from the boundary conditions alone in Sublette County.

To obtain additional information about the origin of lateral boundary ozone concentrations in Sublette County, the lateral boundary ozone concentrations were further processed to tag or mark them by

quadrant (north, south, east, and west boundary) and by vertical height. This tagging process was done to identify, with increased precision, the origins from within the boundaries that have an impact on the ozone concentrations observed in Sublette County. In order to increase computational efficiency and to simplify the analysis, concentrations from the boundary conditions were binned or consolidated into the six vertical layers shown on **Table 3-1**, which also indicates the approximate height above the surface level assigned to each layer. A total of 24 (6 vertical layers for each of the 4 lateral boundaries) unique ozone tracers or source regions were used to identify the origin of ozone coming from the boundaries into Sublette County. After a visual verification was performed on the final BC profiles, both models were executed for the inert tracer simulation.

Table 3-1 Vertical Layering Scheme Used to Tag Boundary Ozone Contributions by Vertical Level of Origin

Tracer Layer Name	Model Layer Range	Altitude Range (AGL)
Layer 1 (L1)	1 to 15	0 to 1-km
Layer 2 (L2)	16 to 19	1 to 2-km
Layer 3 (L3)	20 to 25	2 to 5-km
Layer 4 (L4)	26 to 28	5 to 7.5-km
Layer 5 (L5)	29 to 31	7.5 to 10-km
Layer 6 (L6)	32 to 36	10-km to model top

3.2.2 Boundary Condition Test Analyses

The influence of the lateral boundary concentrations in Sublette County was assessed at the Boulder, Jonah and Daniel sites. The time series in **Figure 3-1** compares the 36-km CMAQ and CAMx total tracer concentrations to available ozone observations. The tracer concentrations represent the total sum of all 24 source regions from the boundaries. The figure illustrates that for all sites there is a gradual build-up of ozone from the clean initial conditions.

Analysis of **Figure 3-1** indicates that the ozone tracer concentrations are typically very close in magnitude to observed background concentrations at all sites except for Daniel in which both models systematically underpredict compared to the observations. Without anthropogenic local sources or chemistry invoked, the model could theoretically never replicate the observed variability in ozone concentrations due to the existing formation/destruction processes inherent in the observations. The figure also indicates that tracer concentrations are very similar between CMAQ and CAMx which suggest similarities in the way both models handle vertical and horizontal transport in this region.

Figure 3-2 provides a snapshot of the spatial differences between the CMAQ and CAMx surface-layer ozone tracers for two days in February 2008, which shows that the spatial distribution of tracer concentrations can vary between the models across the continental U.S. The location of the largest differences can change significantly from day-to-day; however, they are generally lower in the Western U.S. and the area of interest, which is supported by the time series plots provide in **Figure 3-1**.

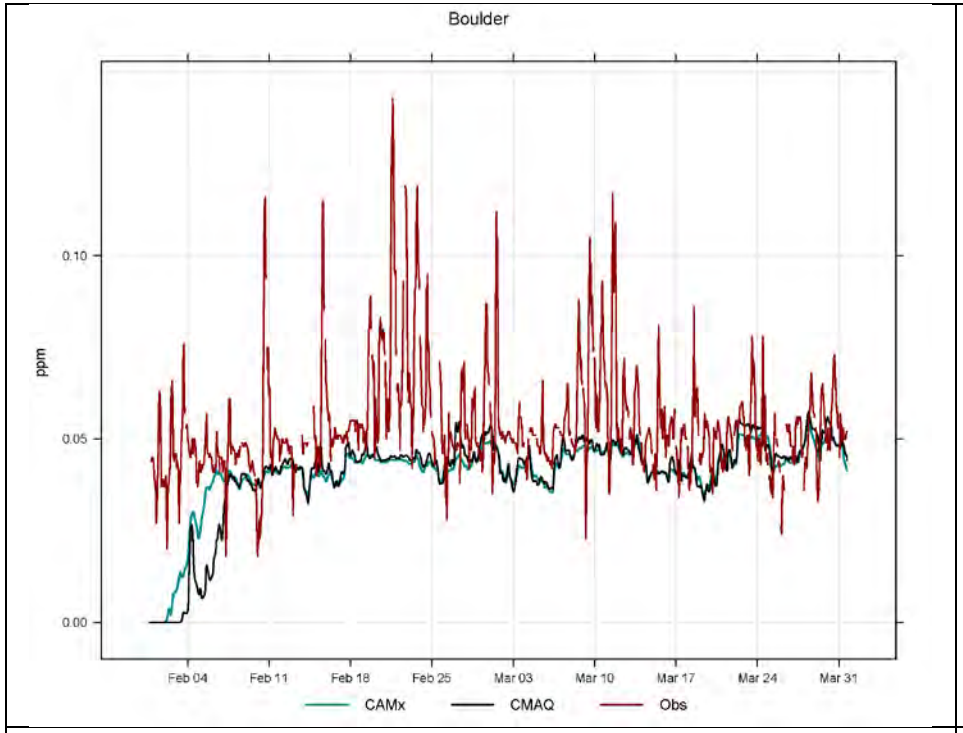

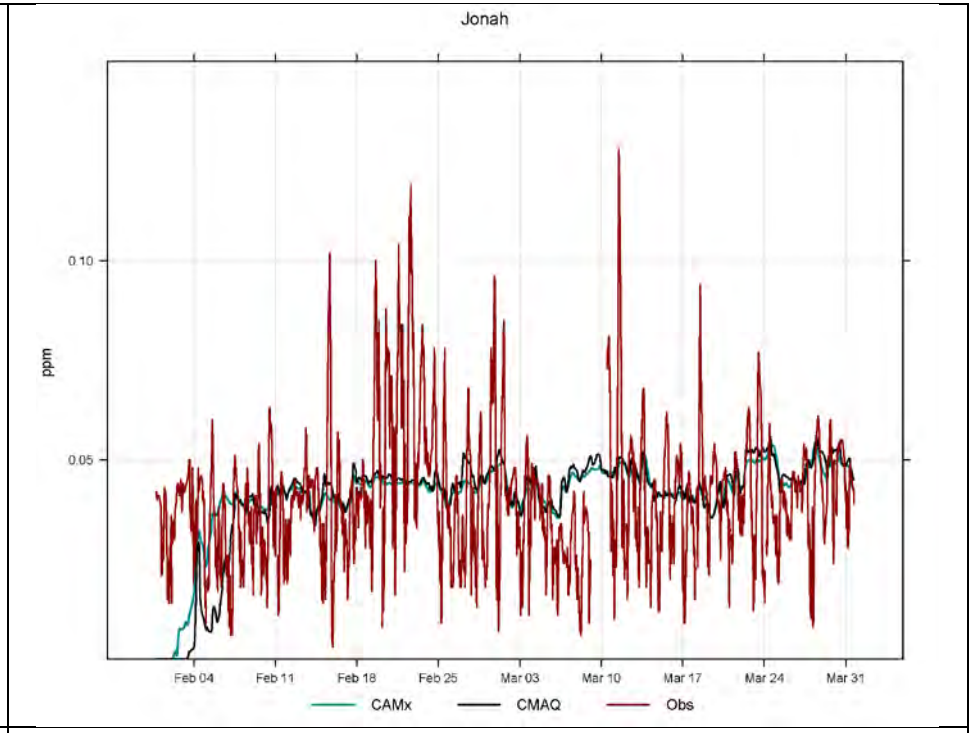

Figure 3-1 Comparison between Observed Ozone Concentrations and 36-km Domain Modeling Results. Total Tracer Concentrations are the Sum of all 24 Tagged Boundary Ozone Species

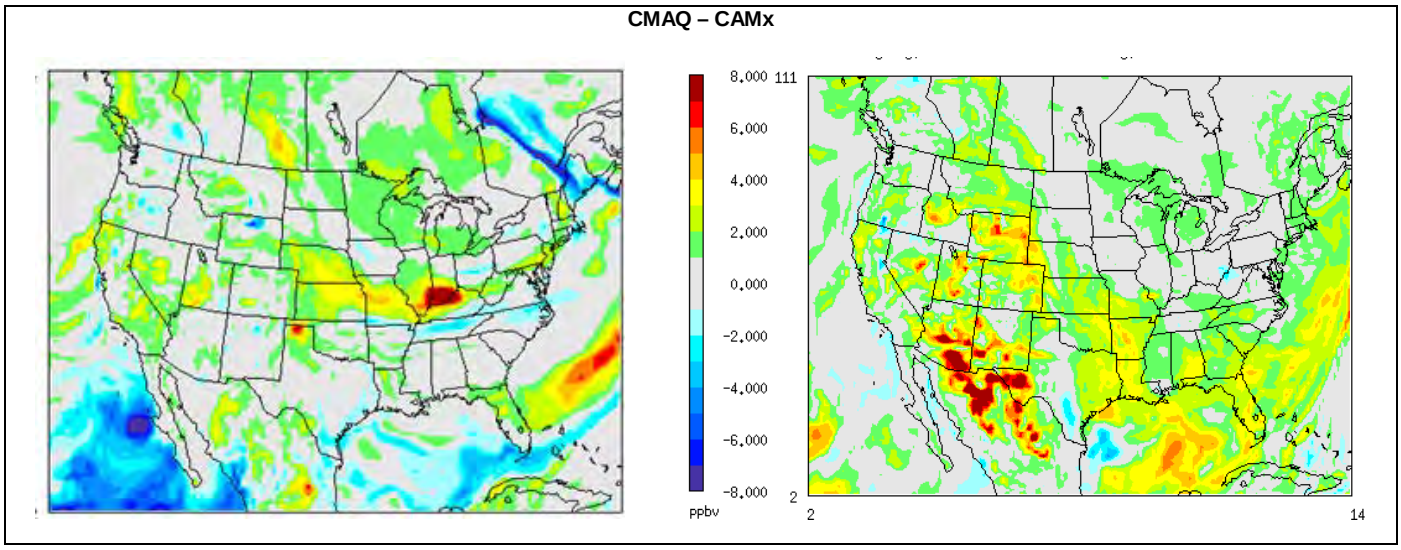

Figure 3-2 Spatial Plots Differences of Daily-Averaged 36-km CMAQ and CAMx Ozone Tracer Concentrations for February 10 and 28, 2008

Figure 3-3 compares the CMAQ 36-km with the 1.33-km domain ozone tracer concentrations at Boulder. This figure demonstrates that the results from each domain are similar, generally within 1 ppb. These small differences in the concentrations are likely due to the spatial resolution of the domains. The CAMx domain inter-comparison (not shown) yields very similar results with no apparent systematic bias between domains. These results demonstrate that both models, with their differing nesting capabilities, provide a consistent treatment of the ozone tracer as it moves towards the area of interest.

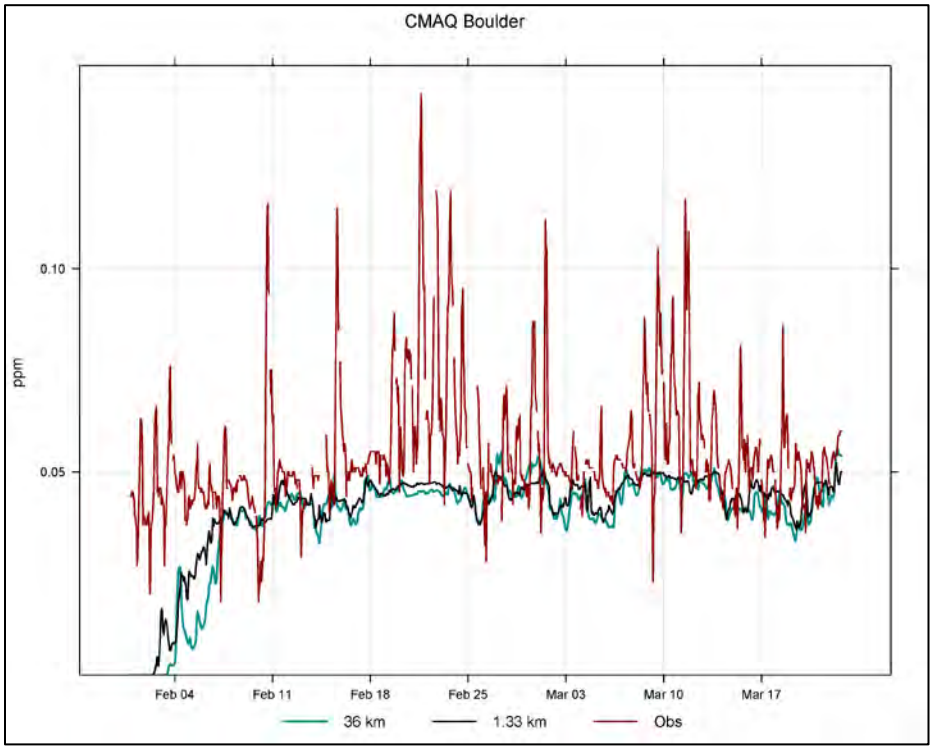

Figure 3-3 Inter-domain Comparison of CMAQ Ozone Tracer Concentrations at Boulder

Figure 3-4 compares the CAMx and CMAQ 1.33-km tracer concentrations at Boulder, by their contribution from the lateral boundary conditions, regardless of the vertical allocation. Each of these contributions is represented with different colors in the figure. Consistent with previous results, CAMx and CMAQ tracer concentrations are similar. The tracer results from both models show that the Northern and Western lateral boundaries have the largest potential to influence ozone concentrations in Sublette County. It also demonstrates that this impact alternates between the north and west boundaries with a period of about 4 to 7 days.

Figure 3-5 compares CAMx and CMAQ 1.33-km tracer concentrations at Boulder by their contribution from each of the six vertical layer boundary conditions regardless of its lateral allocation. Each of these contributions is represented with different colors in the figure. This comparison demonstrates that the differences between CAMx and CMAQ modeling tracers are small when vertical allocation is considered. **Figure 3-5** also illustrates that the most significant source of ozone from the boundaries when the vertical levels are considered is level 3 (L3), which spans from about 1.7 to 4.5-km AGL. After level 3, levels 2 (1 to 1.7-km AGL) and 1 (0 to 1-km AGL) are the other important sources of ozone when considered by vertical level.

Figure 3-6 provides a bar chart of the source of the ozone tracer for modeled concentrations at Boulder by each of the 24 bins (by lateral boundary and vertical layer). The values presented in **Figure 3-6** have been averaged over the entire modeling period and represent the fraction of the total tracer mass from each source region that has an influence over the ozone in the Boulder site. In both models about 56 percent of the tracers originate from levels 2 and 3 (1 to 4.5-km AGL) in the western boundary, while 15 percent of the tracers originate from level 3 in the northern boundary. This figure demonstrates that the concentrations in Sublette County, exclusively from the lateral boundaries, tend to come mostly from the western and northern boundaries and from levels 2 and 3 (i.e., WRF vertical layers 16 – 25) with nominal heights above ground of around 1,000-m to 5,000-m AGL. This finding is reasonable when considering the climatological flow aloft (generally from the west or west-northwest) as well as the time needed for air to descend over time from these heights. Additionally, less than 5 percent of the modeled concentrations in the UGRB originated from layers above 7.5-km AGL.

3.2.3 Boundary Condition Test Findings

- Modeled tracer concentrations between both CAMx and CMAQ are very similar at Boulder, Jonah and Daniel.
- Median tracer concentrations attributable to the lateral boundaries range from 40 to 50 ppb at sites within the UGRB. This compares well with observed median concentrations that range between 37 and 48 ppb at these same sites.
- The tracer results from both models show that the most significant source of ozone from the boundaries by vertical level is level 3, which spans from about 1.7 to 4.5-km AGL.
- Less than 5 percent of the ozone tracer concentrations modeled at Boulder, Jonah and Daniel came from layers higher than 7.5-km AGL.
- Based on the above findings, no anomalous ozone from stratospheric intrusions was expected to impact Sublette County during the periods considered for the base case modeling.

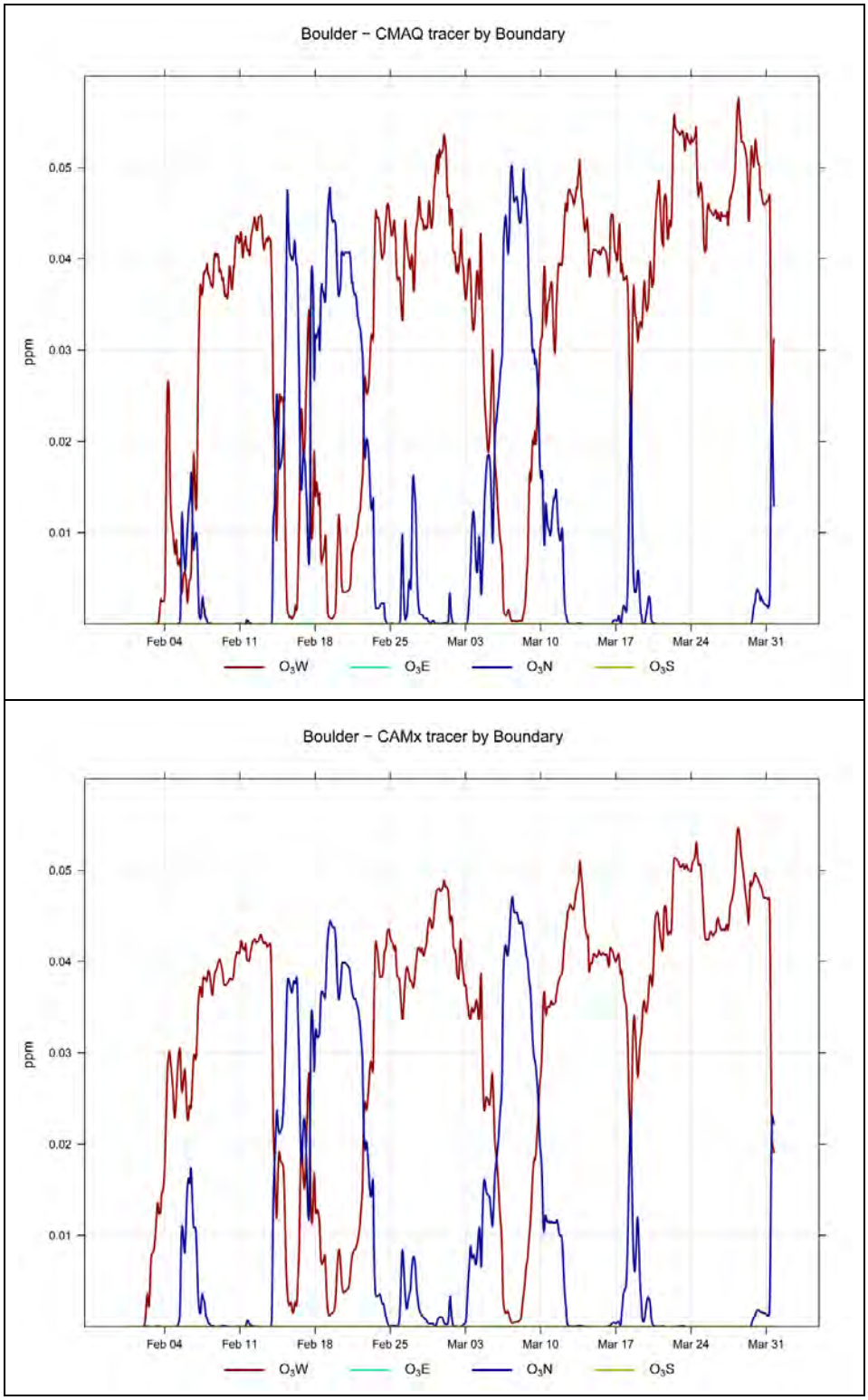

Figure 3-4 CMAQ and CAMx 1.33-km Domain Boundary Ozone Contributions from the 4 Lateral Boundary Directions at Boulder during February and March of 2008

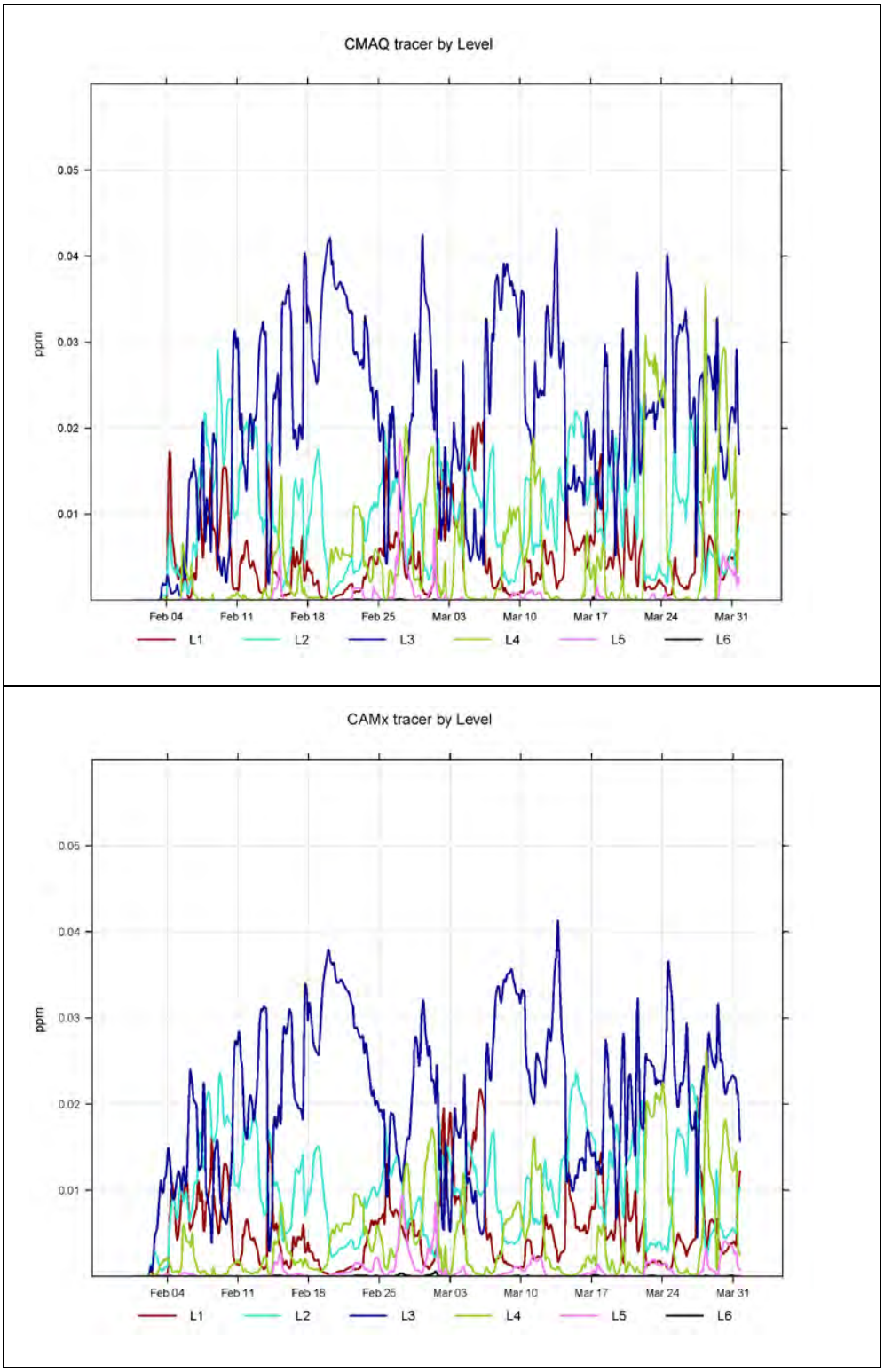

Figure 3-5 Time Series Comparison between CMAQ and CAMx 1.33-km Domain Boundary Ozone Contributions from the 6 Tagged Vertical Level at Boulder during February and March of 2008

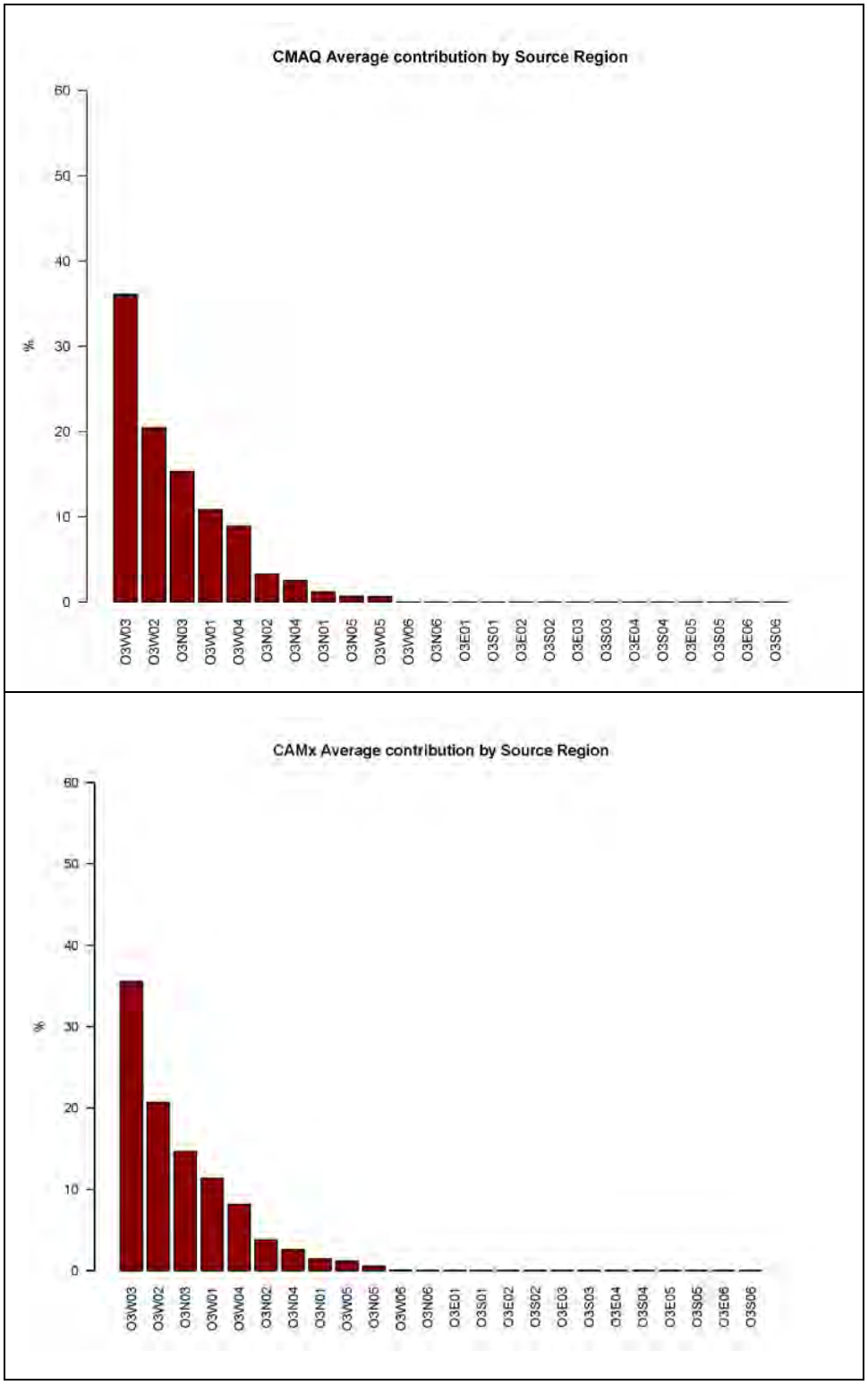

Figure 3-6 Bar Chart Comparison between CMAQ and CAMx 1.33-km Tracer Concentrations by Each of the Source Regions used to Tag Boundary Conditions. O3W03 Means Western Boundary, Level 3, etc.

3.3 36-km Base Case Ozone Modeling

Using the model inputs and configurations described in Chapter 2.0, the base case modeling was executed for both models for the entire 2-month period of February and March 2008. The version of CMAQ used for the base case results presented below contained the albedo patch discussed in Chapter 2.0 and detailed in Chapter 4.0. When possible, the results from the simulations were assessed and analyzed as they were completed. This stepwise process resulted in a detailed analysis of snow cover and albedo inputs during the 36-km base case modeling as well as detailed analyses of the 1.33-km base case results in the surface and aloft layers.

3.3.1 36-km Ozone Analyses

While the 36-km base case simulation was running, the output was checked to identify and remedy any potential issues with the input data or model settings prior to carrying out the more intensive high-resolution modeling. The product of such a check is the CAMx and CMAQ surface-level ozone concentrations at a 36-km resolution for February 23, 2008 as shown in **Figure 3-7**. The CAMx run produced a significant regional ozone enhancement over much of the eastern U.S., with ozone concentrations exceeding 75 ppb over large portions of Oklahoma, Arkansas, and Tennessee. No such ozone enhancement was produced by CMAQ. A qualitative comparison against available monitoring data (not shown) showed the CAMx ozone concentrations to be unrealistic.

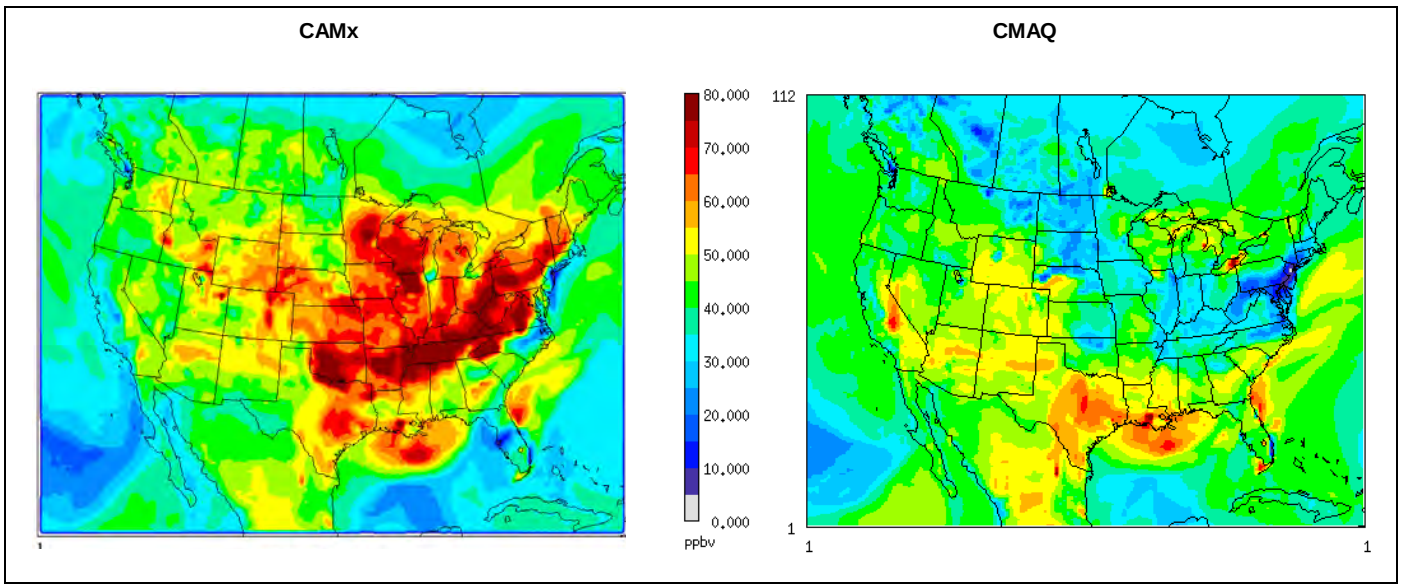

Figure 3-7 CAMx (left) and CMAQ (right) 36-km Domain Surface Layer Ozone Concentration Predicted on February 23, 2008 at 0000 UTC. The CAMx Simulation Used the Default WRFCAMx Snow Cover Conversion Algorithm and a Snow Albedo of 0.8

In light of these results, a review of some CAMx settings was conducted. The CAMx snow albedo was initially set to 0.8 for the base case runs to allow for an enhancement of photolysis expected to be important for ozone events. The CAMx base case simulation also used snow cover inputs generated by the processor WRFCAMx, which contains algorithms for translating the WRF snow cover fractions into model-ready gridded snow cover data. In CAMx, snow cover is treated in a binary fashion, with each grid cell treated as either completely snow-covered or not snow-covered at all. By default, WRFCAMx considers a grid cell to be snow-covered when the WRF snow cover fraction for that grid cell is greater than zero.

In order to address the issue identified in **Figure 3-7**, the CAMx simulation for the 36-km domain was re-run with a lower snow albedo value of 0.5. Although 0.8 is considered an appropriate snow albedo value for fresh snow, this value is likely not representative of snow cover albedo over a 36-km grid cell because of sub-grid scale disruptions to the snow cover field (e.g., trees, urban areas, or localized snowmelt). Although the CAMx ozone field from this second simulation compared much more favorably to the CMAQ results (**Figure 3-8**), CAMx still produced several areas of enhanced ozone not supported by observations.

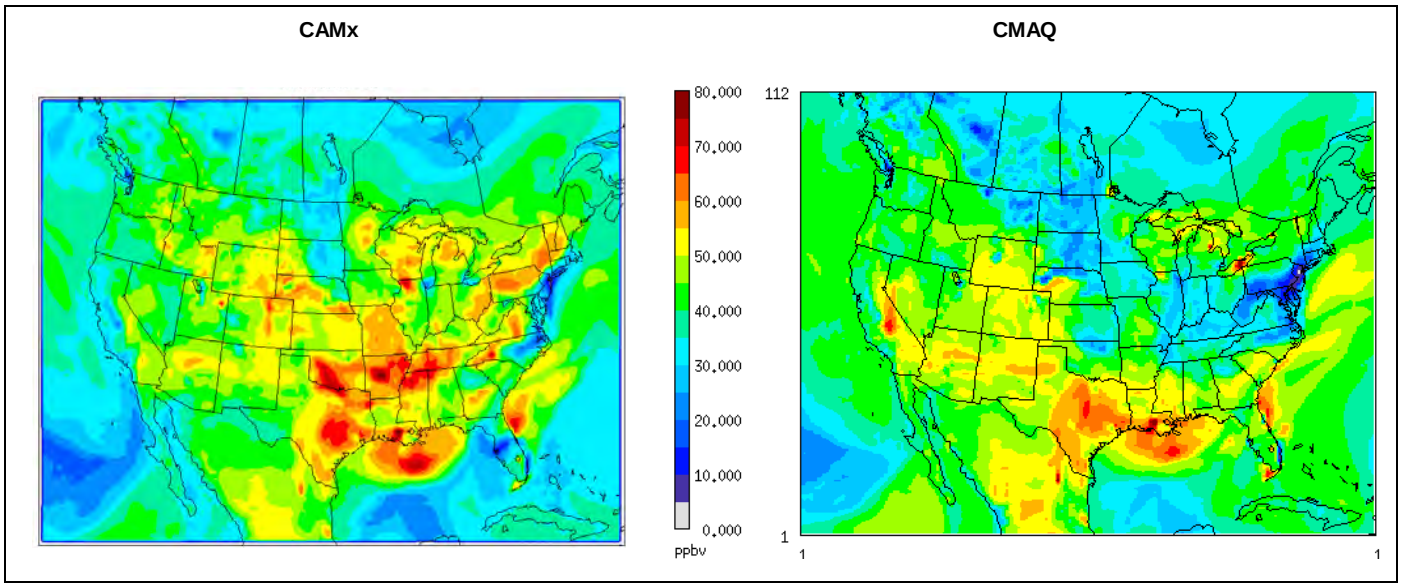

Figure 3-8 CAMx (left) and CMAQ (right) 36-km Domain Surface Layer Ozone Concentration Predicted on February 23, 2008 at 0000 UTC. The CAMx Simulation Used the Default WRFCAMx Snow Cover Algorithm and a Snow Albedo of 0.5

To address the remaining issues with the CAMx 36-km grid simulation, the snow cover fields were further evaluated. The spatial coverage of snow cover predicted by WRF was generally consistent with NOAA snow cover observations throughout the modeling period, as shown in the sample snow cover fields for February 23, 2008, displayed in **Figure 3-9**. However, while the WRF snow cover field compares reasonably well with observations, the CAMx-ready binary snow cover field generated by WRFCAMx shows extensive and unrealistic snow coverage over the northern two-thirds of the U.S., extending south through Arkansas and Tennessee (**Figure 3-10**, bottom left). Upon investigation, it was found that this occurs because WRF snow cover fraction data contain extensive regions of small (less than 0.01) but non-zero snow cover fractions, which were interpreted by WRFCAMx as complete snow cover for that cell. Although the threshold fraction of 0.5 for defining a grid cell as snow covered was supposed to be the default in WRFCAMx, it was found in the code that this was set incorrectly to 0.0 and therefore corrected to its original intent. Use of the threshold fraction set at 0.5 resulted in a more realistic CAMx snow cover field (**Figure 3-10**, bottom right). When used in conjunction with a lower albedo, the improved snow cover fields eliminated the anomalous ozone enhancements shown in the previous tests (**Figure 3-11**).

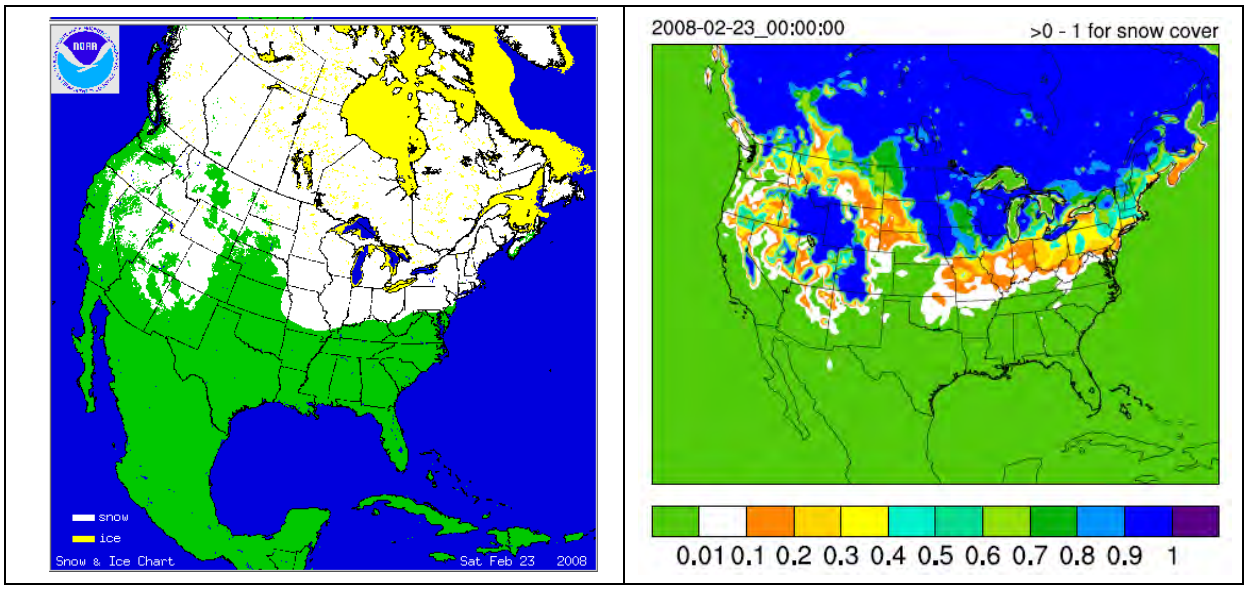

Figure 3-9 Observed (left) and WRF-predicted (right) Snow Cover Fields on February 23, 2008. Observed Snow Cover Fields Obtained from NOAA Snow Cover Maps Website

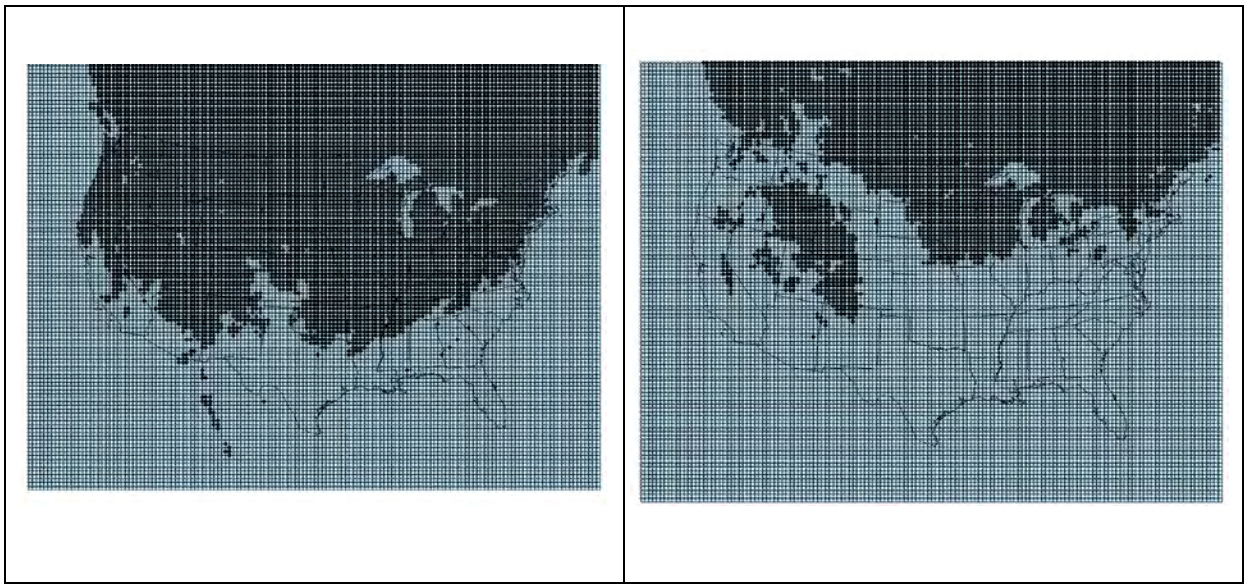

Figure 3-10 CAMx-ready Snow Cover Field for February 23, 2008 Generated from the Default (left) and Modified (right) WRFCAMx Algorithm for Determining CAMx Snow Cover from WRF Fractional Snow Cover

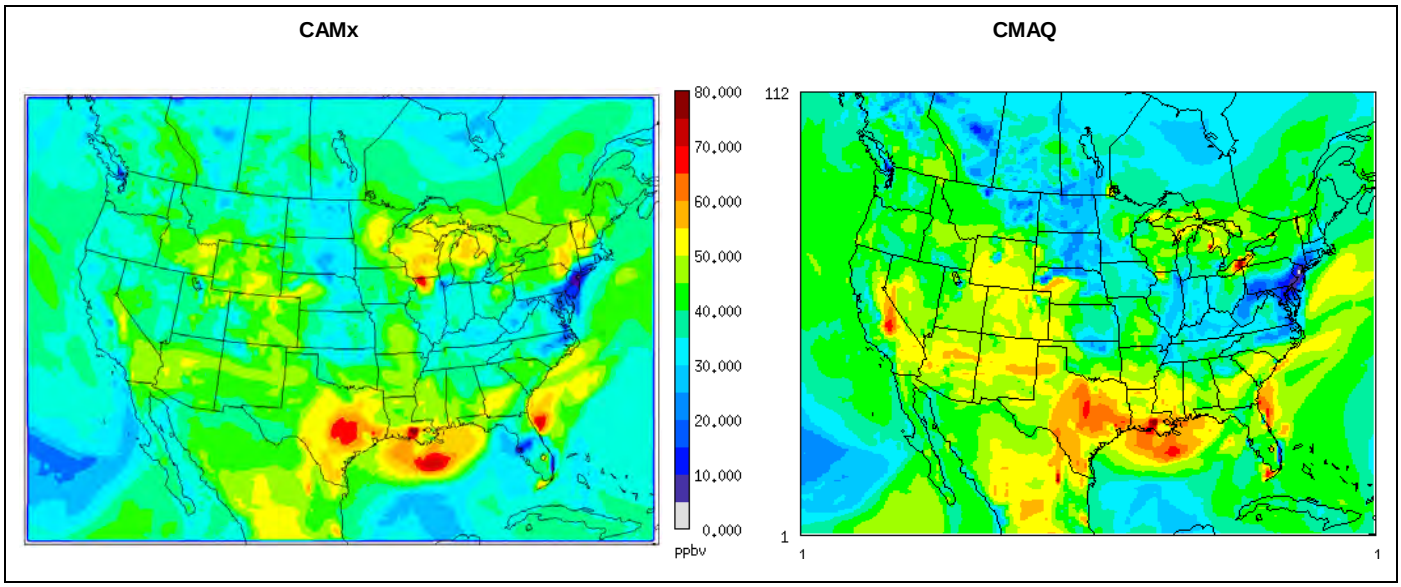

Figure 3-11 CAMx (left) and CMAQ (right) 36-km Domain Surface Layer Ozone Concentration Predicted on February 23, 2008 at 0000 UTC. The CAMx Simulation Used the Revised WRFCAMx Snow Cover Algorithm and a Snow Albedo of 0.5

3.3.2 36-km Ozone Findings

Use of a snow albedo value of 0.5 and a WRFCAMx fractional snow cover threshold of 0.5 in CAMx provides better results on the 36-km domain, which in turn will provide better boundary conditions for the 12-km domain.

3.4 1.33-km Base Case Ozone Modeling

The model performance was assessed during the IOPs by comparing the 1.33-km domain modeled ozone concentrations to the concentrations observed at the monitoring sites shown in **Figure 2-2**. The Boulder, Jonah and Daniel sites are permanent WDEQ aerometric monitors, while Warbonnet, LaBarge, Haystack Butte, and Simpson Gulch sites are mesonet monitors deployed during UGWOS (2008).

3.4.1 1.33-km Ozone Time series

The models' results are compared with observed near-surface ozone concentrations using time series plots. With the exception of the LaBarge site, **Figures 3-12** to **3-18** show that both models systematically underpredict ozone concentrations at most sites during the IOPs, especially during the observed elevated ozone peaks. The modeled ozone concentrations at these observation sites rarely exceed 60 ppb during the IOPs, whereas the peak observed ozone concentrations sometimes exceed 100 ppb during the IOPs.

At Boulder (**Figure 3-12**), both models underpredict the observed ozone concentrations: CAMx generally predicts ozone concentrations that do not exceed 40 ppb, while CMAQ can approach 50 ppb particularly during the diurnal peaks. CMAQ tends to be able to reproduce some level of the observed diurnal cycles, while CAMx generally does not. At Jonah (**Figure 3-13**) and Warbonnet (**Figure 3-15**), both models show significant ozone reduction at night due to local titration by the significant NO_X emissions in the area, although in Warbonnet the effect of titration are more pronounced in CMAQ. The observed ozone titration at Jonah and Warbonnet is most pronounced at night, when the modeled ozone concentrations drop to zero frequently, well below the observations. During the day, CMAQ is able to reproduce the timing (but not the magnitude) of ozone peaks somewhat better than CAMx. At Daniel (**Figure 3-14**),

modeled ozone remains mostly at, but less than, background levels and in both the model and observations there is not a strong diurnal pattern found at the other sites.

At LaBarge (**Figure 3-16**) CMAQ is generally able to predict the timing and magnitude of observed ozone concentrations better than CAMx. CMAQ performance is particularly good during IOP 3 with model concentrations very close to observations. Another feature that both the model and observations have in common is a very strong diurnal cycle during the IOPs. This strong diurnal cycle could be indicative of ozone formed in the vicinity of the LaBarge station. As shown in **Figure 2-2**, the LaBarge station is located in the southwestern part of the 1.33km domain, which is also a region where the models systematically produce the largest ozone concentrations (as shown in the following section). At both Haystack Butte (**Figure 3-17**) and Simpson Gulch (**Figure 3-18**), the observations do not show a pronounced diurnal cycle. Since these sites are located downwind from most emissions sources, the observed ozone on these sites has been subject to at least some long range transport. Both models systematically undepredict ozone concentrations at these two sites.

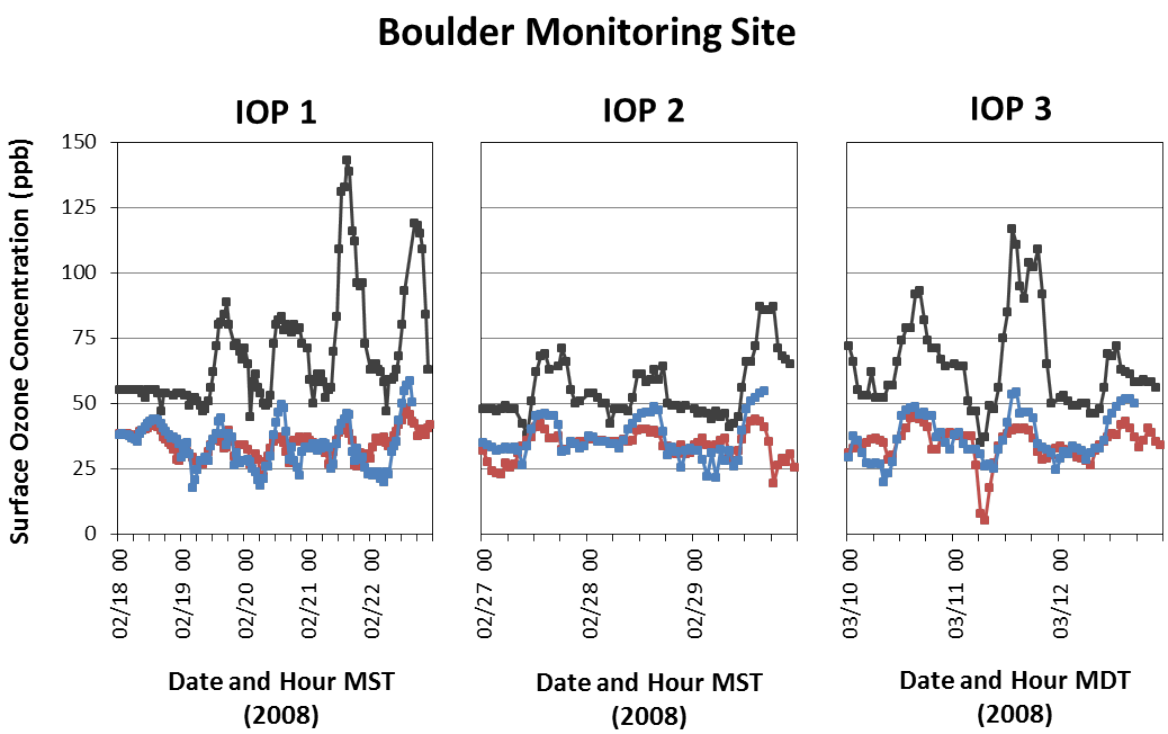

Figure 3-12 Time Series of Observed (black), CAMx (red) and CMAQ (blue) Ozone Concentrations at Boulder During the Three IOPs

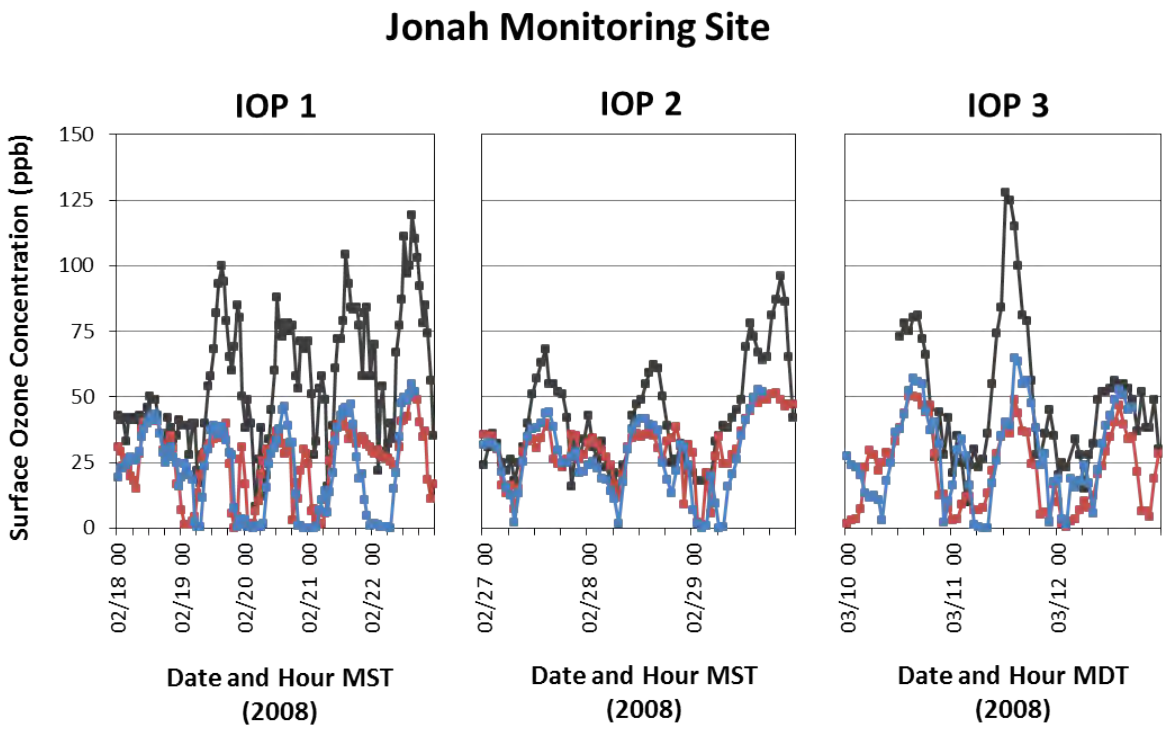

Figure 3-13 Time Series of Observed (black), CAMx (red) and CMAQ (blue) Ozone Concentrations at Jonah During the Three IOPs

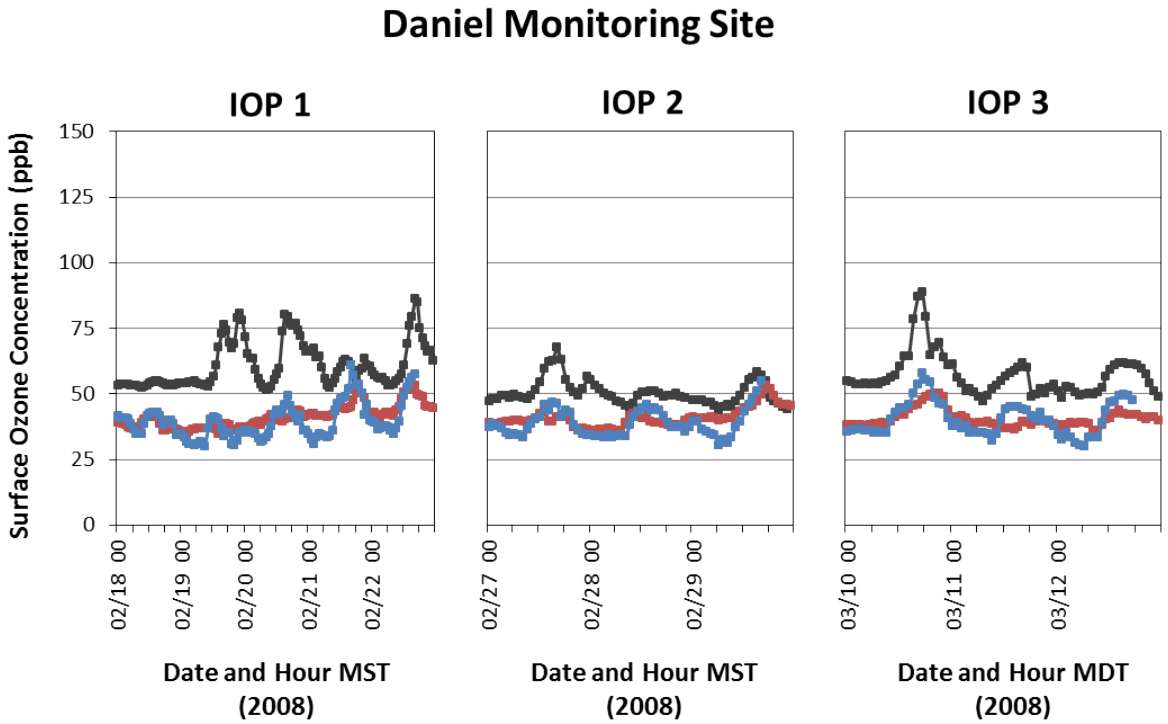

Figure 3-14 Time Series of Observed (black), CAMx (red) and CMAQ (blue) Ozone Concentrations at Daniel During the Three IOPs

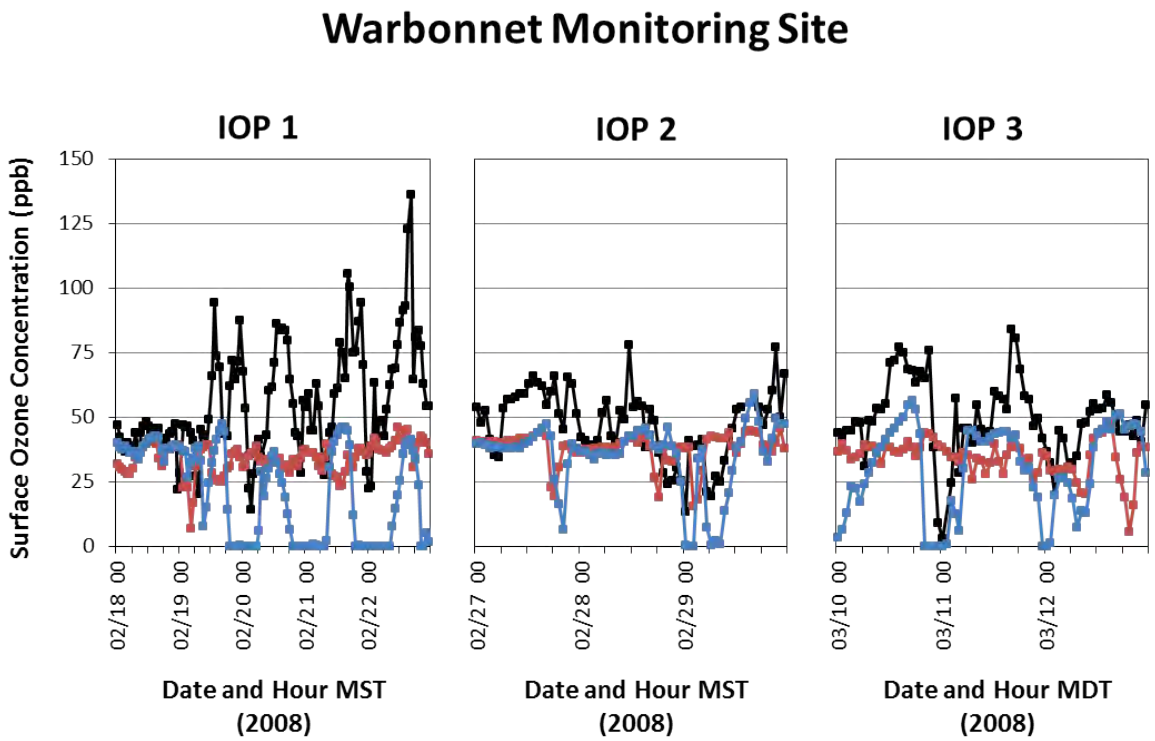

Figure 3-15 Time Series of Observed (black), CAMx (red) and CMAQ (blue) Ozone Concentrations at Warbonnet During the Three IOPs

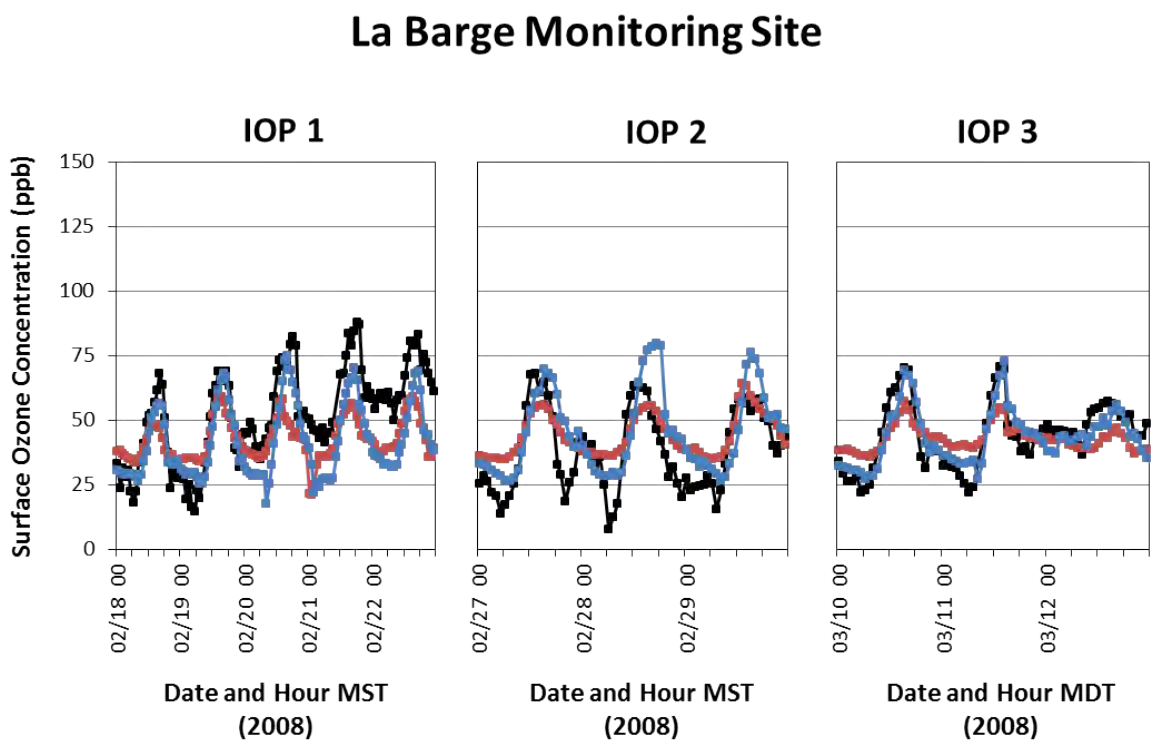

Figure 3-16 Time Series of Observed (black), CAMx (red) and CMAQ (blue) Ozone Concentrations at LaBarge During the Three IOPs

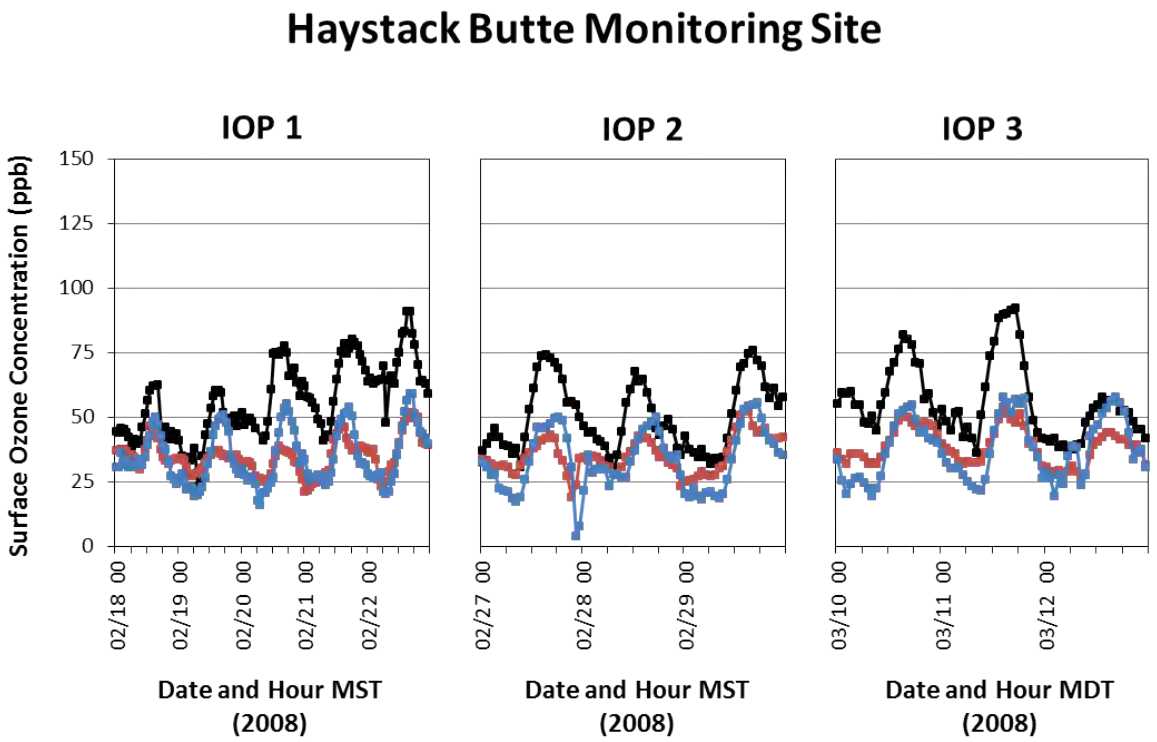

Figure 3-17 Time Series of Observed (black), CAMx (red) and CMAQ (blue) Ozone Concentrations at Haystack Butte During the Three IOPs

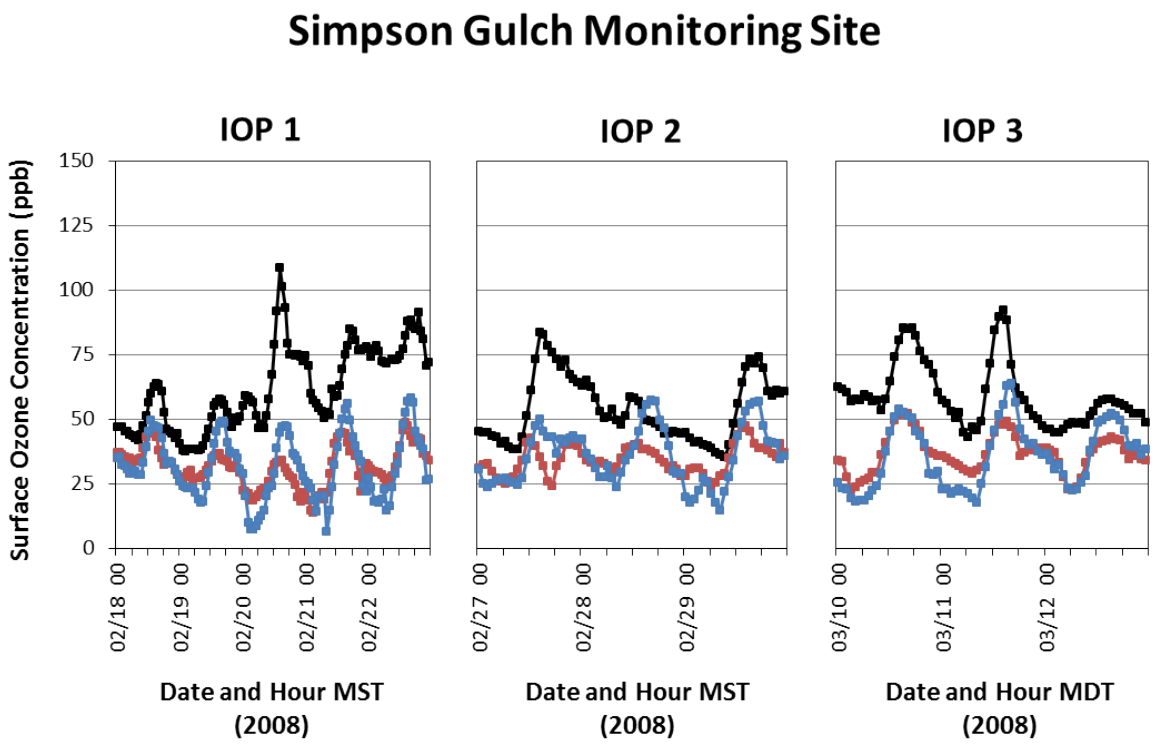

Figure 3-18 Time Series of Observed (black), CAMx (red) and CMAQ (blue) Ozone Concentrations at Simpson Gulch During the Three IOPs

3.4.2 1.33-km Ozone Spatial Plots

Spatial plots of CMAQ and CAMx ozone concentrations from the 1.33-km domain are shown in **Figure 3-19**. These plots, which represent one afternoon from each IOP, suggest that in general both models do not produce significant amounts of ozone in the area, particularly at Boulder, Jonah and Daniel. Around the oil and gas development areas, the predicted ozone concentrations are consistently lower than the surrounding areas, as the presence of large NO_X sources titrate the ozone during the day. The titration-effects are even more pronounced during the nighttime hours (not shown explicitly but evidenced in the time series plots above). The titration effect is particularly noticeable around the Warbonnet station during February 28 and March 11, 2008.

The spatial plots also show that for both models local ozone production occurs in southwest Sublette County and in neighboring Lincoln and Sweetwater counties. For CAMx, this production is more modest than CMAQ, which could be related to increased photolysis in CMAQ due to the in-line photolysis module. The peak modeled ozone concentrations in these areas are around 70 ppb for CAMx and 85 ppb for CMAQ for the period shown. The aircraft measurements of ozone concentrations during UGWOS do show some elevated ozone concentrations in extreme southern Sublette County and in the neighboring counties, which is discussed in more detail in Section 3.5 and 3.6. CMAQ consistently generates the highest ozone concentrations in the southwest part of the 1.33km domain. The LaBarge ozone observations tend to be most consistent with the CMAQ results. Simpson Gulch and Haystack Butte are generally located downwind from oil and gas sources, **Figure 3-19** shows that CMAQ is able to produce ozone near LaBarge which is then transported in a southeast direction (particularly on February 28 and March 11), impacting both Haystack Butte and Simpson Gulch.

.

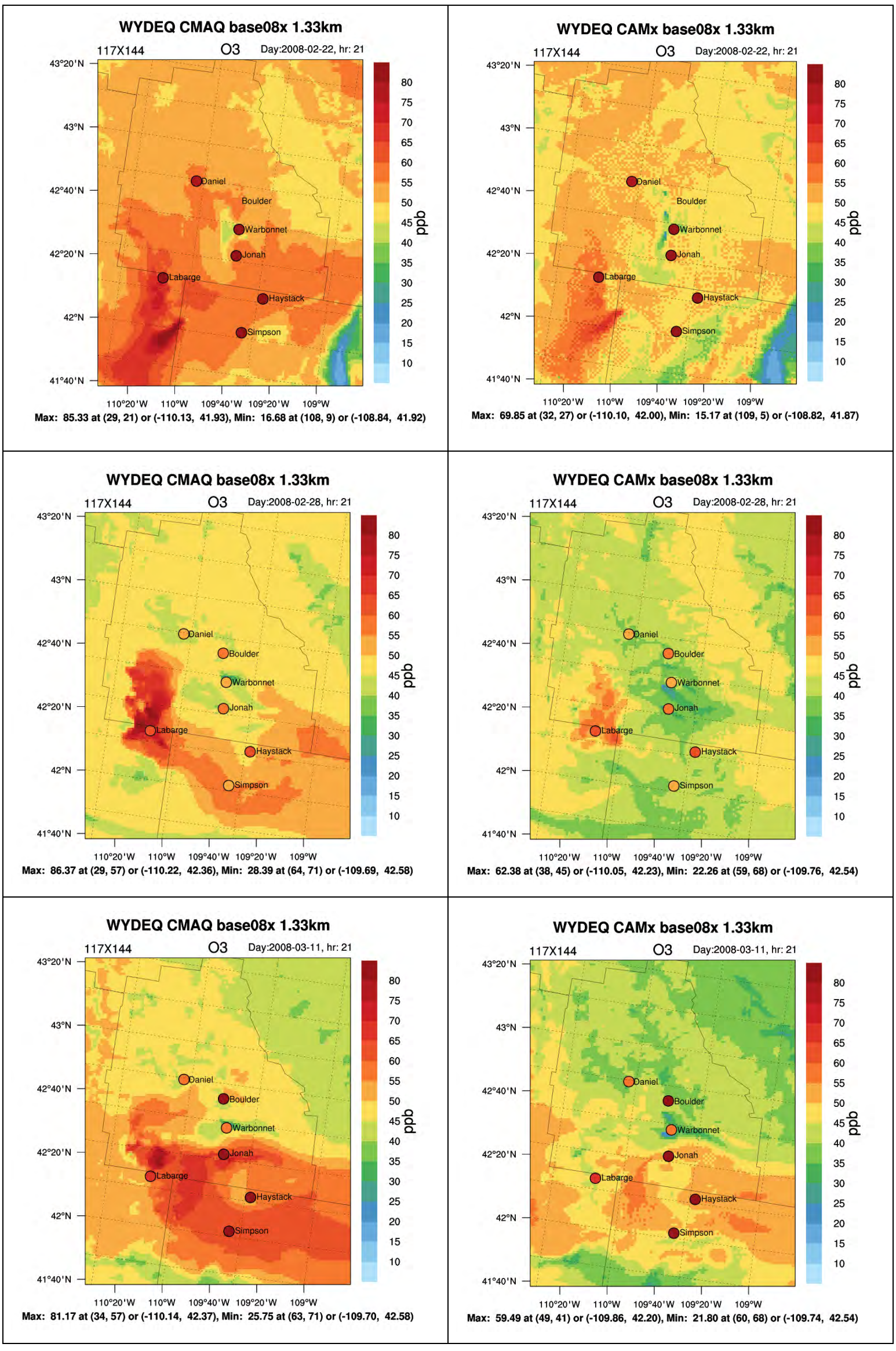

Figure 3-19 Spatial Plots of CMAQ (left) and CAMx (right) Near-Surface Ozone Concentration from the 1.33-km Domain at 1400 MST on February 22, February 28, and March 11, 2008. The observed ozone concentrations for multiple sites are shown in circles overlaid on model results

.

3.4.3 1.33-km Ozone Findings

- Base case modeling results show that neither CMAQ nor CAMx were able to fully replicate the measured 1-hour peak ozone concentrations during the IOPs. Both models show ozone estimates that consistently under-predict observations at Boulder, Jonah and Daniel. This general lack of skill in both models led to additional surface and aloft analyses as well as sensitivity simulations described in detail in the next sections.
- Both models show daily ozone reductions at Jonah, Boulder and Warbonnet due to titration by fresh NO_X emissions in the area. The modeled ozone titration is most pronounced at night (see Jonah and Warbonnet time series), but also occurs during the day and is more noticeable at the Jonah and Warbonnet sites (see spatial plots).
- The spatial plots show that peak ozone concentrations in the 1.33-km domain are larger in magnitude and spatial extent for CMAQ than for CAMx. While both models perform well at the LaBarge site, they perform poorly at and around the Boulder, Jonah and Daniel sites.
- Both models produce local ozone in southwest Sublette County and in neighboring Lincoln and Sweetwater counties. The peak modeled ozone concentrations occur in the vicinity of LaBarge with values around 70 ppb for CAMx and 85 ppb for CMAQ during the periods analyzed. The magnitude of the modeled peak concentrations is consistent with observations at the LaBarge site; however, the observed peak concentrations occur at the Boulder site.

3.5 Base Case Surface Layer Analyses

The modeled surface ozone precursor concentrations for the base case are assessed through a series of analyses performed for all three IOPs. For these analyses, the Boulder, Jonah and Daniel sites are compared to the CAMx modeling results since these sites collected VOC measurements during the IOPs. Results from the CAMx model were used as the basis of these analyses because of its post-processing software capabilities and efficiencies in the model. As detailed in Section 2.2, CAMx uses the Carbon Bond mechanism, which simplifies the hydrocarbon chemistry associated with ozone formation by grouping or “lumping” molecules or parts of molecules into reactivity classes. For example, all alkanes are modeled as paraffinic carbons (or paraffin) that react at identical rates. The selection of only two of the VOC modeled species (paraffin and xylene) was made here for efficiency and simplicity of the analysis. Paraffins were selected since alkanes are a significant portion of the oil and gas emissions although they are not considered very reactive and therefore are less conducive to ozone formation. Although xylene emissions are not as significant, this species was selected since it is considered very reactive and potentially important in the formation of ozone. Formaldehyde was selected given its importance in the formation of hydroperoxyl radical which is a major oxidizer throughout the entire atmosphere and is central to catalytic cycles generating ozone in the troposphere.

The following products were generated and evaluated during the surface layer analyses:

- Time series of modeled and observed NO_X, CO, paraffin VOCs, xylene, and formaldehyde concentrations at the grid cells that contain the Boulder, Jonah and Daniel sites;
- Spatial plots of NO_X, CO, paraffin VOCs, xylene, and formaldehyde concentrations overlaid with available observations in Sublette County, and with near-surface wind vectors produced by WRF and the WRFCAMx pre-processor; and
- Emissions density plots of near-surface NO_X, CO, paraffin, xylene, and formaldehyde emissions.

This section shows some example plots from the full analysis and summarizes the key results from these work products.

3.5.1 Surface Layer Time Series Comparisons

Figure 3-20 shows time series comparisons of modeled and observed NO_X concentrations at Daniel and Jonah for all three IOPs. The Boulder site did not have adequate data recovery for hourly NO_X. Since Jonah was situated within a large oil and gas production area in 2008, NO_X concentrations are much higher at Jonah than at Daniel. At Jonah, CAMx generally underpredicts NO_X, particularly when the observed NO_X concentration exceed 100 ppb. At Daniel, which is not close to any large NO_X sources, the modeled NO_X concentrations generally agree well with observations; however, the model does not capture the occasional periods of elevated NO_X concentrations.

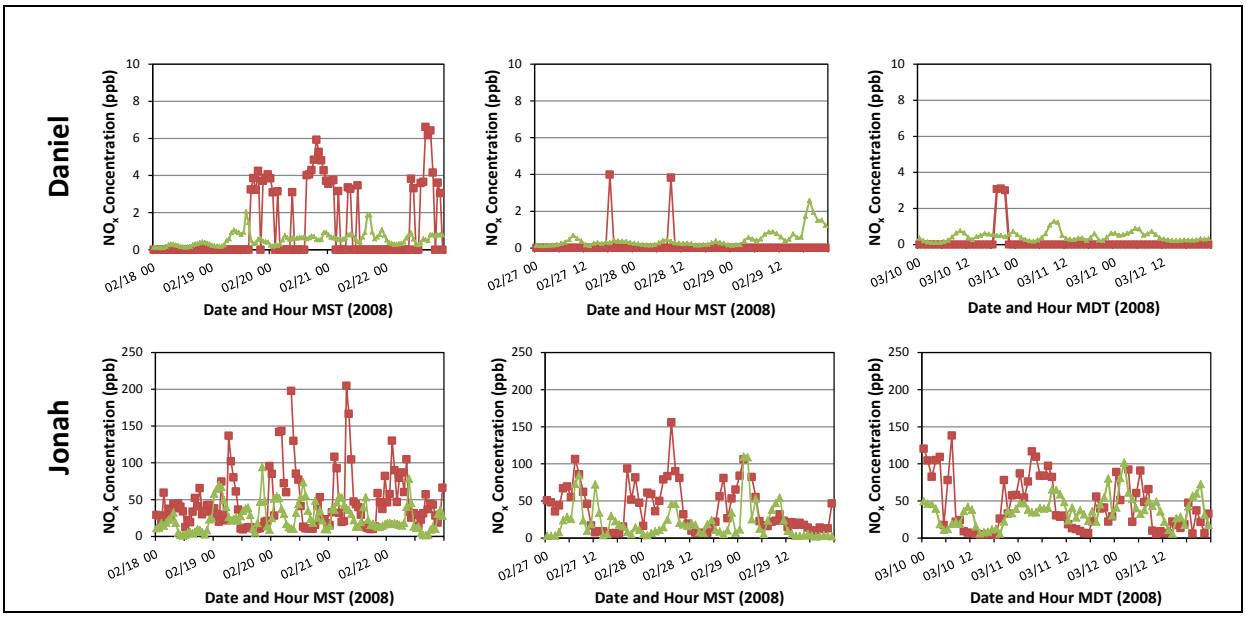

Figure 3-20 Time Series Comparison of Modeled (green) and Observed (red) Near-Surface NO_x Concentrations During Each IOP at Daniel and Jonah.

The model significantly underpredicts paraffin VOC concentrations at all three Sublette County monitoring locations during the IOPs, as shown in **Figure 3-21**. At times, the model underpredicts paraffin VOCs by an order of magnitude. The model also underpredicts more reactive VOC compounds, such as xylene (not shown here).

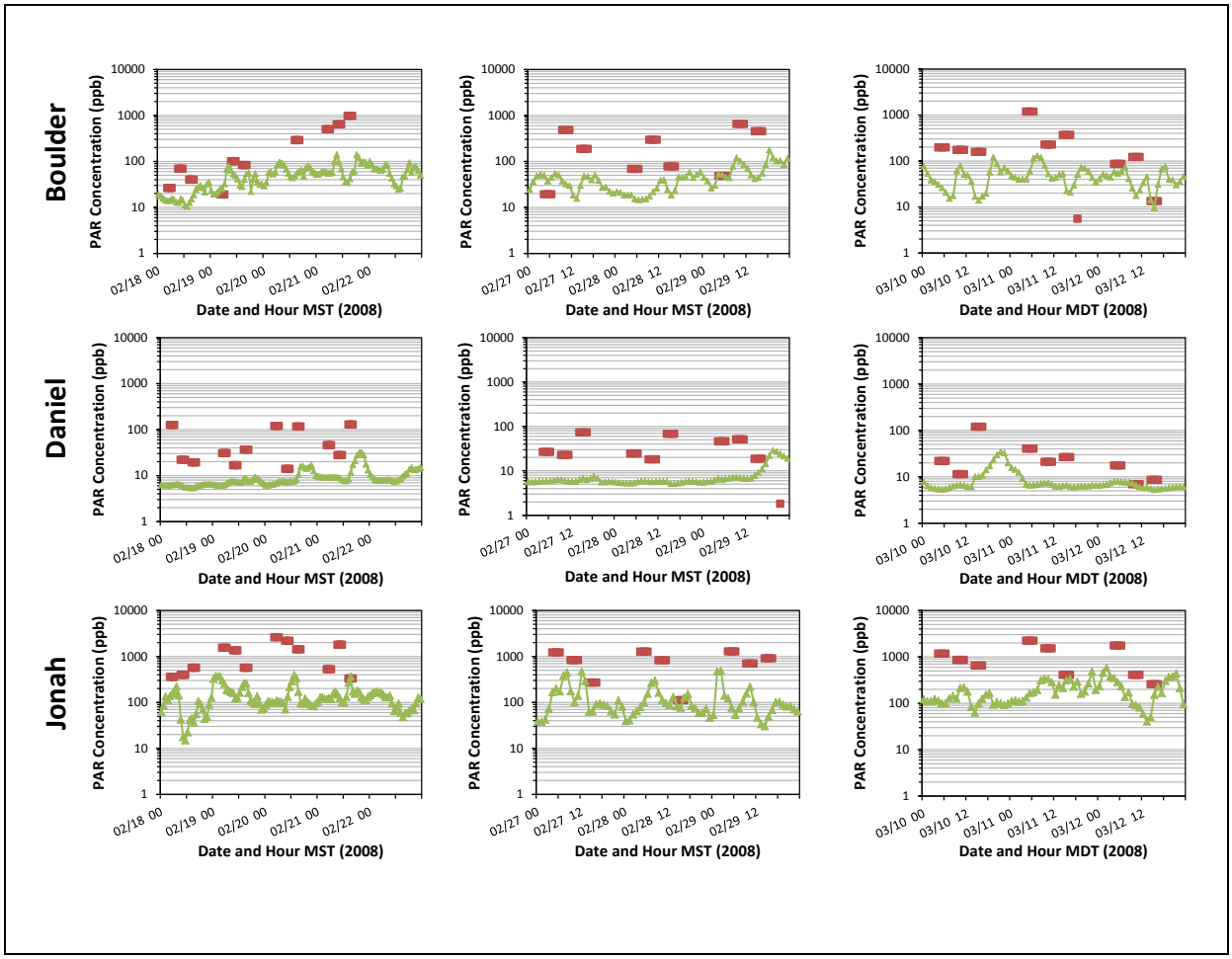

Figure 3-21 Time Series Comparisons of Modeled (green) and Observed (red) Paraffin Concentrations During Each IOP at Boulder, Jonah and Daniel Plotted on a Log Scale

3.5.2 Surface Layer Spatial plots

Spatial plots of modeled near-surface ozone and NO_X concentrations from CAMx in the 1.33-km domain for February 22, 2008 at 1500 Mountain Standard Time (MST) are shown in **Figure 3-22**. The ozone spatial plot is overlaid with modeled wind vectors, while the NO_X spatial plot is overlaid with ambient measurement data where available. During the IOPs, the modeled near-surface winds are generally light and variable within the UGRB, allowing the modeled near-surface pollutants to remain within the UGRB. The ozone spatial gradients within the 1.33-km domain do not show the expected elevated ozone seen in observations. The NO_X impacts were generally lower than observed at the monitoring sites and the spatial fields show a large area of NO_X less than 10 ppb to the south of the oil and gas sources with higher concentrations closer to the sources. **Figure 3-23** shows spatial plots with observation overlays for paraffin VOCs and xylene for February 21, 2008 at 0900 MST. The time series for VOCs (paraffins and xylene) show consistent and substantial underpredictions. The spatial plots of these emissions show locations with elevated concentrations near oil and gas sources.

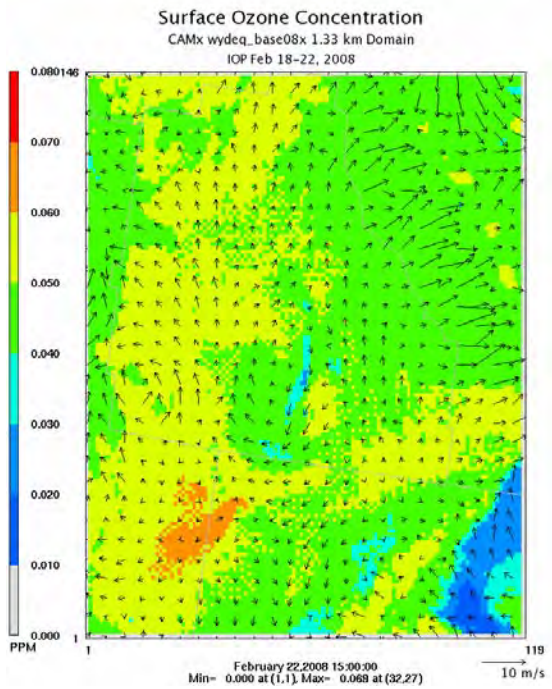

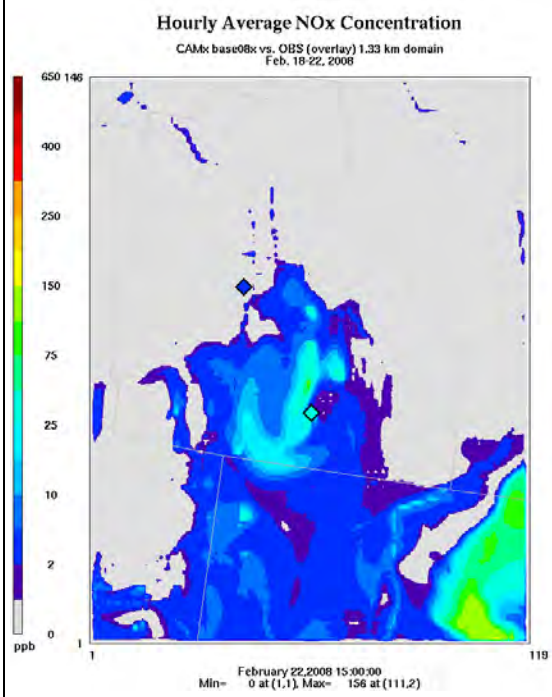

Observed Ozone Concentrations

Daniel: 79.5 ppb
Boulder: NA
Jonah: 119 ppb

Figure 3-22 CAMx Spatial Plot of Modeled Surface Layer Ozone Concentrations Overlaid with Wind Vectors (left), and Modeled NO_x Concentrations Overlaid with Ambient Data (right) on February 22, 2008 at 1500 MST.

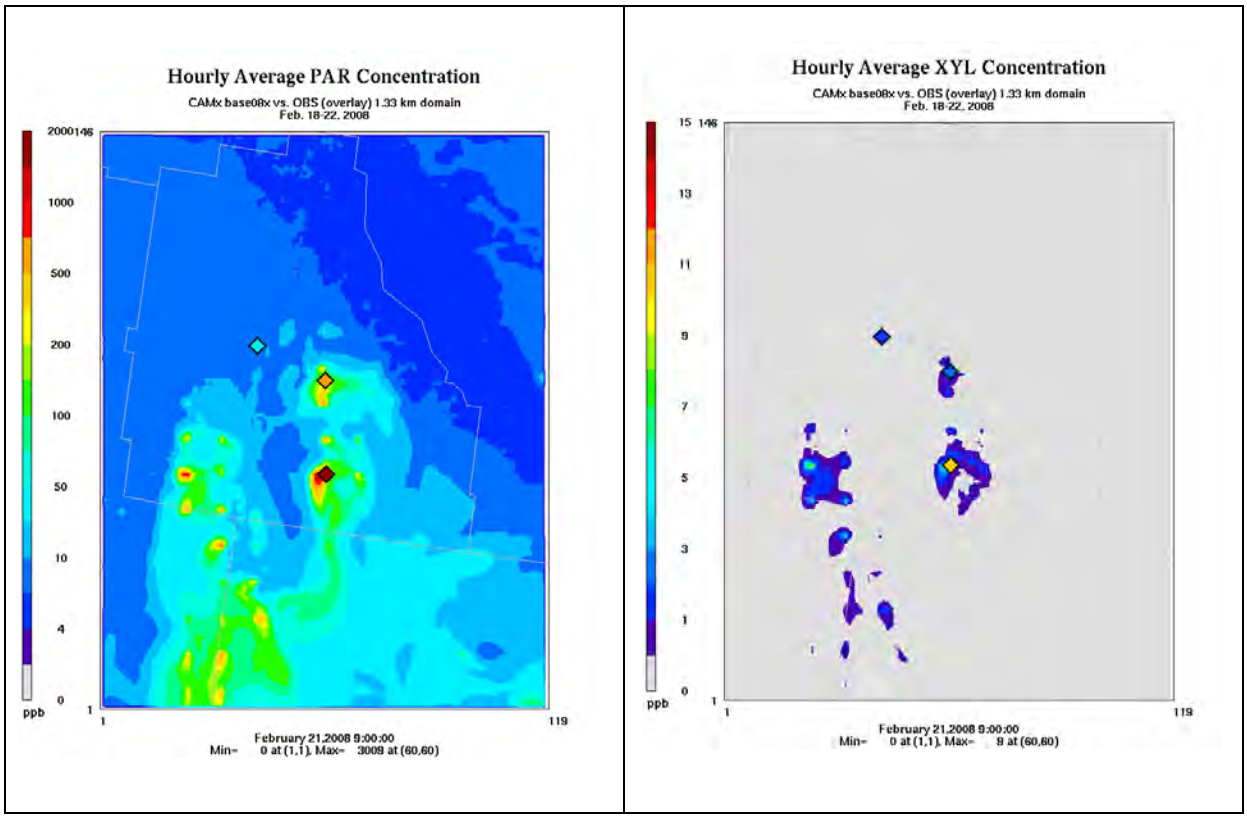

Figure 3-23 CAMx Spatial Plot of Modeled Surface Layer Paraffin VOC (left) and Xylene (right) Overlaid with Ambient Data on February 21, 2008 at 0900 MST

3.5.3 Surface Layer Emissions Density Plots

As part of the surface analysis, the emissions density plots from the lowest model layer were also evaluated. **Figure 3-24** shows an example emission density plot for NO_X and paraffin VOCs on March 11, 2008. As expected, the most prominent feature in the NO_X emissions density plot is the road network, with some additional emissions from the oil and gas development areas. Note that much of the combustion-related NO_X emissions associated with the oil and gas development occur above layer 1, but within the lowest few model layers. Also expectedly, the paraffin VOC emissions density plot shows the presence of VOC emissions associated with the oil and gas development in the region.

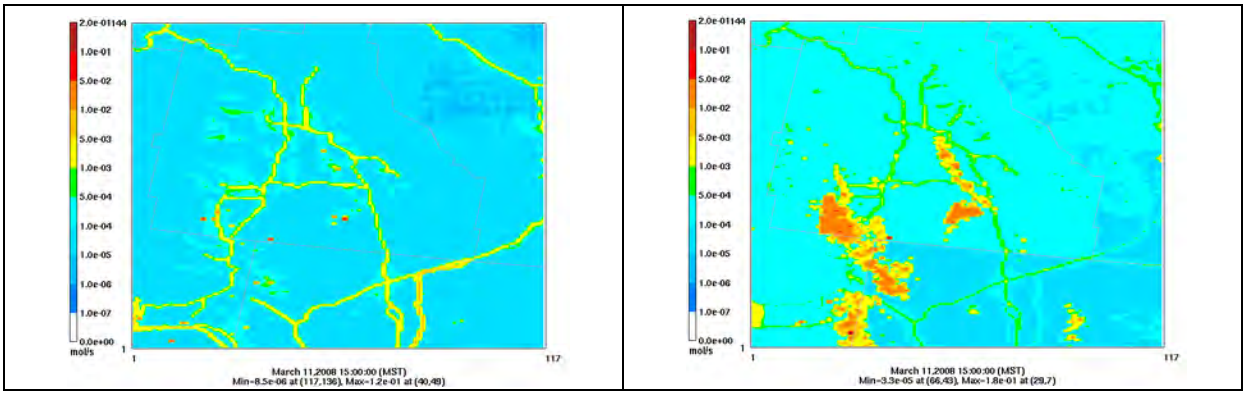

Figure 3-24 CAMx Layer 1 Emission Density Plots for NO_x (left) and Paraffins (right) on March 11, 2008 at 1500 MST

3.5.4 Surface Layer Analyses Findings

- Both models produce near-surface ozone concentrations that are consistently low compared to observations for all IOP days (see Section 3.4).
- At the monitor sites, modeled NO_X and VOC concentrations are consistently low compared to observations for all IOP days. At times, modeled VOC concentrations are an order of magnitude lower than observed concentrations.
- During the IOP days, modeled surface wind speeds in the UGRB are sufficiently light and variable (usually less than 5 m/s) to keep pollutants and precursor emissions within the UGRB.
- The spatial plots provide information about domain-wide model-predicted concentrations and generally seem reasonable, but cannot be validated without additional monitoring data. The poor performance at the monitored locations is also a consideration in the interpretation of these results.
- The location and distribution of ozone precursor emissions is consistent with expectations based on the input emission inventory as shown in the emission density plots.

3.6 Base Case Vertical Analyses

A series of additional analyses of the vertical modeling outputs from the 1.33-km domain was also conducted in order to evaluate the vertical distribution of emissions, the three-dimensional structure and movement of pollutants, and boundary layer structure and stability in the base case modeling. This analysis was performed for the three IOPs identified during the 2008 UGWOS field campaign. Similar to the surface analyses these vertical analyses focused on locations with aloft measurements and used the CAMx model results due to its post-processing software capabilities and efficiencies with this model. As a reference for the vertical analyses, **Table 3-2** shows the height of the model vertical layer interfaces up to 1,100-m AGL. The analysis focused on model results in the lowest 1,000-m AGL.

Table 3-2 Height of Model Vertical Layer Interfaces up to 1100-m AGL

Model Layer	Height (m)
1	0
2	12.0
3	24.1
4	40.1
5	56.2
6	72.4
7	96.6
8	120.9
9	161.5
10	243.2
11	325.6
12	408.6
13	492.3
14	576.6
15	747.5
16	921.2
17	1,098.0

The following products were generated and evaluated during this analysis:

- Vertical distributions of CO, NO_X, and VOC emissions, along with spatial plots of emissions densities at various levels;
- Vertical profiles of modeled wind and ozone compared to ozonesonde measurements;
- Aloft modeled ozone concentrations compared to aircraft observations;
- Modeled vertical cross-sections of ozone across Sublette County; and
- Spatial plots of ozone concentrations through 1,000-m AGL.

Select plots from the IOPs that summarize key results from the analysis are provided below.

3.6.1 Vertical Emissions Distribution

The vertical placement of emissions in the model is important as it dictates their exposure to different wind regimes and subsequent transport as well as modeled VOC/NO_X ratios that directly relate to local ozone formation. As a result, the vertical distribution of modeled CO, NO_X, and VOC emissions in the 1.33-km domain was evaluated. As shown in Section 4.4 and **Figure 4-11**, about 85 percent of the daily CO and NO_X emissions from combustion sources are injected in the 4 lowest model layers (up to 50-m AGL), while 95 percent of VOC emissions are injected into the lowest 3 model layers (up to 40-m AGL). **Figures 3-25** and **3-26** show sample spatial plots of NO_X and paraffin emissions at 25 to 40-m AGL (layer 3), and 250-m AGL (layer 10). These analyses confirm that the emission injection heights are reasonable and consistent with expectations, and that minimal emissions are being injected above the shallow boundary layers of the UGRB.

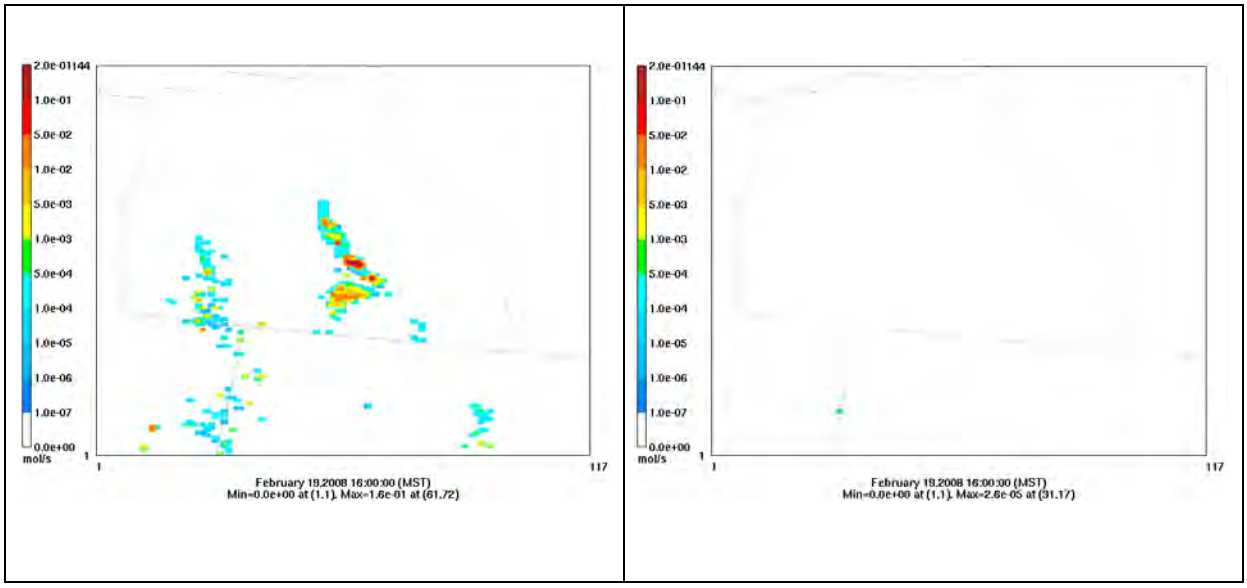

Figure 3-25 Spatial Plot of NO_x Emissions in Layer 3 (left) and Layer 10 (right) on February 19, 2008 at 1600 MST

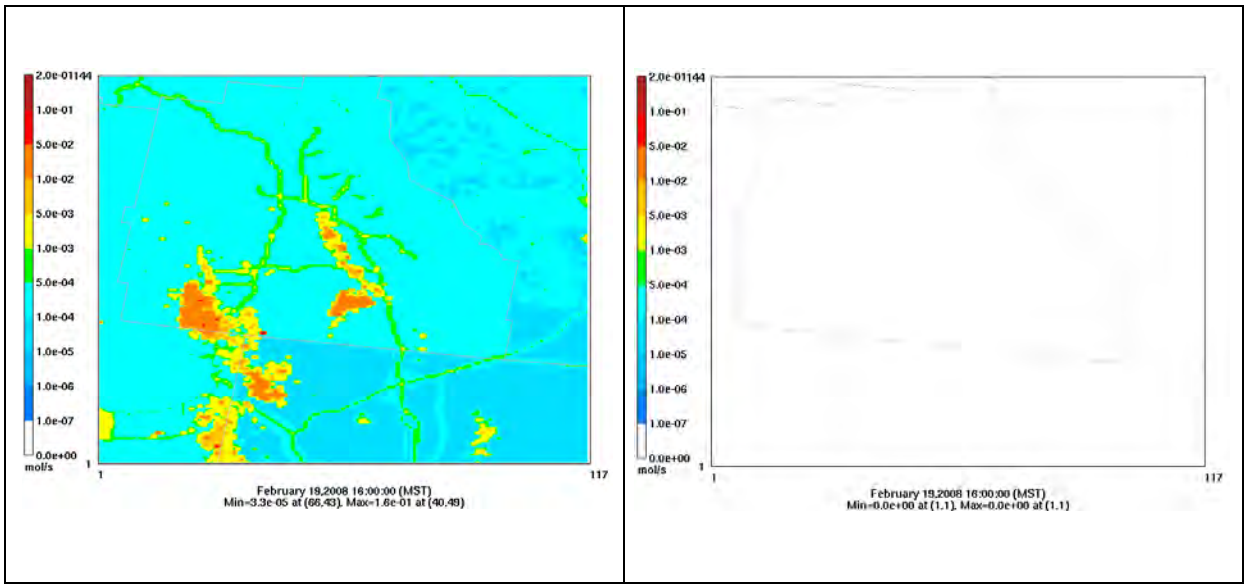

Figure 3-26 Spatial Plot of Paraffin VOC Emissions in Layer 3 (left) and Layer 10 (right) on February 19, 2008 at 1600 MST

3.6.2 Vertical Profiles

Figure 3-27 and **3-28** compare vertical profiles of observed and modeled ozone concentrations below 600-m AGL. The observed values were generated from ozonesondes released twice during the afternoon from the Pinedale airport during the first and second IOP. These observed values were plotted alongside vertical profiles of CAMx ozone concentrations for the same time and location. Profiles from the third IOP were also analyzed with similar conclusions, but are not shown here. Observed ozone production in the UGRB is typically confined to the lower layers due to the shallow mixing that results from wintertime cold pool conditions. During all three IOPs, CAMx consistently underpredicts ozone concentrations below 300-m AGL. Above 300-m AGL, the modeled ozone profiles agree well with the ozonesonde observations.

3.6.3 Vertical Cross-Sections

Vertical cross-sections of ozone, NO_X, CO, and xylene concentrations modeled by CAMx for the afternoon of February 20 are presented in **Figure 3-29**. These cross-sections follow a west-east transect through the Jonah monitoring site and extend across the entire 1.33-km modeling domain with the Jonah site located around the middle of the cross-section. The Jonah site was selected for analysis of vertical cross-sections due to the site's proximity to emissions sources and monitored levels of ozone during the IOPs. Because the vertical dimension is not plotted to scale, each plot has reference lines indicating the approximate position of 250-m (lower line) and 1,300-m AGL (higher line).

The cross-section plots show that the highest modeled concentrations of NO_X, CO, and xylene over the Jonah site are confined below 250-m AGL, suggesting that CAMx is mixing pollutants through a reasonably shallow boundary layer (likely no greater than 200 to 250 m). It is important to note that the high NO_X concentrations (upper left) over Jonah are coincident with the reduced ozone concentrations (lower right) due to titration shown in the ozone cross-section. Similar ozone reduction over Jonah in the vertical was seen during the second and third IOP (not shown).

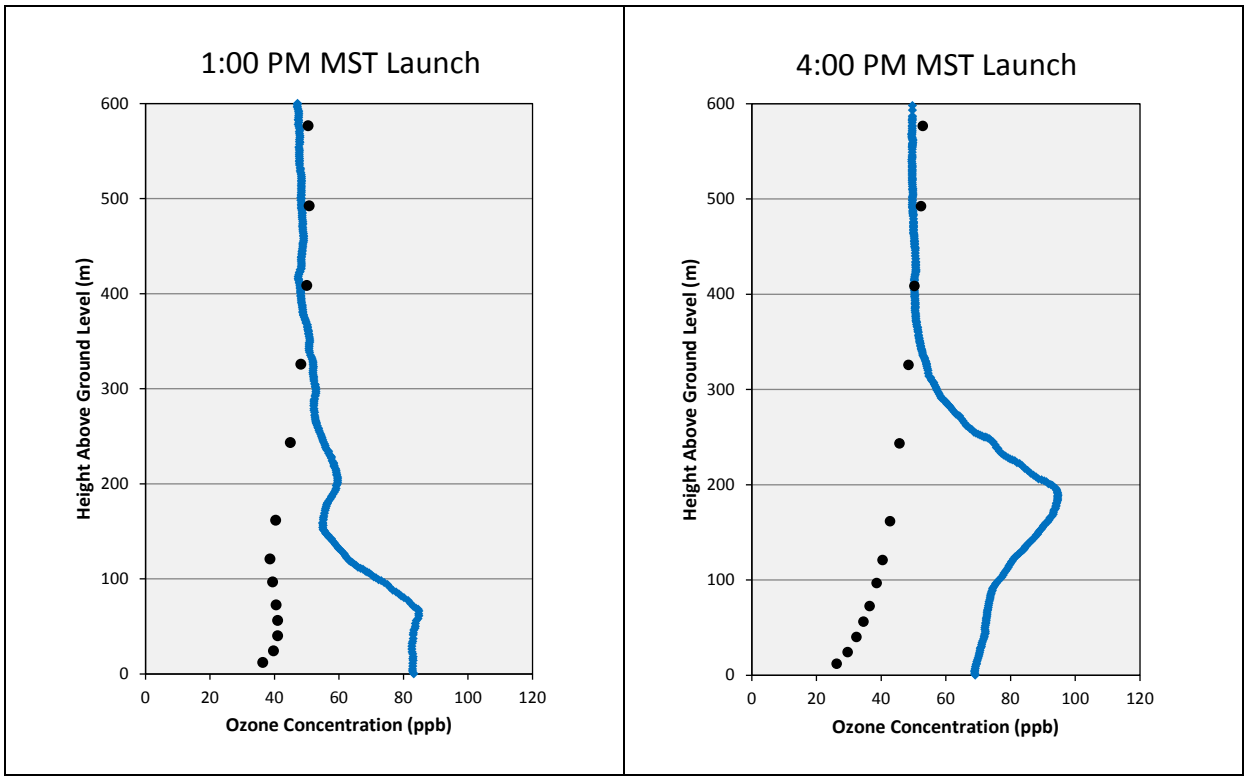

Figure 3-27 CAMx Modeled (black dots) and Observed Ozone Profiles (blue lines) at Pinedale Airport on February 20, 2008 at 1:00 PM (left) and 4:00 PM (right) MST

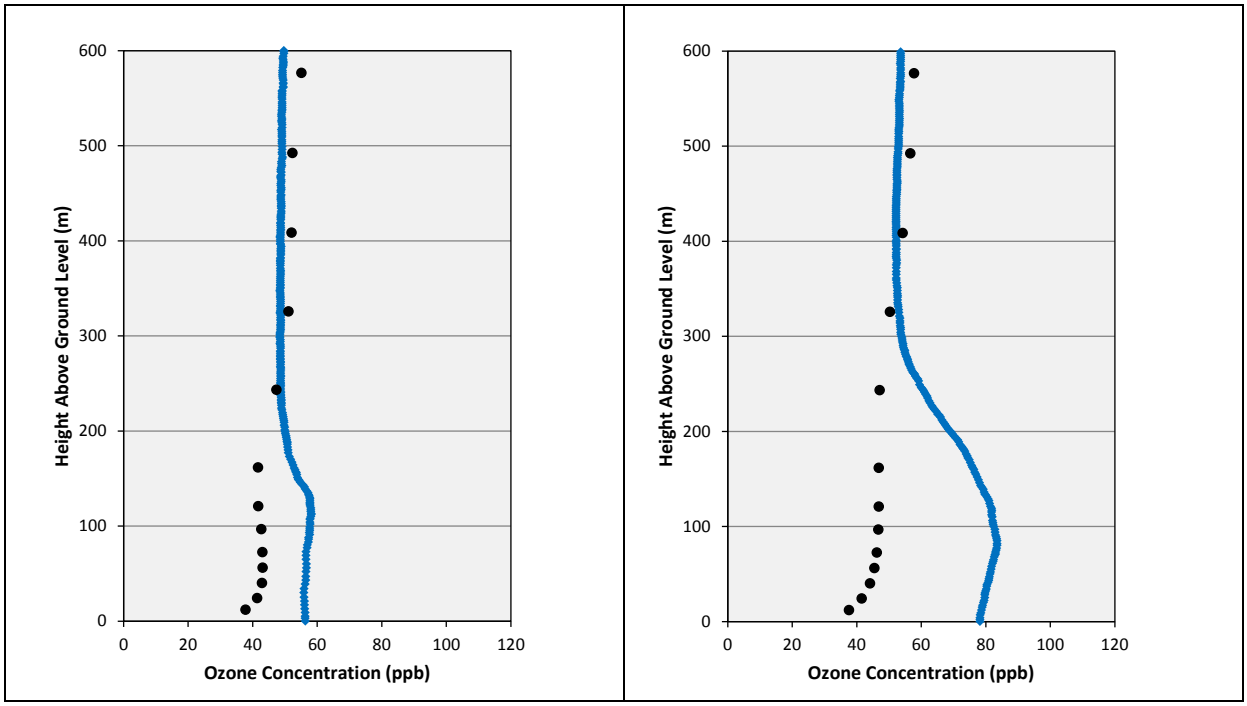

Figure 3-28 CAMx Modeled (black dots) and Observed (blue lines) Ozone Profiles at Pinedale Airport on February 29, 2008 at 1:00 PM (left) and 4:00 PM (right), MST

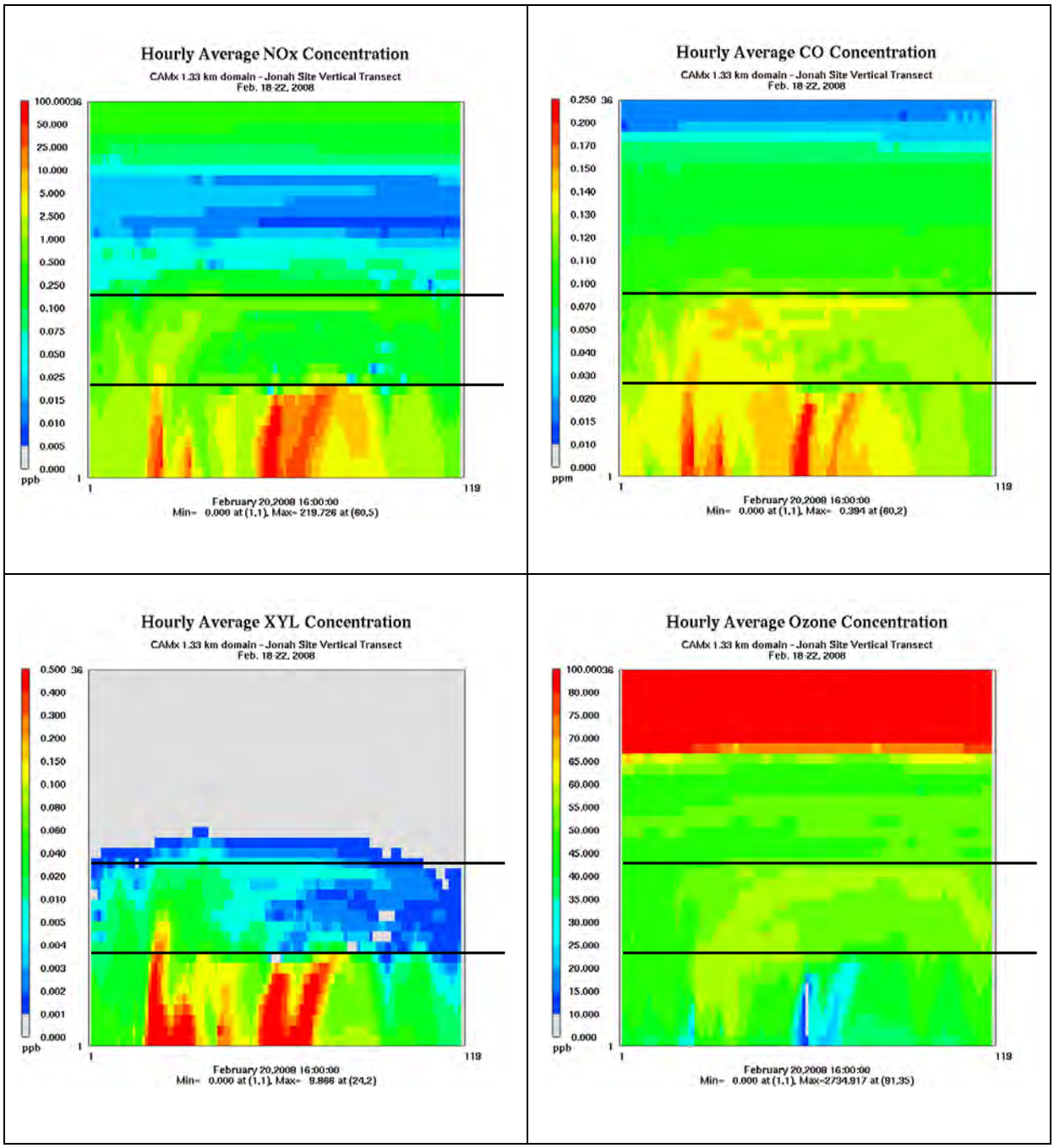

Figure 3-29 CAMx Vertical Cross-Sections of NO_x, CO, Xylene and O_3 on February 20, 2008 at 1600 MST Along a West-East Transect Taken Across the 1.33-km Modeling Domain Through Jonah. Black Reference Lines Indicate the Position of 250-m and 1,300-m AGL.

Midday mixing heights on February 20 calculated from the CAMx vertical diffusivity (**Figure 3-30**) are between 80- to 150-m and coincide reasonably well with the 100-m mixing height estimated from Sonic Detection and Ranging (SODAR) observations on this date during the UGWOS 2008 study. Based on the pollutant cross-sections in **Figure 3-29**, CAMx may be slightly overestimating the extent of mixing. It should be noted however, that mixing heights are not rigid lids and some vertical mixing will still occur across this boundary. Furthermore, pollutant concentrations between 100- and 250-m AGL are resolved by only three vertical layers; therefore, diffusion across two neighboring layers would change the apparent depth of mixing in the model by 50 m or more. Since CAMx largely confines pollutants within 250-m AGL during the IOPs, it is a positive indication that the vertical mixing processes in the model are reasonable.

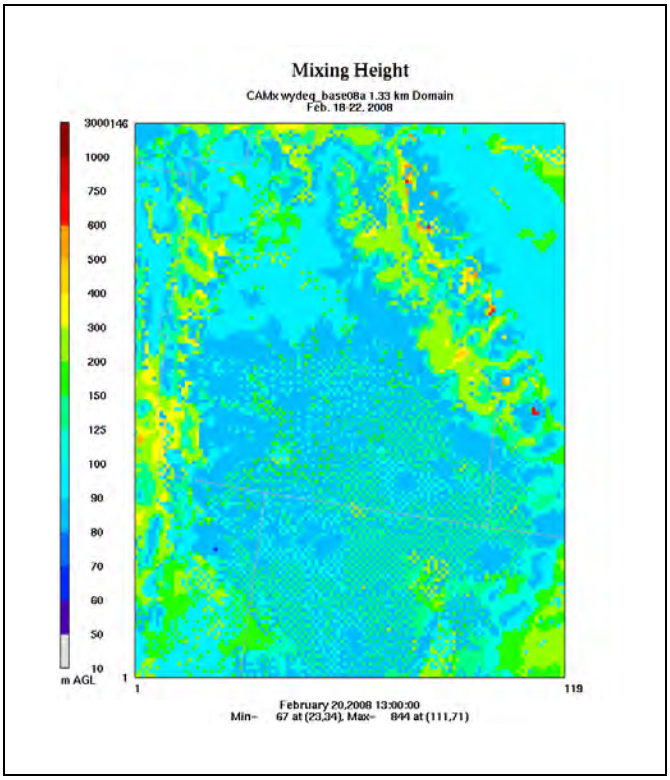

Figure 3-30 Mixing Heights Predicted by CAMx on the 1.33-km Domain on February 20, 2013 at 13:00 MST.

3.6.4 Vertical Spatial Plots

A series of spatial plots of modeled pollutant concentrations at various levels below 1-km AGL, overlaid with modeled wind vectors, were analyzed to provide a more refined understanding of the three-dimensional structure and movement of pollutants within the UGRB in the CAMx base case simulation. As an example, representative plots of modeled NO_X concentrations at 100-m and 250-m AGL (CAMx model layers 7 and 10, respectively) for February 20 at 1600 MST are shown in **Figure 3-31**. In this example, modeled winds within the UGRB at 100-m AGL are light and variable, and pollutants at this altitude will generally remain within the UGRB. At 250-m AGL, however, the modeled northwest wind is sufficiently strong to advect pollutants toward the southeast and out of the UGRB. Notably, NO_X concentrations at 250-m AGL are substantially lower than at 100-m AGL since most of the NO_X emissions are injected below 250-m AGL. Throughout the IOPs, modeled winds in the lowest 100-m AGL were typically light and variable, while modeled wind speeds above 250-m AGL were typically strong enough to remove pollutants from the UGRB. At night, a modeled northwest (down-valley)

low-level jet often formed above the nocturnal boundary layer. This modeled flow may be a combination of synoptic and terrain forcing, but the presence of this feature in observations has not been fully investigated. Overall, the aloft wind vector plots showed significant vertical wind shears but most of the emissions modeled from the local oil and gas activity are expected to remain within the UGRB due to their limited plume rise.

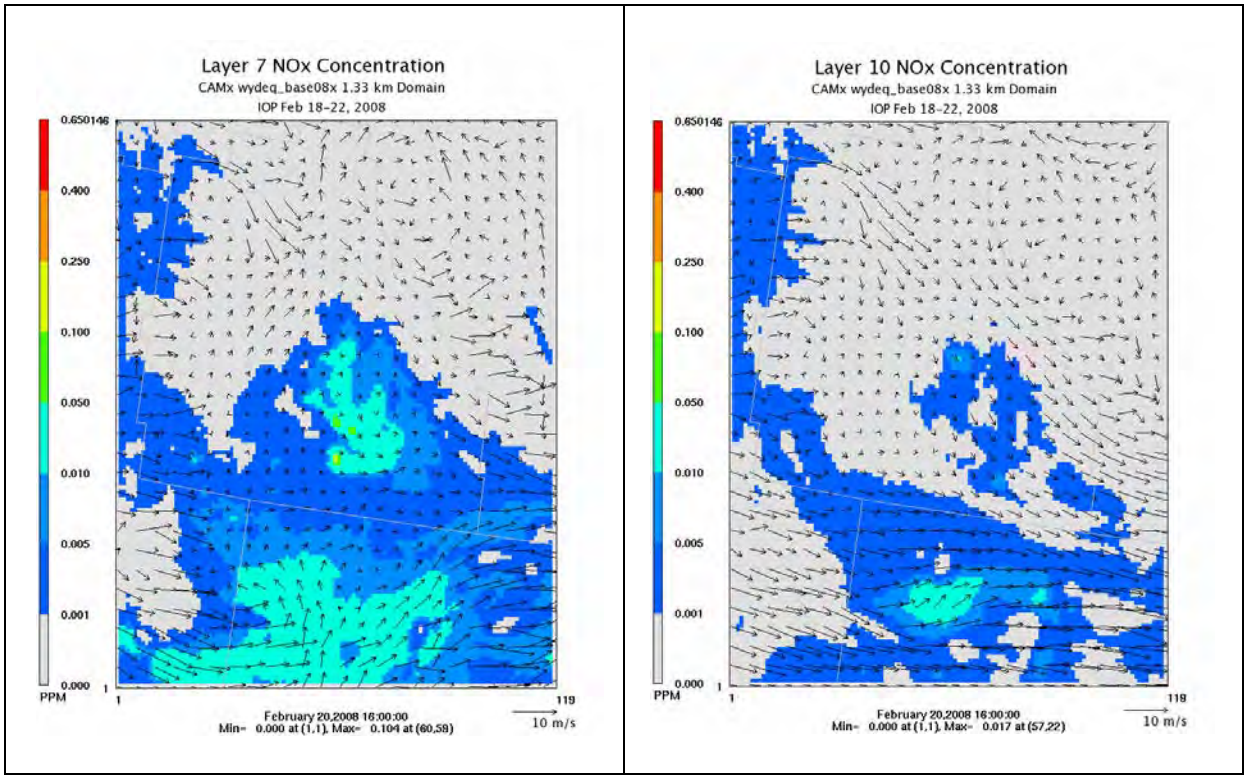

Figure 3-31 CAMx NO_x Concentrations at 100-m AGL (left) and 250-m AGL (right) Overlaid with Modeled Wind Vectors on February 20, 2008 at 1600 MST

Spatial plots of CAMx ozone concentrations above the surface were compared against aircraft measurements of ozone collected during the IOPs. The CAMx predictions were extracted at layer 7, or approximately 100-m AGL, which corresponds to the typical altitude of the long aircraft transects. **Figure 3-32** shows this comparison on the afternoon of February 20, during the first IOP. The aircraft observations show two regions of enhanced ozone with concentrations in excess of 100 ppb: one in southern Sublette County southwest of Jonah, and a second larger region in central Sublette County to the south of Boulder and Daniel. The corresponding CAMx spatial plot suggests that no significant ozone production was modeled in Sublette County (maximum value less than 60 ppb). In and around the Jonah oil and gas development region, CAMx actually predicts ozone concentrations that are lower than the surrounding areas, which is the result of ozone titration by the NO_X sources in that area. Modeled winds below 100-m AGL during this event were light and variable (see **Figure 3-32**), and therefore any modeled pollutants emitted or created below 100-m AGL within the UGRB would likely remain within the Basin.

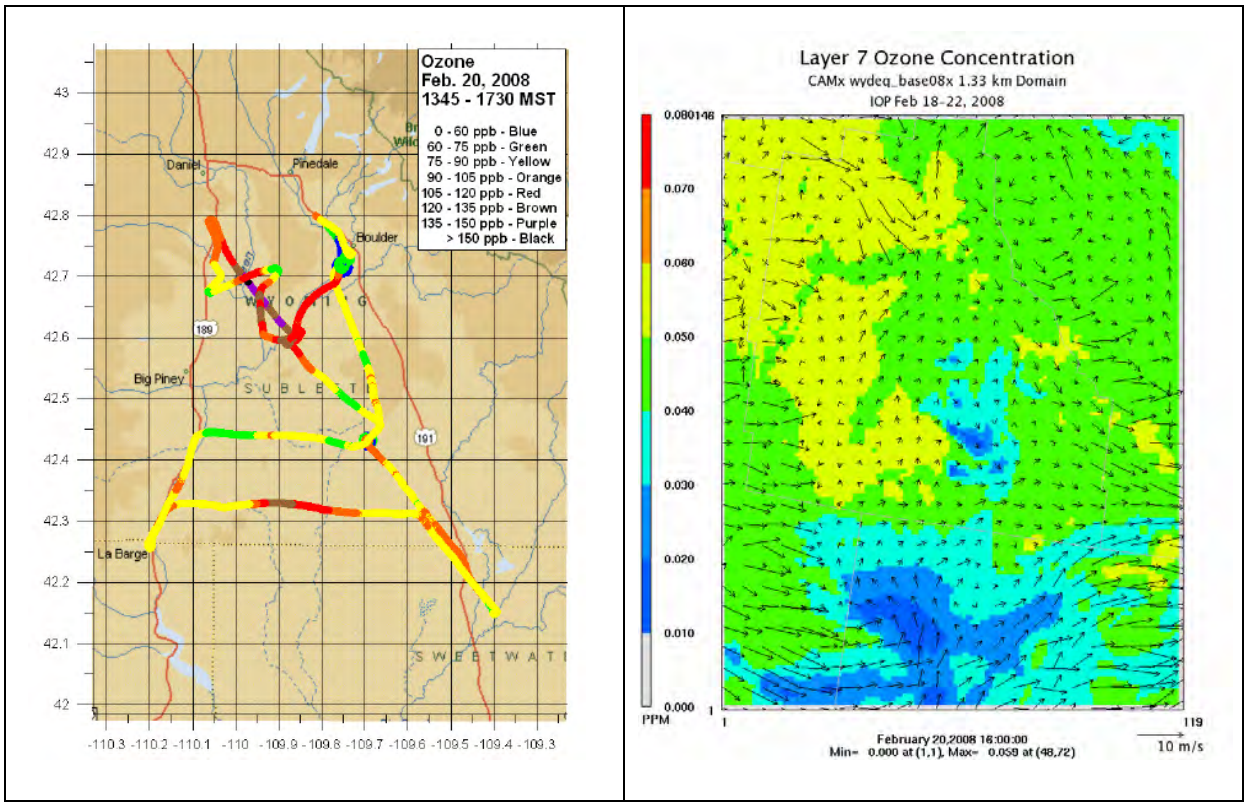

Figure 3-32 Ozone Concentrations from Aircraft Observations (left) and CAMx Predictions at Layer 7 (right) During the Afternoon of February 20, 2008. Modeled Wind Vectors at Layer 7 are Overlaid on the CAMx Ozone Plot. Note the Different Spatial Scales Between the Plots

Figure 3-33 provides a similar comparison with aircraft observations of ozone during IOP 3, on March 11 1600 MST, and modeled ozone concentrations and wind vectors at 100-m AGL (layer 7). During IOP 3, ozone concentrations in excess of 90 ppb were observed across large areas of Sublette County, with concentrations above 150 ppb observed northeast of Jonah. As in IOP 1 (**Figure 3-32**) and IOP 2 (not shown), CAMx did not produce any significant ozone in the UGRB. During the afternoon hours, 100-m AGL winds were light and variable in the east side of the Basin. Earlier that morning, although CAMx winds at the surface were light and variable, CAMx predicted moderate northwest winds across the entire Basin at 100-m AGL. The observational data are insufficient to determine whether the modeled morning winds at this altitude are correct.

Figure 3-34 shows the NO_X concentrations at the surface and 100-m AGL at 0800 on March 11. The modeled winds within the UGRB at the surface are light and variable, and pollutants mostly remain within the UGRB. At 100-m AGL, the modeled northwest wind is sufficiently strong to advect pollutants toward the southeast and out of the UGRB.

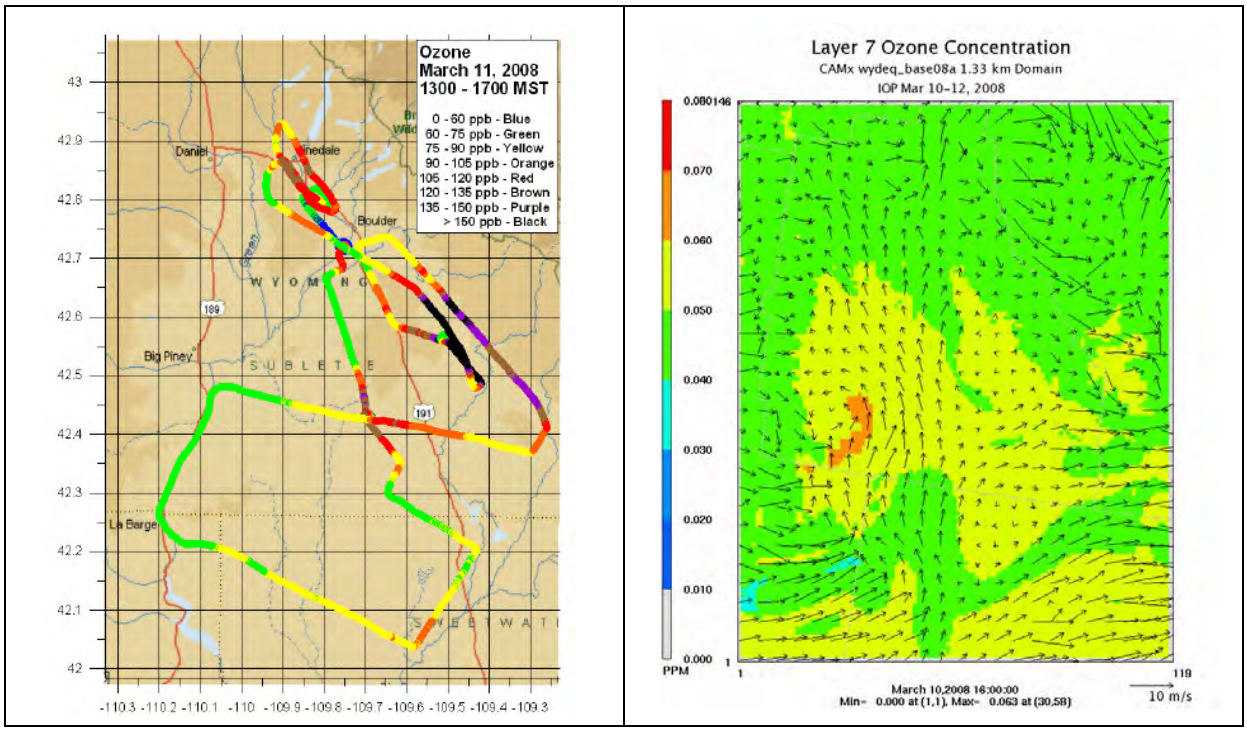

Figure 3-33 Ozone Concentrations from Aircraft Observations (left) and CAMx Predictions at Layer 7 (right) During the Afternoon of March 11, 2008. Modeled Wind Vectors at Layer 7 are Overlaid on the CAMx Ozone Plot. Note the Different Spatial Scales Between the Plots

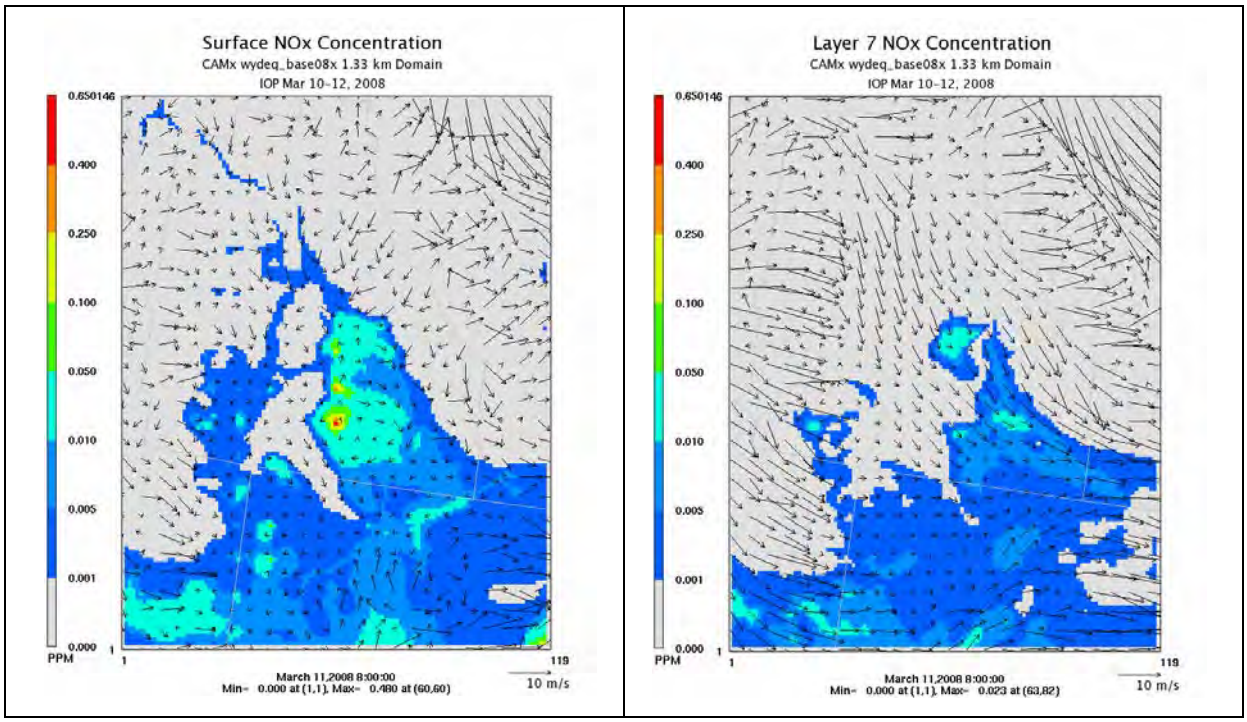

Figure 3-34 CAMx NO_x Concentrations at the Surface (left) and 100-m AGL (right) Overlaid with Modeled Wind Vectors on March 11, 2008 at 0800 MST

3.6.5 Vertical Analyses Findings

- The vertical distribution of modeled precursor emissions from oil and gas sources varies by pollutant, but all pollutants are emitted primarily in the lowest 4 model layers (below 50-m AGL) as expected.
- The ozone model concentrations in the vertical compare well to ozonesonde observations above 300-m AGL, but poorly below it.
- Very little local ozone is produced in the vicinity of oil and gas emission sources at any level above the ground in the UGRB. Ozone depletion is evident over the oil and gas development regions as a result of titration from fresh NO_X plumes.
- The spatial distribution and magnitude of modeled ozone within the mixed layer does not match that observed in the aircraft transects.
- WRF predicts vertical wind shears in the UGRB and significant spatial and temporal variability in winds throughout the UGRB.
- WRF frequently predicts moderate northwest (down-valley) winds at 50 to 250-m AGL during the night and morning hours. This flow may be a combination of synoptic and terrain forcing.
- CAMx mixing heights in the UGRB are typically less than 200-m AGL during the IOPs, suggesting that vertical mixing is weak as expected.

4.0 Sensitivity Runs

4.1 Introduction

This chapter presents the results of a series of sensitivity simulations that were explored in order to improve and optimize the base case modeling described in Chapter 3.0. The tests were only simulated for the first IOP (February 18 to 22) using CMAQ because its one-way nesting methodology allows simulations of only one computational grid (1.33km) at a time without the need to run coarser ones. This approach provides a computationally efficient way to run multiple sensitivities. Three sensitivity tests described in more detail below provided opportunities to investigate model response to several aspects of the CMAQ modeling. These tests include:

- A change to CMAQ version 5.0 to fix albedo over snow covered surfaces;
- The introduction of a pseudo-HONO source in an attempt to match the observed HONO diurnal concentrations; and
- A test of model sensitivity to plume heights.

The results of these sensitivity tests are assessed at the Boulder, Jonah and Daniel sites since these sites would derive the most benefit from improved model performance.

4.2 CMAQ Albedo Test

4.2.1 Albedo Test Background

The in-line photolysis module in CMAQ version 5.0 was originally updated to adjust the surface albedo based on land-use type and time-varying snow/ice coverage. However, Gail Tonnesen with USEPA Region 8 found that the largest albedo and photolysis rate enhancement occurred almost exclusively over the regions set as “sea ice”; while for any other regions covered by snow the enhancement was very limited. It is expected that for Wyoming the areas covered by snow are significantly larger than those set as “sea ice” and therefore the effect of the in-line photolysis module was originally under-estimated.

As discussed in Chapter 2.0, these limitations to the original CMAQ version 5.0 were identified by USEPA Region 8, who provided updated CMAQ codes, an albedo patch that uses an alternative treatment of surface albedo in snow cover areas. The update modifies the in-line albedo calculation to set the albedo to 0.85 times the fractional snow cover. The purpose of the CMAQ albedo test described below is to identify the differences between the original CMAQ v5.0 code and the revised version with the albedo patch. Both versions of CMAQ were run through the first IOP with the same inputs (emissions and meteorology) and configuration settings with the exception of the patched in-line photolysis described above.

4.2.2 Albedo Test Analyses

Time series comparisons at Boulder, Jonah, and Daniel for both ozone and NO_X modeled concentrations and observations are presented in **Figures 4-1** and **4-2**, respectively. **Figure 4-1** shows that the ozone concentrations from the revised code are systematically higher relative to CMAQ v5.0, especially during the daylight hours and in the days when peak ozone occurs (February 19 to 21). This is the result of increased photolysis rates due to enhanced albedo on snow covered areas in the revised in-line photolysis module in CMAQ. However, this enhancement is not enough to place the modeling results at similar levels to observed ozone concentrations. While the increased photolysis increases ozone formation in the model, there is some increased NO_X destruction relative to CMAQ v5.0, which is shown in **Figure 4-2**.

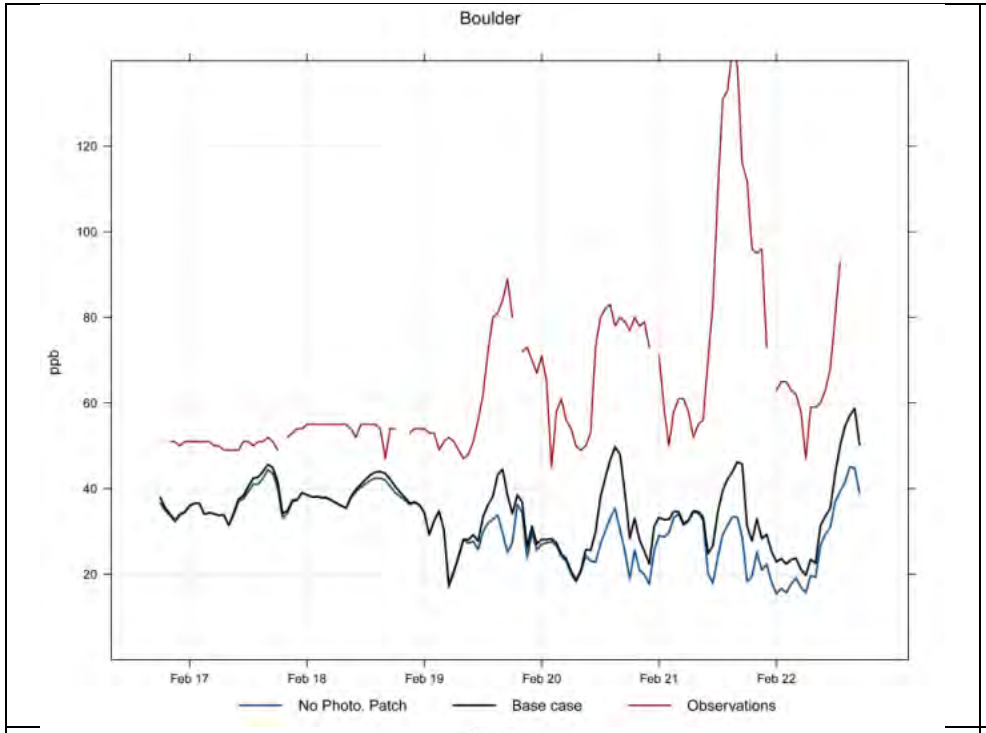

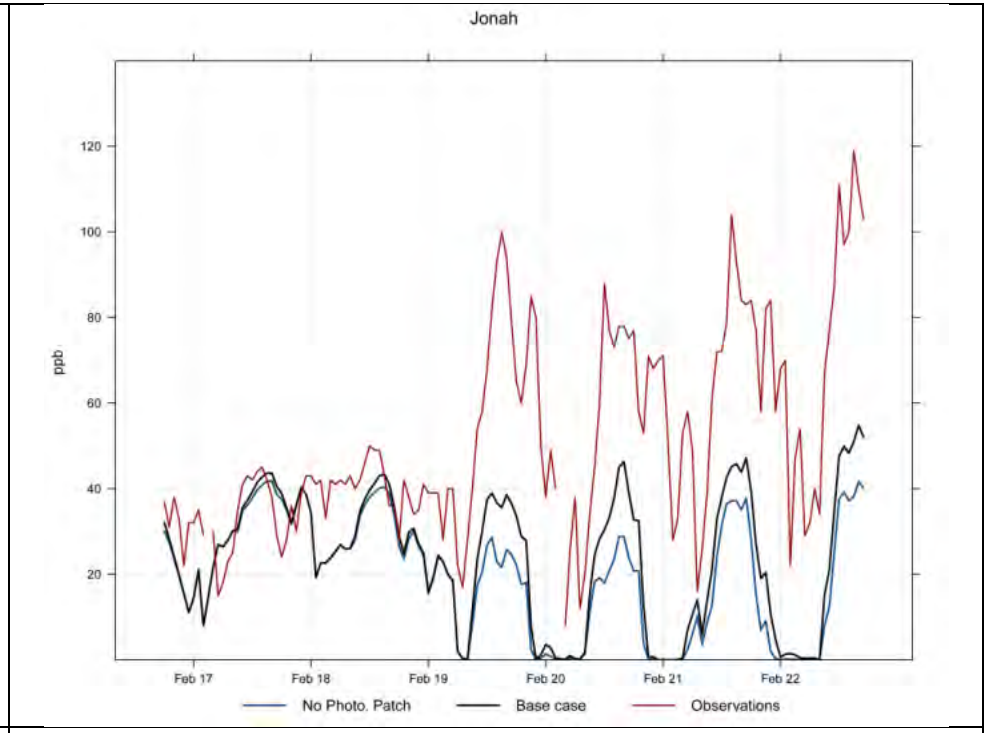

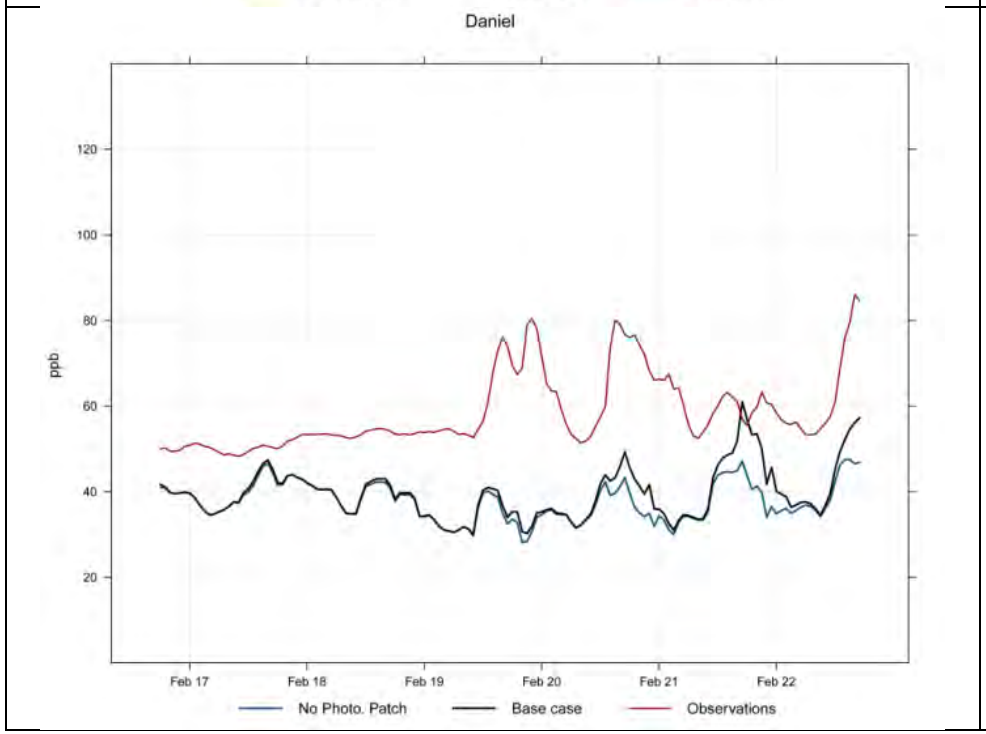

Figure 4-1 Time Series Comparison of Ozone Concentrations Between Original CMAQ Version 5.0 (blue), the Updated in-line Photolysis Module CMAQ (black) and observations (red).

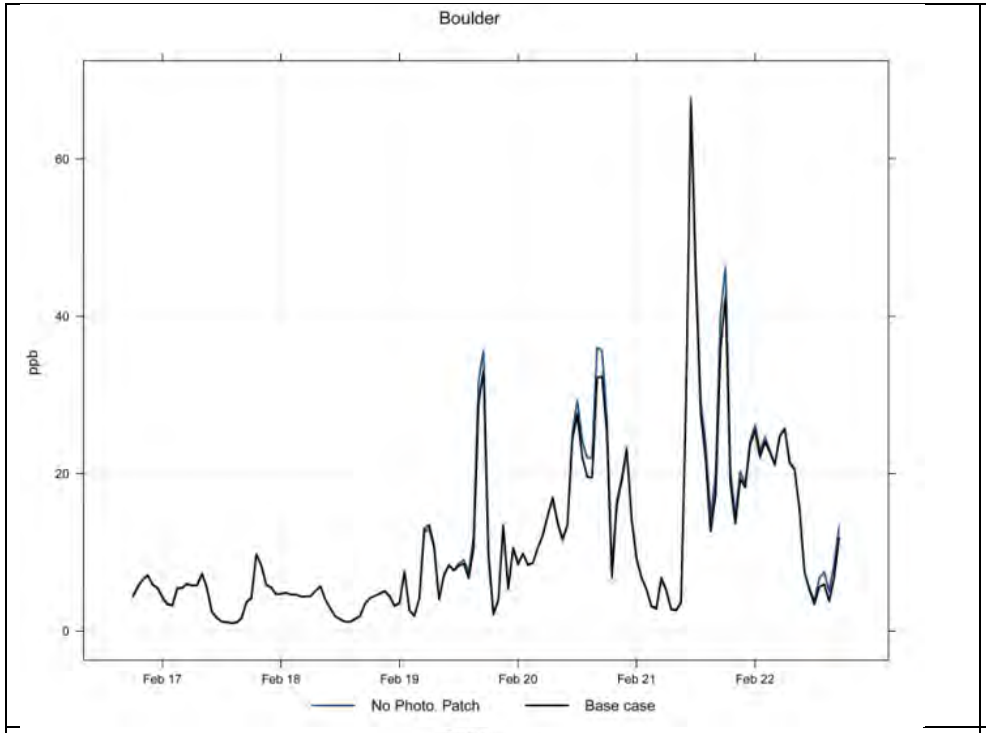

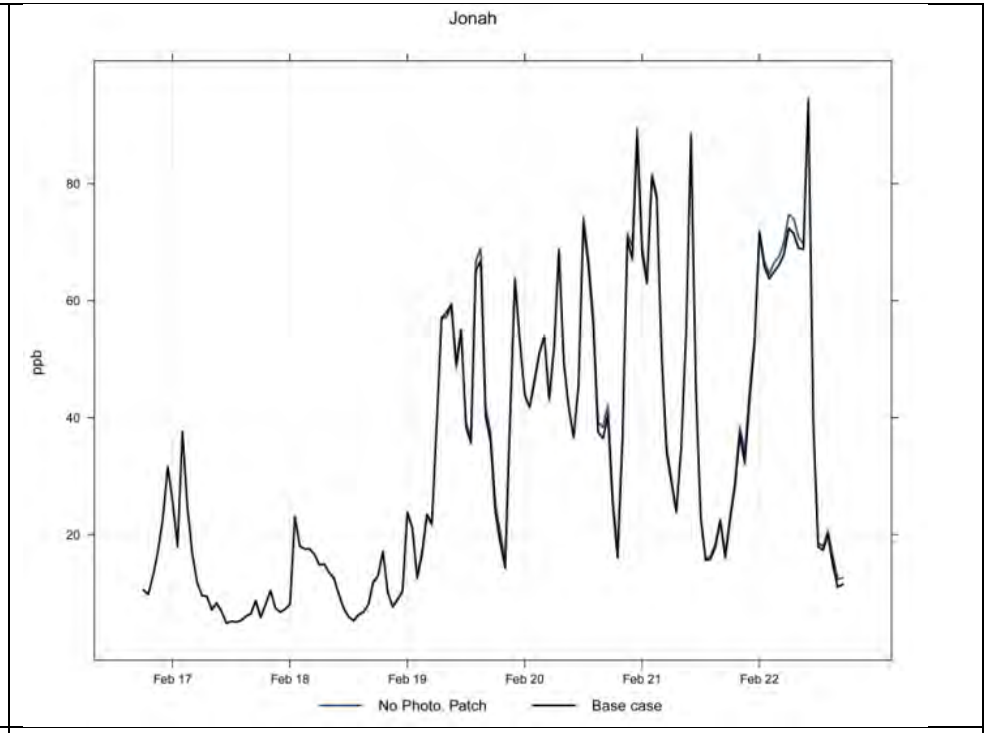

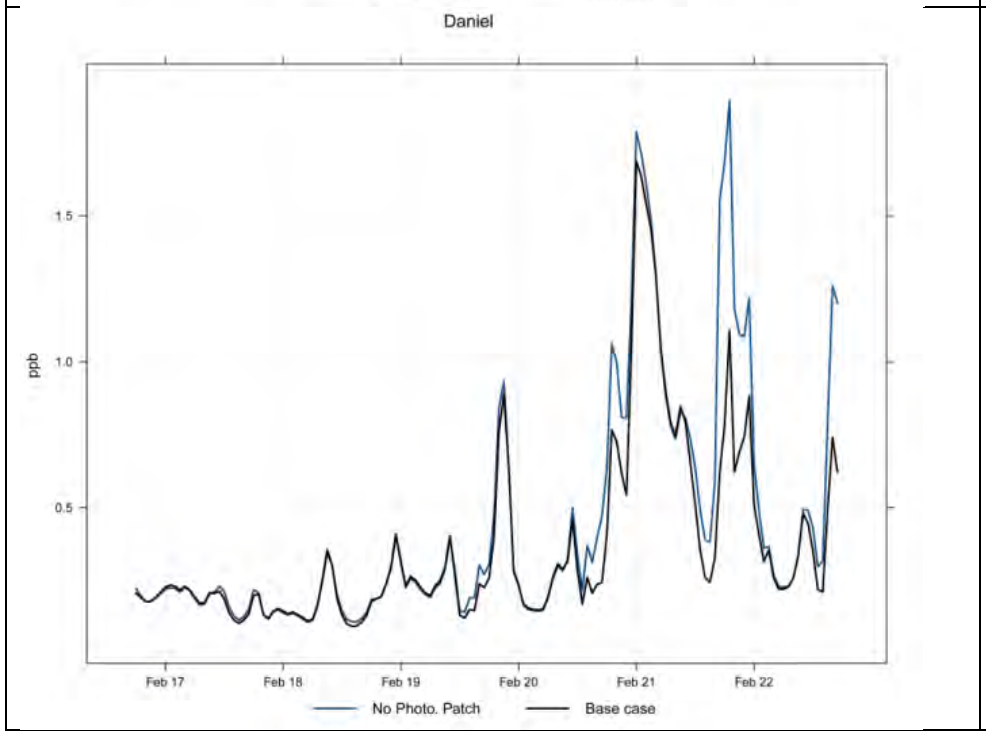

Figure 4-2 Time Series Comparison of NO_x Concentrations Between Original CMAQ Version 5.0 (blue) and the Updated in-line Photolysis Module CMAQ (black).

Figure 4-3 presents ozone spatial plots for February 21 at 0800 and 1600 MST. The figure compares the base case (with the albedo patch) to the default CMAQ version (no albedo patch) and also shows the differences spatially. During hours with low photochemical activity (0800) both versions of the model have ozone concentrations generally low (ranging from 10 to 40 ppb) with the small differences shown in the difference plot likely due to the cumulative effect of the enhanced photolysis over time. At hour 16:00 when there is active photochemistry in the area the spatial patterns change substantially between the two model versions. The distribution of ozone in the base case with enhanced photolysis shows a significant increase in concentrations exceeding 60 ppb in the southwestern region to the central part of the 1.33-km domain with a maximum domain-wide concentration of 75 ppb. In contrast, the default version shows that the maximum concentrations occur in the western side of the domain and they range from 40 to 50 ppb with a domain-wide maximum of 54 ppb. The difference plot emphasizes the fact that the default CMAQ version results in domain-wide lower ozone concentrations relative to the base case. The enhancement in the base case ozone is significant with large areas showing increases in ozone up to 20 ppb with a maximum change of 28 ppb.

4.2.3 Albedo Test Findings

- Time series comparisons at Boulder, Jonah, and Daniel shows that increased photolysis rates due to enhanced albedo on snow covered areas in the revised CMAQ in-line photolysis module lead to systematically higher ozone concentrations relative to the original CMAQ v5.0, especially during the daylight hours and in the days when peak ozone occurs.
- Spatial plots show that when there is active photochemistry (late afternoon) ozone concentrations experience a significant increase exceeding 60 ppb in the southwestern region to the central part of the 1.33-km domain. In contrast, the default version shows that the maximum concentrations occur in the western side of the domain and they only range from 40 to 50 ppb. Difference plots show that the revised CMAQ is able to produce an additional 28 ppb of ozone relative to the CMAQ v5.0 version.
- As a result of these analyses, the CMAQ version with the albedo patch was used in the base case modeling.

4.3 HONO Test

4.3.1 HONO Test Background

HONO, which is usually present during the nighttime hours in urban atmospheres, can be rapidly photolyzed during the daytime hours to yield hydroxyl (OH) radicals. The photodissociation of HONO can be a significant source of OH radicals before other sources become dominant and therefore a significant driver for enhanced ozone production. Surface chemistry may have important implications for ozone episodes during the winter, influencing both the chemical composition and vertical concentration profiles of precursor emissions. One of the prominent reactions is the photolysis of nitrate, which leads to the formation of OH radicals in the snow and to the release of reactive nitrogen compounds, like nitrogen oxides (NO and NO_2) and HONO to the atmosphere (shown in Equation 4-1). Observations in the Pinedale area show high HONO concentrations concurrent with the onset of ozone events during wintertime. In addition, recent modeling by USEPA Region 8 has shown a significant increase in ground-level ozone during the winter when HONO is explicitly modeled (Tonnesen 2013) in the West. It is thought that heterogeneous reactions[8] on the snow surface may lead to production of HONO (Honrath et al. 2002; Amorosa et al. 2006). To evaluate the effects of a HONO emissions source derived from the

[8] Heterogeneous reactions are a class of chemical reactions in which the reactants are in two or more phases (solid and liquid, gas and solid, etc) or in which one or more reactants undergo chemical change at an interface. In the context of this study the chemical reactions might be occurring in the interface gas/solid formed between the atmosphere and the snow covered surfaces.

snowpack, sensitivity runs with CMAQ were performed to include an area source of HONO emissions covering the 1.33-km domain.

$$NO_3^- \xrightarrow{h\nu} NO_2(g) + O^-$$
$$NO_3^- \xrightarrow{h\nu} NO_2^- + O(^3P) \xrightarrow{H^+} HONO(g)$$

Equation 4-1

4.3.2 HONO Emissions Preparation

During the 2011 Upper Green Winter Ozone Study (UGWOS), continuous HONO measurements were collected at the Boulder site from January 11, 2011 until March 31, 2011, though data was lost for a 2 week period in mid-February due to a power outage that damaged electronic units in the HONO instrument (ENVIRON et al. 2011). It was found that HONO measurements typically peaked near midday at around 0.5 ppb, though peaks occasionally reached the 1.5 to 2 ppb range, as shown in **Figure 4-4**. For the HONO sensitivity test, and with input from USEPA Region 8, a HONO emissions source for the 1.33-km modeling domain was created with the goal of replicating the magnitude and timing of these measured peaks.

Hour (MST)	Base Case	Default Version	Difference (Default – Base)
08	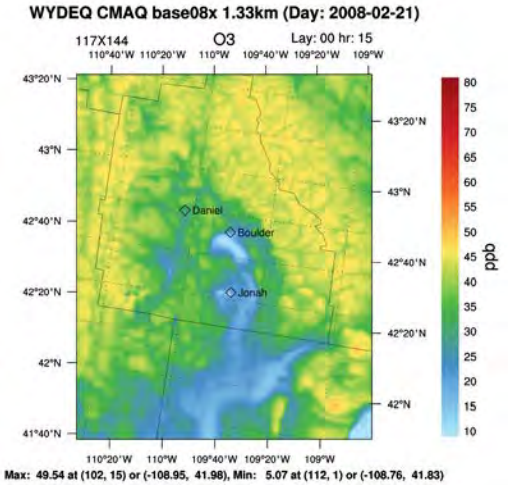	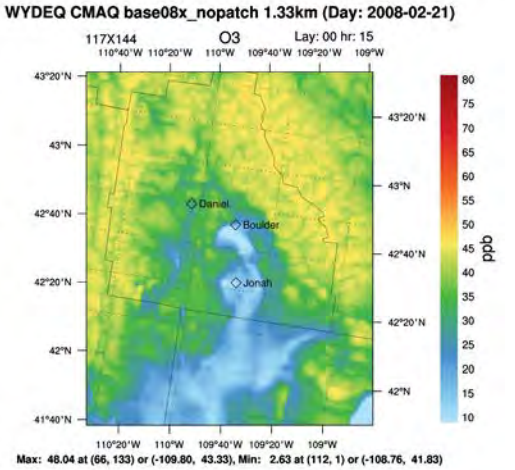	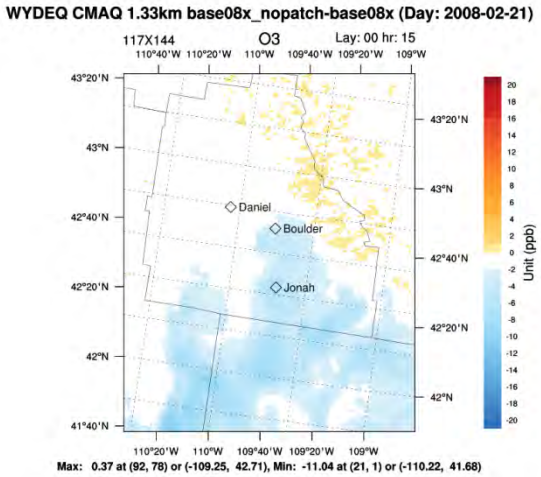
16	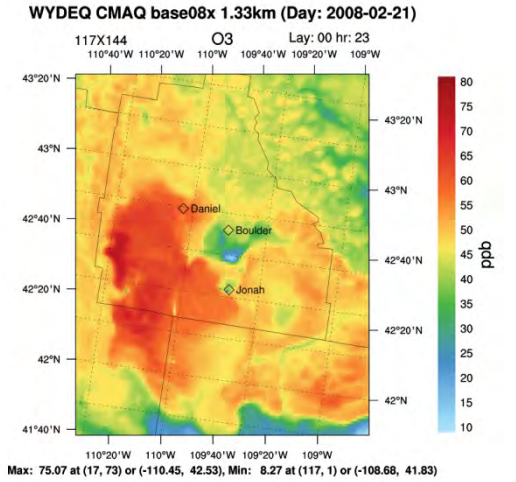	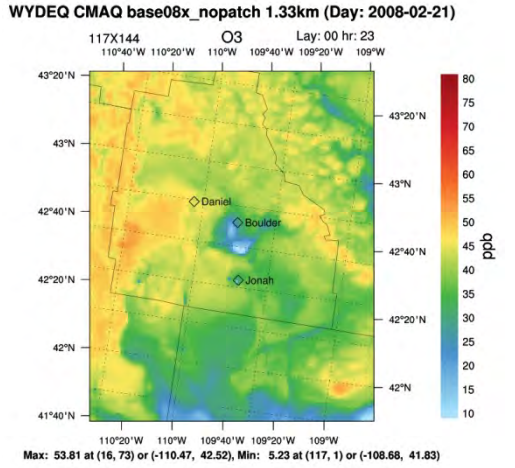	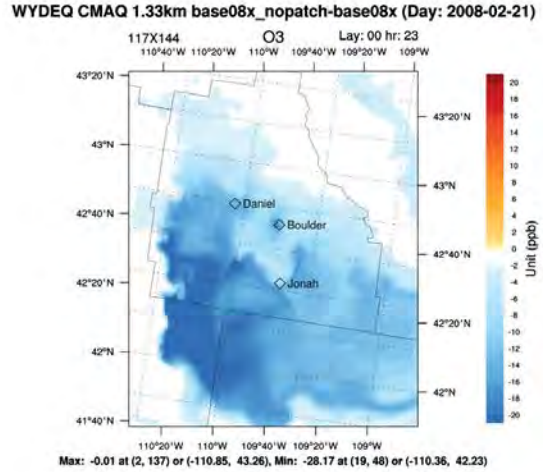

Figure 4-3 Spatial Plots of CMAQ Near-Surface Ozone Concentration from the 1.33-km Domain at 0800 and 1600 MST on February 21 2008. From Left to Right: Base Case with Updated Photolysis Module, Default Version Without Updated Photolysis, Difference Between Both Cases (Default Case Minus Base Case)

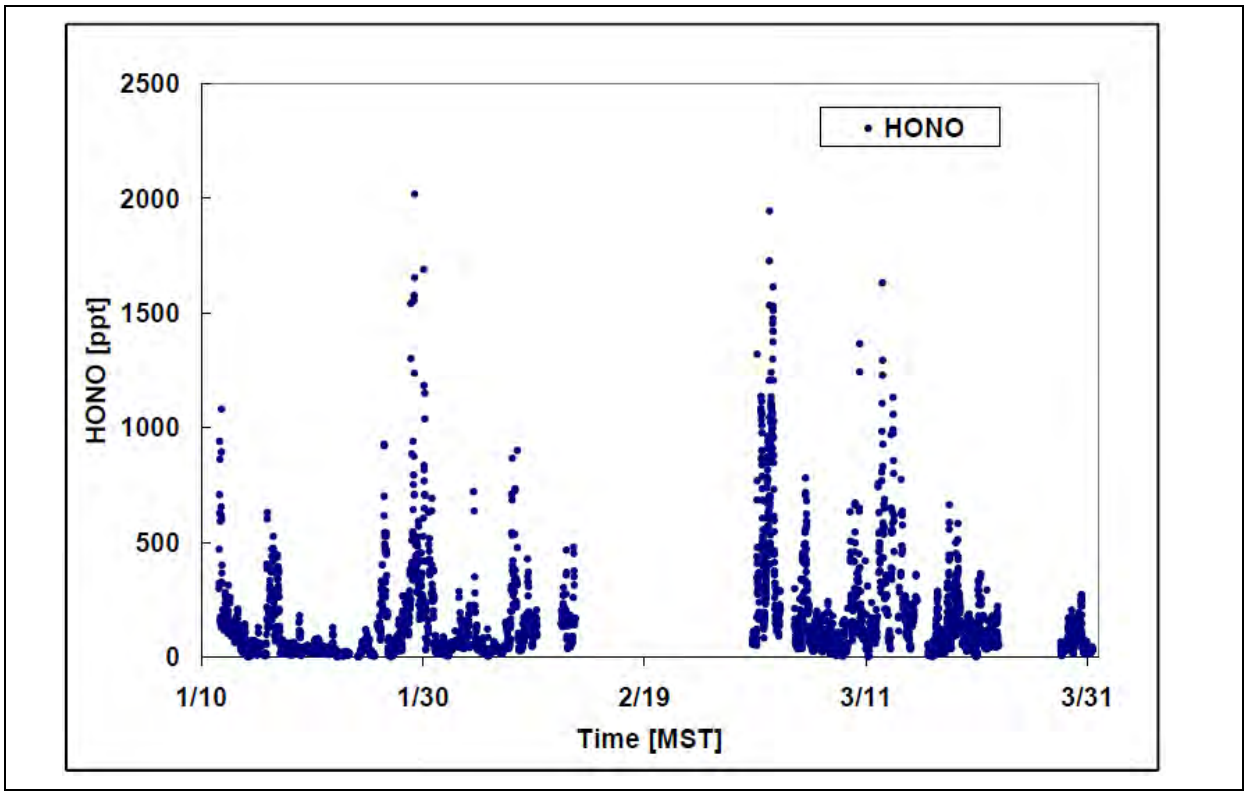

Figure 4-4 Time Series Plot of 10-minute HONO Data for January 11 – March 31, 2011 (ENVIRON et al. 2011)

Prior to this sensitivity test, the emissions inventory prepared for the base case modeling included small amounts of HONO emissions, primarily from oil and gas-related sources. In the oil and gas inventories provided by WDEQ, it was assumed that 3 percent of NO_X emissions from combustion sources were emitted as HONO, resulting in total HONO emissions of about 0.7 tons per day (tpd) across the 1.33-km modeling domain. The HONO emissions were concentrated in oil and gas development areas and HONO emission rates varied little temporally.

Upon analysis of the base case modeling results, it was found that peak HONO concentrations at the Boulder site were similar in magnitude to observed concentrations (i.e., typically 1 to 2 ppb) during periods with elevated ozone levels; however the timing was anti-correlated. The modeled HONO concentrations from the base case were highest at night and fell to very low levels (< 0.1 ppb) during the midday hours when observed HONO concentrations were highest.

At the suggestion of Gail Tonnesen with USEPA Region 8, an initial test run set the domain-wide HONO emissions source to a value 20 times higher than the total HONO emissions in the base case modeling (0.7 tpd) during both day and night (an emission rate of 14 tpd). After this initial simulation and in consultation with WDEQ and USEPA Region 8, a second sensitivity simulation set the domain-wide HONO emissions source to a value 20 times higher than the total HONO emissions in the base case modeling during the night and a value of 50 times higher than the original HONO emissions in the base case modeling during the day (an emission rate of 35 tpd). The increase during the day was intended to sustain elevated HONO concentrations during periods of active photochemistry. The results of this sensitivity simulation are described in Section 4.3.3. A comparison exploring the model results differences between these emission scenarios is presented in Section 4.3.4.

To spatially and temporally allocate HONO emissions in SMOKE, a new spatial surrogate was prepared that evenly distributed total HONO emissions across all grid cells in the 1.33-km modeling domain. A diurnal profile for the new source was prepared by averaging hourly HONO observations for high ozone episodes during the winter of 2011 and calculating hourly temporal allocation factors that fit the observed HONO concentration variations. **Figure 4-5** shows the shape of the modeled, diurnal profile derived from HONO measurement data.

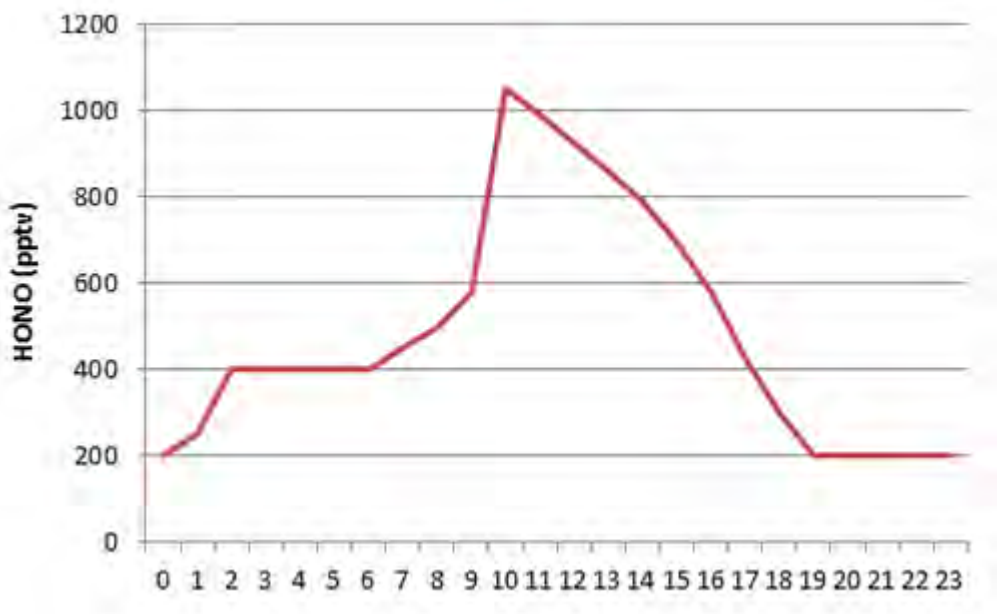

Figure 4-5 Diurnal Profile Developed for HONO Emissions from the Snowpack

4.3.3 HONO Test Analyses

As mentioned above, this section presents the modeling results when the domain-wide HONO emissions are increased 20 times the base case values during the nighttime and 50 times during the daytime. **Figure 4-6** shows the effects of the additional HONO emissions on ozone concentrations at Boulder, Jonah and Daniel. This figure shows that ozone increases relative to the base case but in most cases this enhancement is modest with the most pronounced change at the Daniel site. Although the resulting ozone concentrations are closer to observations, they still show a systematic negative bias, particularly when the largest ozone peaks are observed. **Figure 4-7** compares HONO concentrations between the base case and the HO

NO test. At all sites the HONO concentrations increase, but the most noticeable difference is at Daniel, which it is not in close proximity to major NO_X sources (the source of HONO in the base case modeling). Nevertheless, all sites have higher HONO concentrations as a result of the additional HONO pseudo-source.

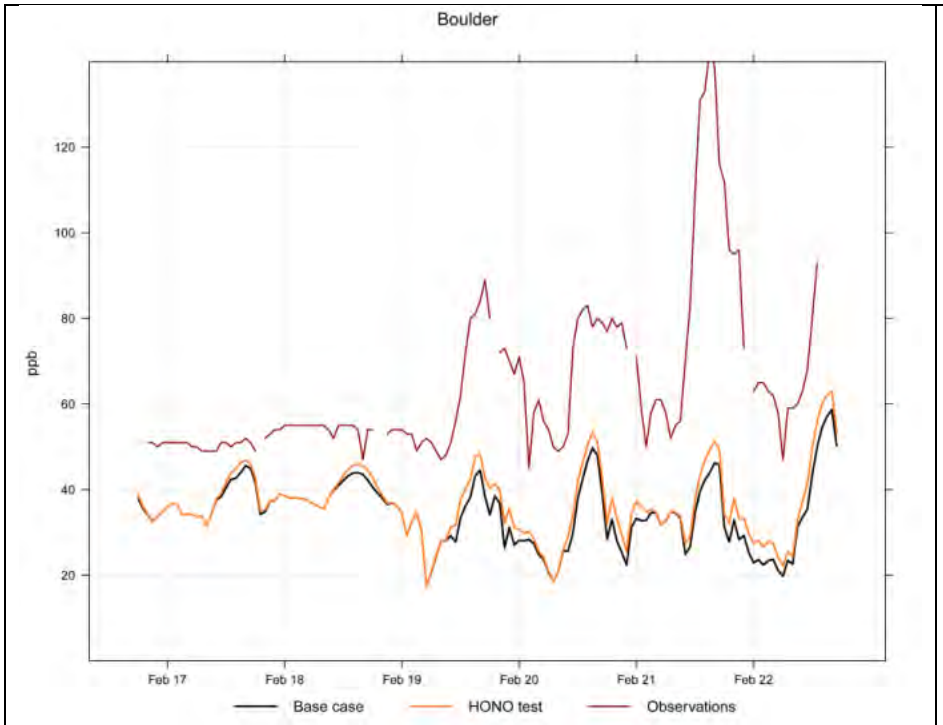

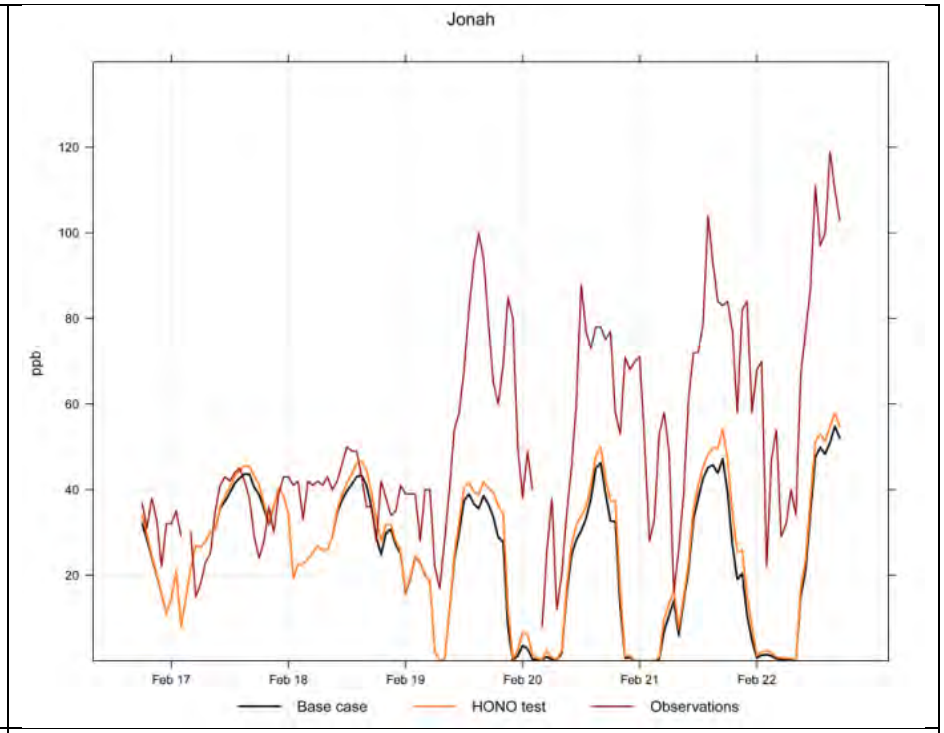

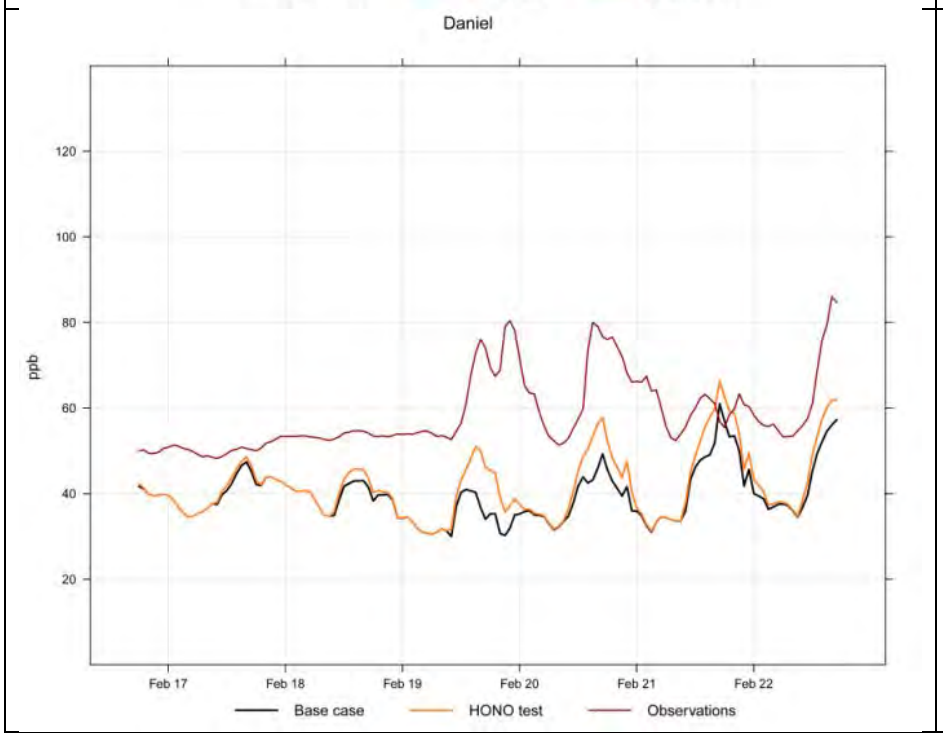

Figure 4-6 Time Series Comparison of CMAQ Ozone Concentrations Between the Base Case (black) ,the HONO Emissions Test Simulations (orange) and Observations (red).

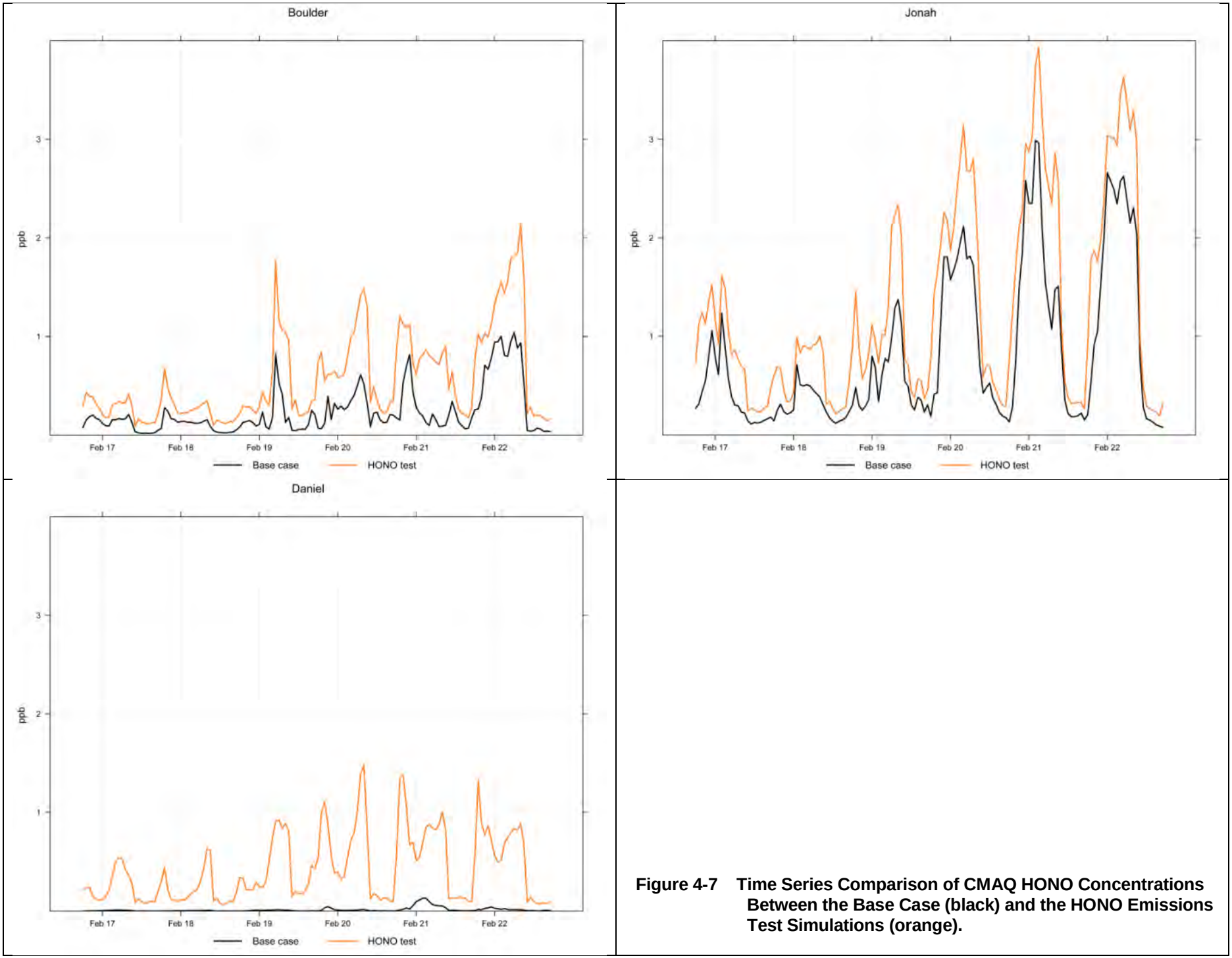

Figure 4-7 Time Series Comparison of CMAQ HONO Concentrations Between the Base Case (black) and the HONO Emissions Test Simulations (orange).

In order to investigate the diurnal variation in modeled HONO concentrations and assess if the model is able to reproduce the observed midday peak, all hourly concentrations for all days were averaged during the first IOP. **Figure 4-8** shows the average, along with the 95 percent confidence interval, diurnal variation of HONO concentration for each hour of the day. For all sites and both the base case and the HONO test, modeled HONO concentrations are the largest at night and during the first hours of the morning then rapidly decreasing at around 0800 or 0900 MST remaining at their lowest concentrations during the daylight hours (between 1000 and 1700 MST) and then starting to increase again around 1800 MST. These results only confirm that the model is not able to produce or sustain any large HONO concentrations during the daytime hours.

Figure 4-9 presents ozone spatial plots for February 21 at 0800 and 1600 MST. The figure compares the base case to the HONO test results and also shows their difference. In the morning when there is low photochemical activity both the base case and the HONO test show low concentrations in very similar spatial patterns; however the difference plot illustrates that the HONO test produces slightly higher ozone concentrations with maximum enhancement of up to 5 ppb. At hour 1600 when there is significant photochemical activity, the spatial distribution of ozone in the HONO test generally resembles the base case, although the values are systematically higher. For instance, the domain-wide maximum concentration for the HONO test is 83 ppb, while the base case maximum is 75 ppb. The location of this domain-wide value is exactly the same in both cases. The last panel in the figure underscores the fact that the HONO test leads to higher domain-wide ozone concentrations relative to the base case. The enhancement in the HONO test ozone varies between 1 ppb up to 14 ppb.

4.3.4 HONO Tests Comparison

An initial test with domain-wide HONO emissions set at 20 times higher than the base during both the day and night was performed before the test described in detail in Section 4.3.3. This section provides a comparison exploring the differences in the model results between these two HONO tests.

Figure 4-10 presents spatial plots with the difference in ozone concentrations between the 50 times and the 20 times HONO tests for different days within the first IOP. The hourly snapshots at 1:00 MST show that the difference in ozone concentrations between both cases is no larger than 7 ppb, while during the day (1500 MST) the difference is at most 3 ppb. The general spatial patterns from day to day during this period are very similar. During the day, when the emissions difference is the largest, the results show that despite the multiple attempts at modifying the magnitude of the HONO source, very little effect was observed in ultimately enhancing the surface ozone concentrations.

4.3.5 HONO Test Findings

- With a domain-wide HONO emission rate of 20 tpd during the nighttime hours, the model was able to generate high HONO concentrations (greater than 1 ppb) at night.
- With a domain-wide HONO emission rate of 35 tpd during daylight hours, the model was unable to sustain the HONO reservoir created during the night and replicate the observed HONO peaks during the day.
- The above findings indicate that either the HONO source from the snowpack is larger than what was modeled or the chemical mechanism(s) may need to be updated to include additional pathways. The difference in time scales between HONO photolysis and model output may also need to be further assessed.
- The domain-wide HONO source resulted in modest increases in ozone at Boulder and Jonah with somewhat larger increases at Daniel. Ozone concentrations increased systematically across the entire domain, with some areas seeing an increase of 14 ppb compared to the base case modeling during the day.

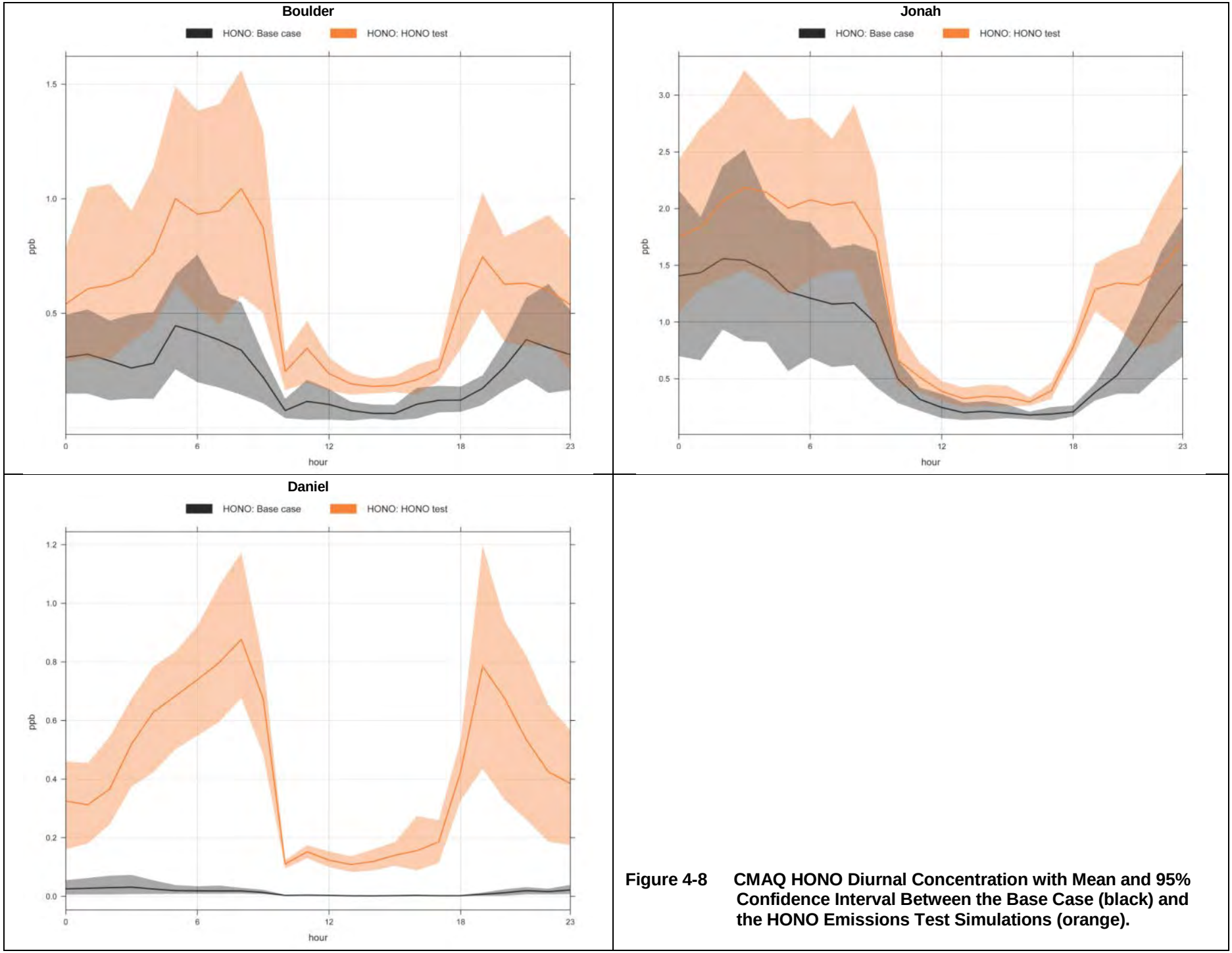

Figure 4-8 CMAQ HONO Diurnal Concentration with Mean and 95% Confidence Interval Between the Base Case (black) and the HONO Emissions Test Simulations (orange).

Hour (MST)	Base Case	HONO Test	Difference (HONO – Base)
08	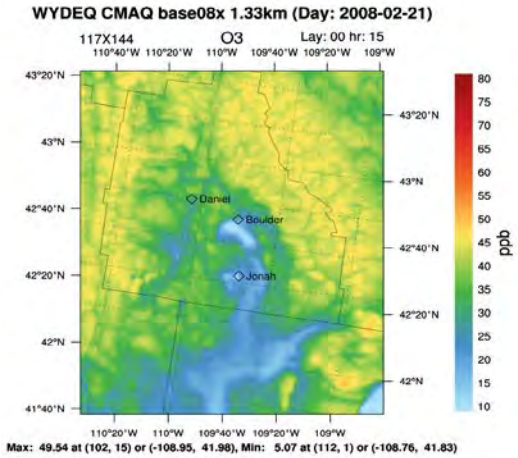	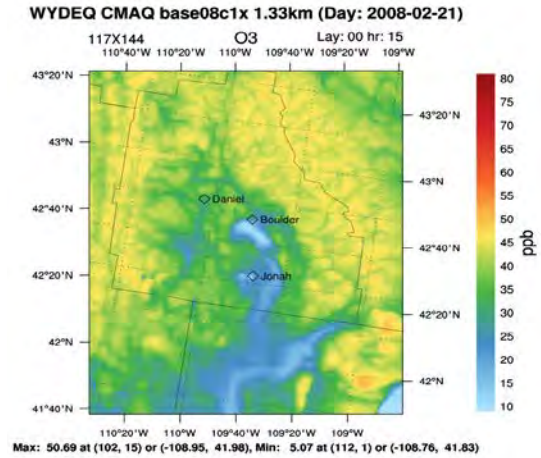	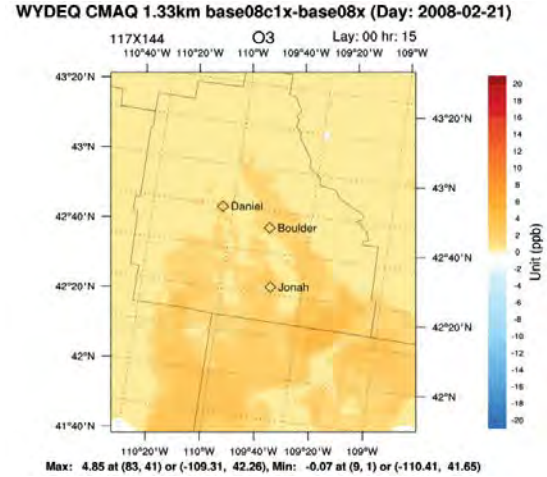
16	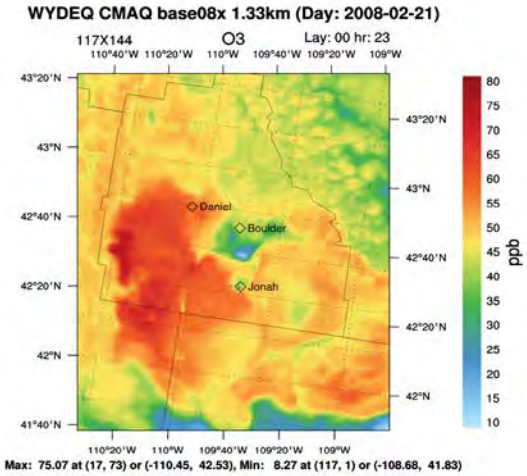	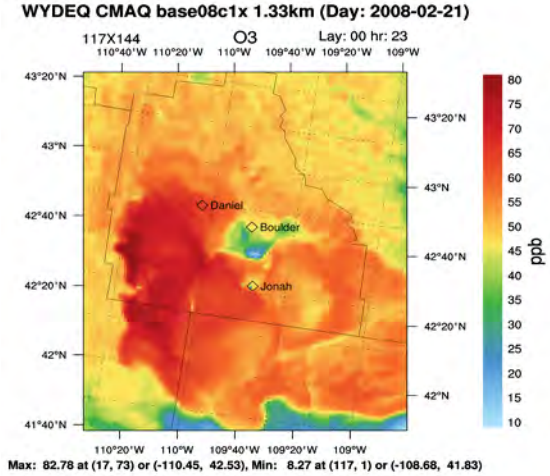	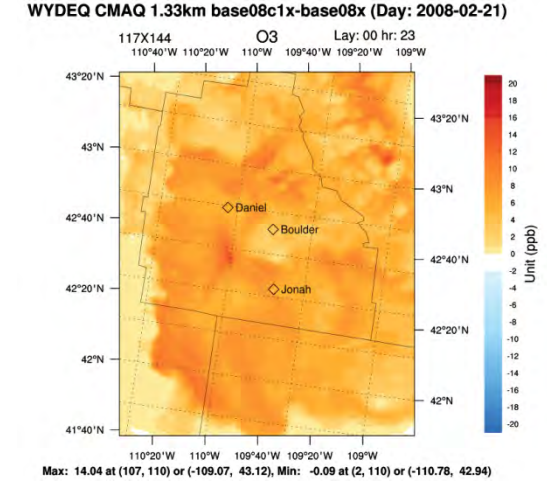

Figure 4-9 Spatial Plots of CMAQ Near Surface Ozone Concentrations from the 1.33-km domain at 0800 and 1600 MST on February 21 2008. From Left to Right: Base case with Updated Photolysis Module, HONO Test and Difference Between Both Cases (HONO Test minus Base Case)

Hour (MST)	February 20	February 21	February 22
01	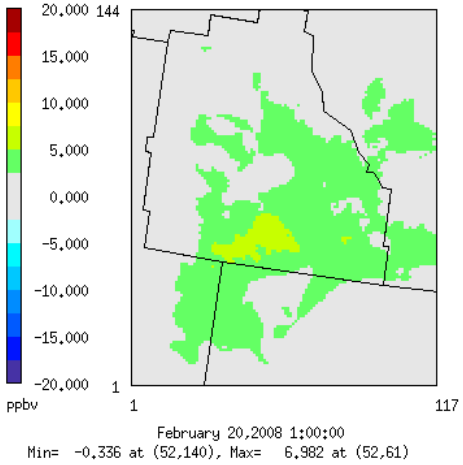	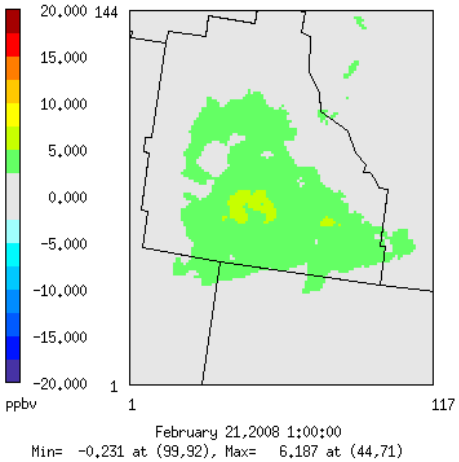	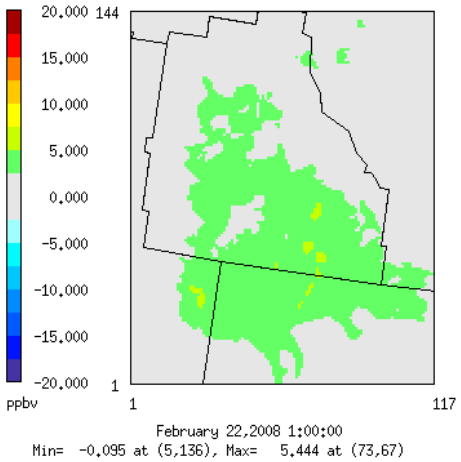
15	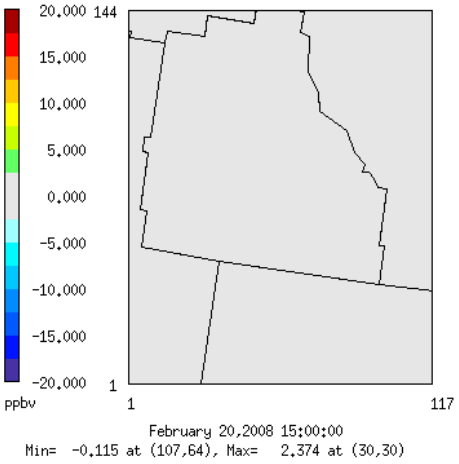	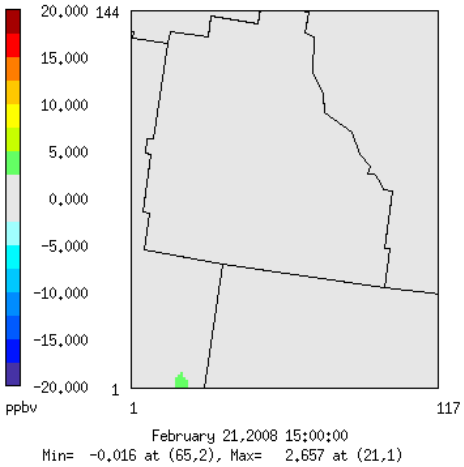	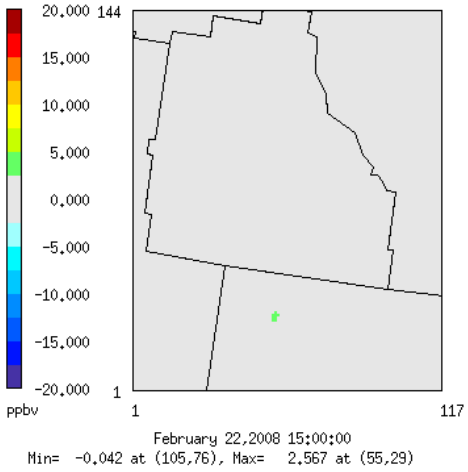

Figure 4-10 Spatial Difference Plots of CMAQ Surface Ozone Concentrations from the 1.33-km domain at 0100 and 1500 MST for selected days during the first IOP. In all cases, the difference is between the results for the test with HONO at a source strength of 50 times higher at night and 20 times higher during the day and the HONO test with a source strength of 20 times higher during the day and night.

4.4 Area Source Test

4.4.1 Area Source Test Background

Since ozone events in the UGRB during the winter typically occur under stagnation conditions when mixing depths are low, the estimation of plume rise for stationary sources is a critical issue. Small errors in the calculation of plume rise can result in emissions being placed incorrectly either in or above the mixed layer, resulting in an incorrect mix of ozone precursors. In addition, fugitive VOC emissions have different plume rise characteristics than high-temperature NO_X emissions from combustion sources, which could impact the VOC to NO_X ratio in the mixed layer. For example, **Figure 4-11** displays the vertical distribution of oil and gas-related emissions across the 1.33-km domain for a sample date in February of 2008. This plot shows that about 85 percent of VOC emissions are injected into the first two model layers, while about 60 percent of NO_X and CO emissions are injected into layer 3 and above.

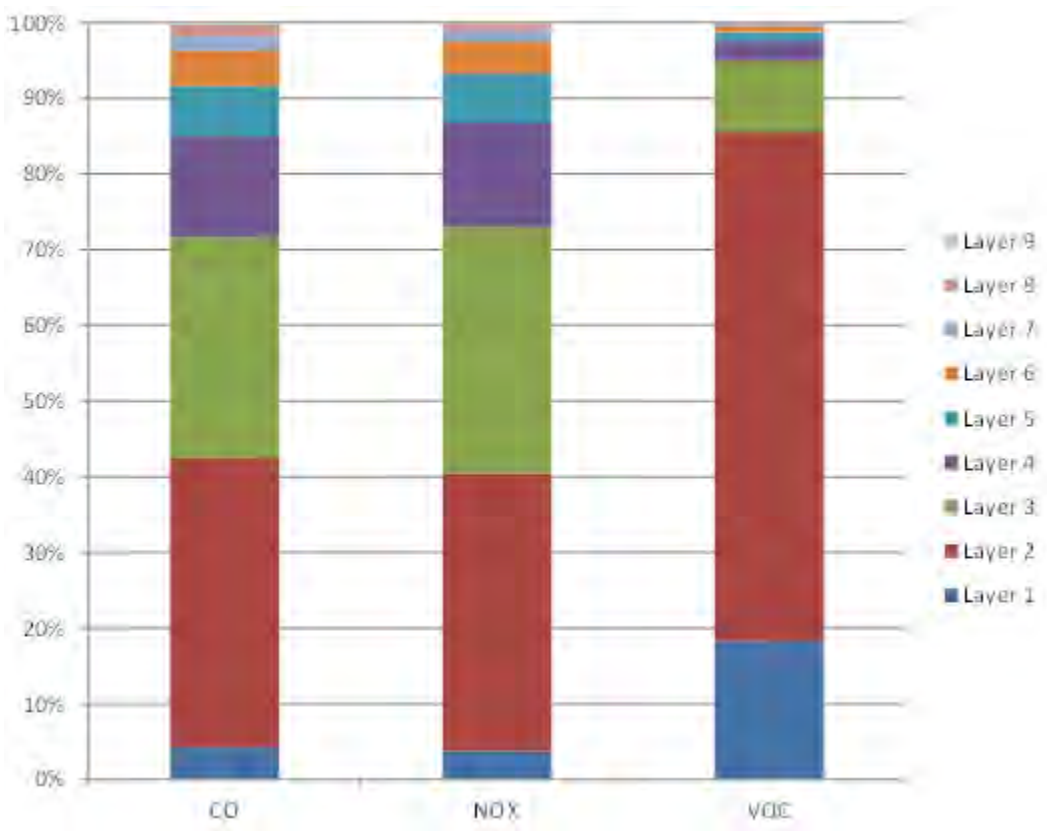

Figure 4-11 Vertical Distribution of CO, NO_x, and VOC Emissions from Oil and Gas Sources in the 1.33-km Domain for February 19, 2008.

To examine the impact of the vertical distribution of emissions from the oil and gas sector, an alternative emissions input was prepared in which all oil and gas-related processes were treated as area sources (i.e., plume rise characteristics are not considered, and all emissions are injected into the first model layer). This is a common method of modeling poorly defined oil and gas-related sources, and performing air quality modeling with these alternative emissions inputs provides information on the impact of the vertical distribution of emissions in the base case modeling.

4.4.2 Area Source Test Emissions Preparation

In the base case modeling, all oil and gas-related processes were modeled as discrete point sources with unique stack parameters and location coordinates. For the area source test, spatial distribution of these sources was preserved (i.e., continue to assign the emissions to specific latitude/longitude coordinates) while forcing the SMOKE model to inject all emissions into the first model layer. To accomplish this, the source-specific stack parameters in the oil and gas emissions inventory data provided by WDEQ was replaced with default parameters that would minimize point source plume rise as shown in **Table 4-1**.

Table 4-1 Stack Parameters Used for all Oil and Gas-related Emissions Sources in the Area Source Test

Parameter	Value
Stack height (feet)	2.0
Stack diameter (feet)	0.5
Gas exit temperature (ºF)	70
Gas flow rate (feet^3/sec)	0.002
Gas exit velocity (feet/sec)	0.01

In addition, a minor modification was made to the source code for the SMOKE plume rise module to ensure that all emissions were injected into the first model layer. For point sources with plume rise limited to the first layer, SMOKE applies a correction that sets the plume height as the center of the second layer. Since this correction results in point source emissions being distributed to the first two model layers, it was disabled. After processing the revised oil and gas emissions inventory through SMOKE, its reporting feature was used to summarize emissions by model layer and verify that all emissions were contained in the first layer. **Figure 4-12** shows a comparison of layer 1 NO_X emissions from oil and gas sources before and after the plume rise was adjusted. These plots demonstrate that the emissions processing for the area source test resulted in a sharp increase in layer 1 NO_X emissions in the 1.33-km modeling domain.

4.4.3 Area Source Analyses

Figure 4-13 compares ozone concentrations between the base case and the area source test through time series plots at the three sites. This figure shows that in Boulder the area source test shows a systematic underprediction of ozone relative to the base case for about 2 days before the start of the IOP, after this time the area source test shows an anti-correlated ozone time series compared to the base case. During the day, the ozone concentrations show the lowest values that then increase rapidly at night. For Jonah a very similar behavior is observed, namely the ozone concentrations are anti-correlated with the base case with ozone peaking in the evening hours and showing the lowest values during the daylight hours. For Daniel, the area source test ozone concentrations are substantially underpredicted at all times. **Figure 4-14** shows the corresponding NO_X time series comparison for these sites. Since NO_X emissions have explicitly been placed at the surface for all sites the NO_X concentration are consistently higher than for the base case. Furthermore the NO_X concentrations show a very strong diurnal cycle. Based on these two figures, it seems that a systematic titration or destruction of ozone during the daylight hours is occurring in this area source test.

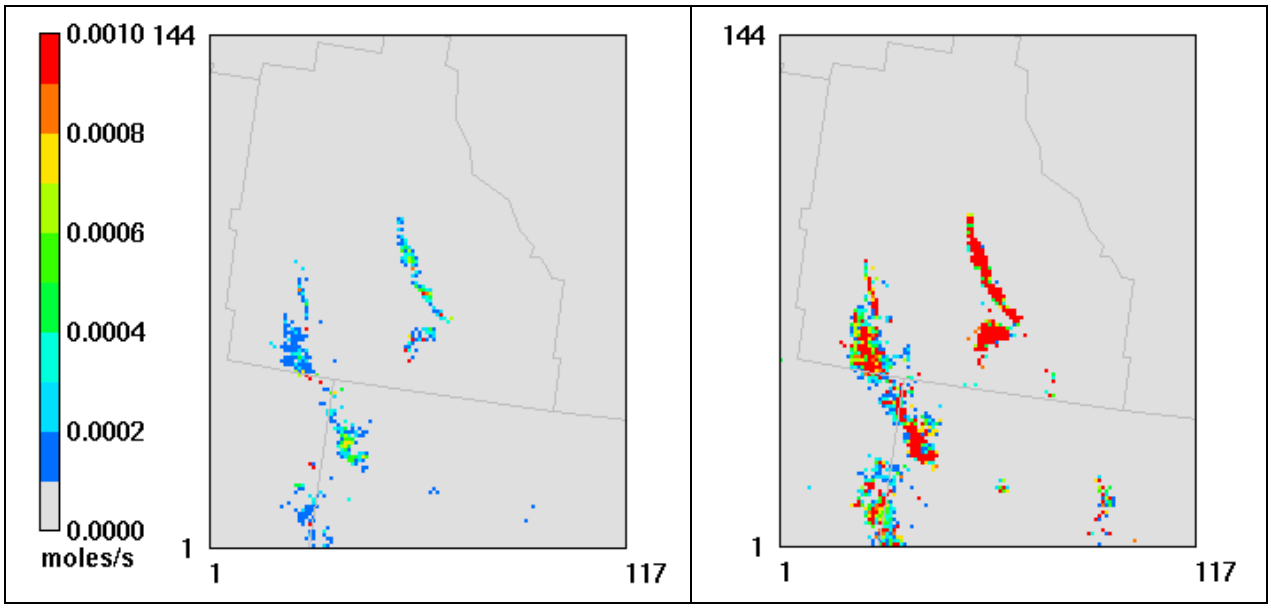

Figure 4-12 Layer 1 NO_x Emissions from Oil and Gas-Related Sources for the Base Case Modeling (left) and the Area Source Test (right).

Figure 4-15 presents ozone spatial plots for February 21 at 0800 and 1600 MST. The figure compares the base case, the area source test results and also their difference. During the morning (0800) the difference between base case and the area source test shows a region very close to the location of oil and gas sources with a heterogeneous response. Namely, there are areas close to each other with both increases and decreases in ozone concentrations; the increases could be as large as 10 ppb while at the same time reductions are as much as 22 ppb. At hour 1600, the ozone spatial distribution for the area source test generally resembles the base case with the exception of the area with the oil and gas sources in the central part of the domain. The last panel shows the differences between these two cases and indicates that for large parts of the domain there is no significant change. However there are two distinct areas with large changes that spatially correlate very well with the NO_X emissions from oil and gas – related sources. These are the regions where ozone concentrations are systematically lower than the base case and where the titration effect decreases ozone concentrations by as much as 27 ppb.

4.4.4 Area Source Test Findings

- Across the domain, there are slightly higher ozone values as the result of the test, but in the vicinity of Boulder and Jonah the model response is much more complex. In this area, near the large NO_X sources, the ozone concentrations can change dramatically over a very small distance.
- Boulder and Jonah are near large NO_X sources and this area shows substantial ozone reductions (decreases up to 30 ppb from the base case) due to titration from the NO_X plumes. This titration, also seen in the base case runs, further demonstrates that NO_X emissions around Boulder and Jonah consistently destroy the modeled ozone.
- The spatial heterogeneity of NO_X and VOC emissions in the area is also demonstrated as there is also some ozone enhancement near the Boulder and Jonah sites, outside of the NO_X plumes.

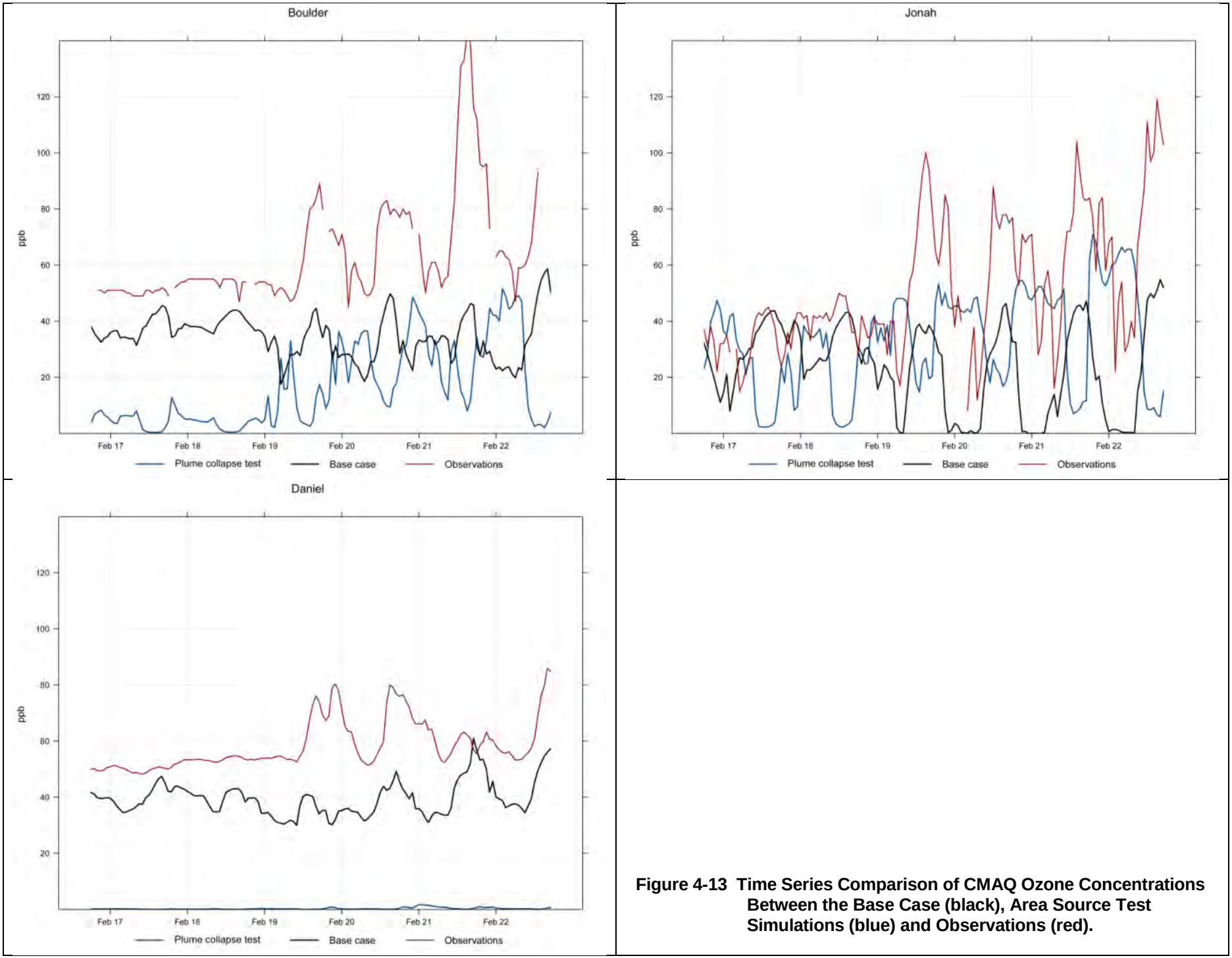

Figure 4-13 Time Series Comparison of CMAQ Ozone Concentrations Between the Base Case (black), Area Source Test Simulations (blue) and Observations (red).

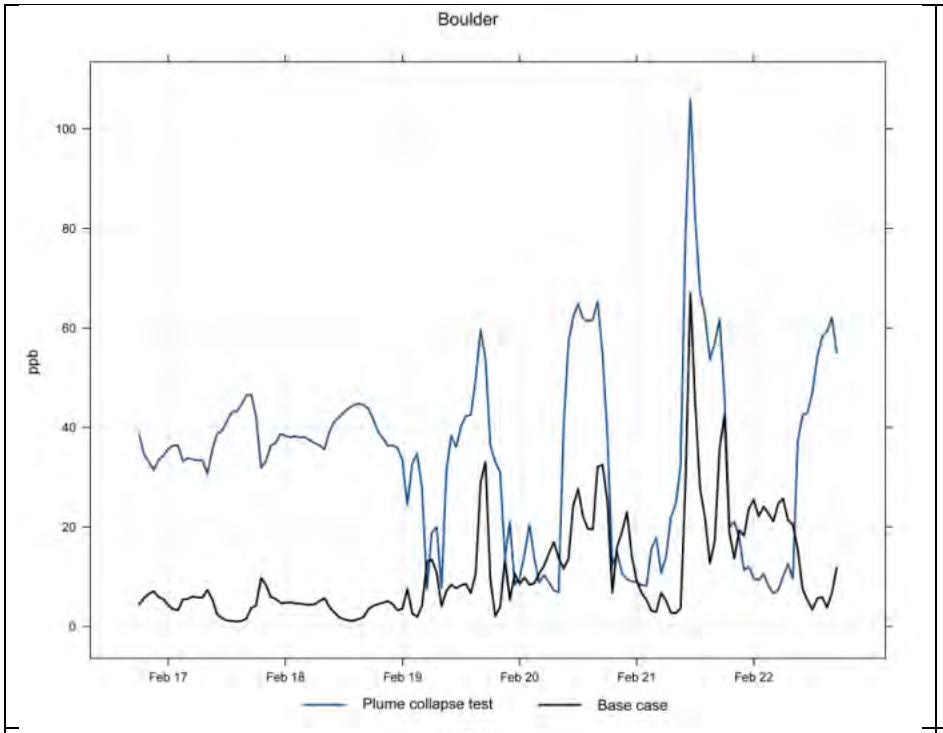

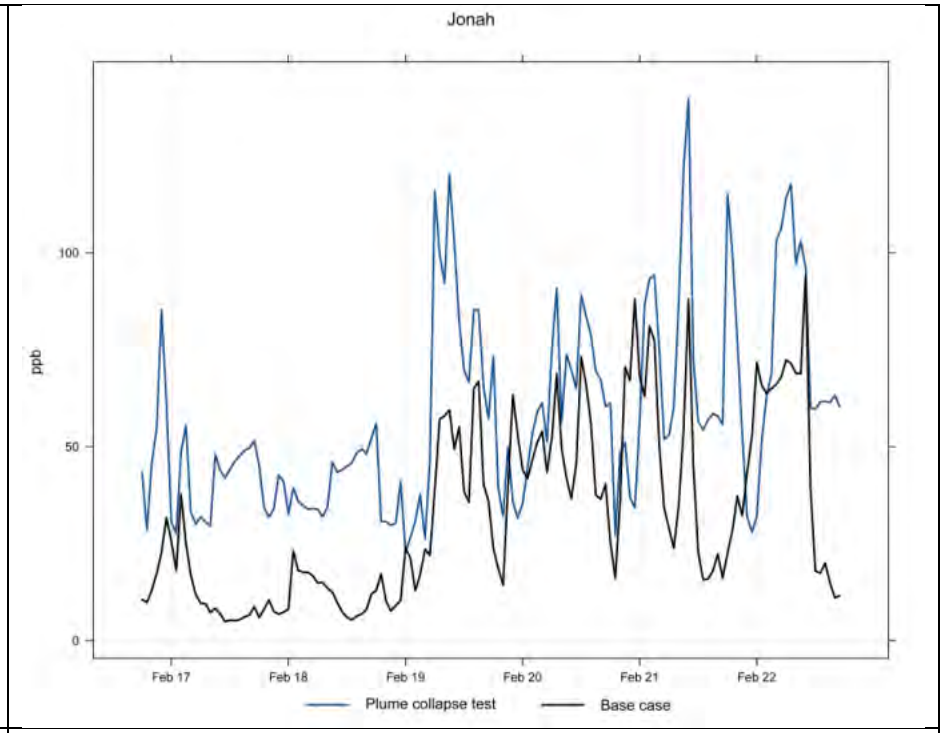

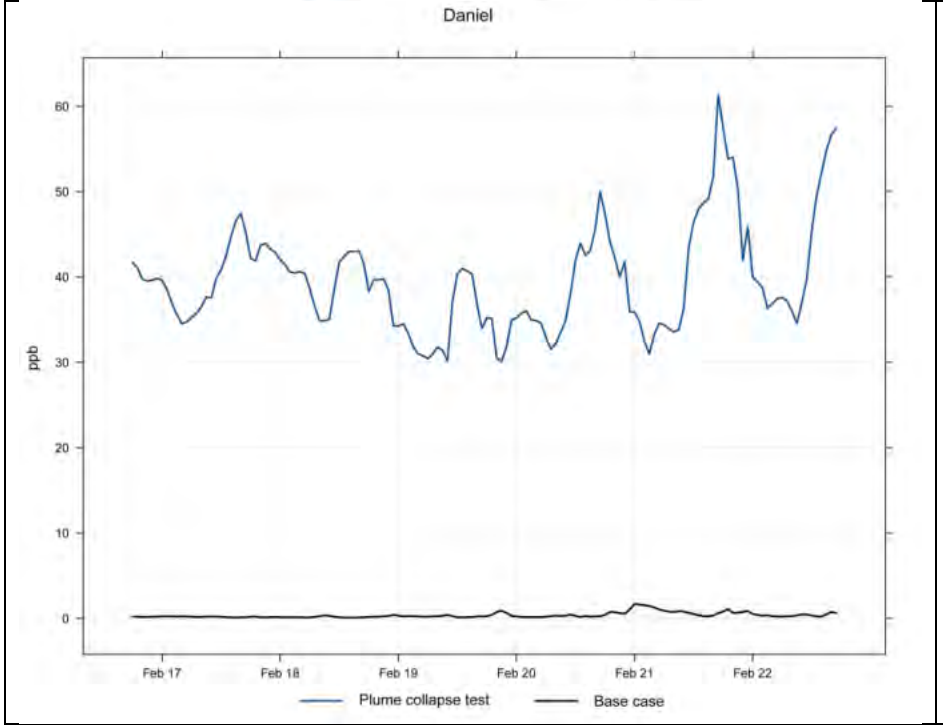

Figure 4-14 Time Series Comparison of CMAQ NO_x Concentrations Between the Base Case (black) and Area Source Test Simulations (blue).

Hour (MST)	Base Case	Area Source Test	Difference (Area Test - Base)
08	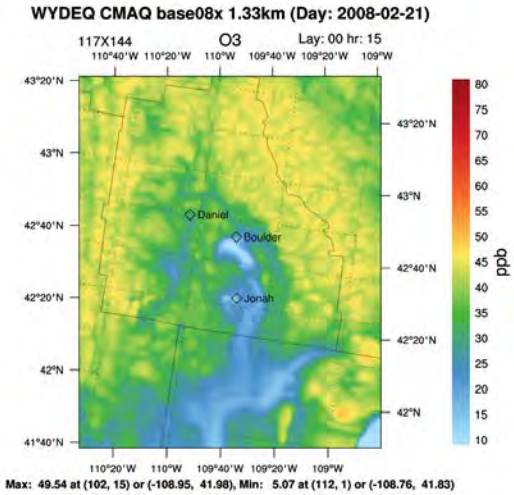	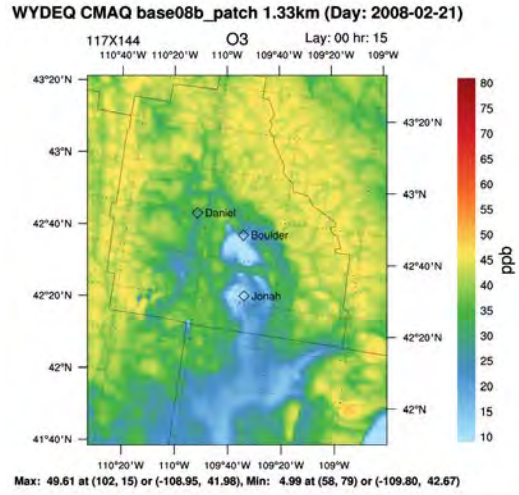	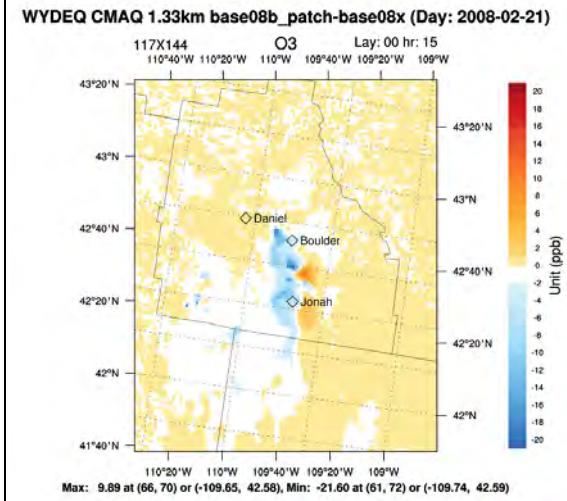
16	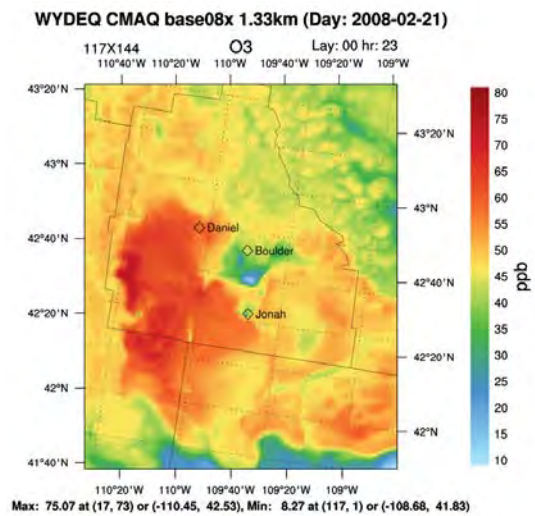	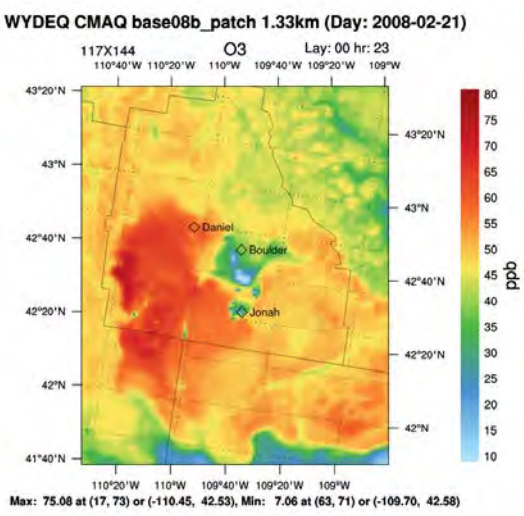	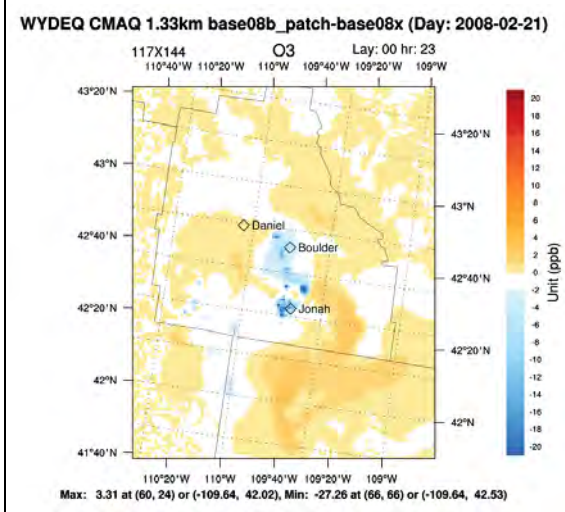

Figure 4-15 Spatial Plots of CMAQ Near Surface Ozone Concentrations from the 1.33-km domain at 0800 and 1600 MST on February 21 2008. From left to right: Base Case, Area Source Test, and the Difference Between Both Cases (Areas Test minus Base Case).

5.0 Summary of Findings

Both the CMAQ and CAMx models were run for the months of February and March 2008 in an effort to replicate the high ozone values that were observed in the UGRB, specifically at the Boulder, Jonah and Daniel monitor locations where intensive monitoring has been conducted during field studies. The models were setup with the domains, meteorology, emission inventory, other ancillary inputs and configurations described in Chapter 2.0. As noted in Chapter 2.0, the version of the CMAQ model that was run applied a patch to the snow albedo algorithm available in version 5.0 (and its importance quantified in Section 4.2); while CAMx version 5.40 used a fixed snow albedo value of 0.5.

Prior to running the base case modeling, an ozone tracer analysis was performed to determine the potential influence of boundary conditions on concentrations in the UGRB. This analysis demonstrated that less than 5 percent of the modeled ozone tracers in the UGRB came from layers higher than 7.5-km AGL. As a result, it was concluded that stratospheric intrusions or other anomalies from the boundary conditions were not likely to affect or influence the ozone concentrations modeled in the UGRB during the base case modeling.

The results of the base case modeling for both models showed ozone concentrations that were well below the observed values at Boulder, Jonah and Daniel. As shown in Section 3.4, both models underpredicted ozone at Boulder, Jonah and Daniel with modeled concentrations generally between 40 and 50 ppb and no replication of the magnitude of the observed ozone peaks. At Boulder, Jonah and Warbonnet the destruction of ozone in the model is also evident. This is likely due to the process of ozone titration given the presence of nearby, large NO_X sources (see **Figure 3-25** for the location of oil and gas NO_X sources) as well as the spatial shape, extent and behavior of the areas of suppressed ozone around the monitors. The ozone titration is most noticeable at night (e.g., **Figure 3-13** shows ozone concentrations falling to zero at night at Jonah, well below the observed values), but is also present during the day in and around the Boulder, Jonah and Warbonnet sites (see the spatial plots **Figures 3-19** and **3-32** as well as the vertical plots **Figure 3-29**). Since both models use the same emission inventory, they both produce similarly low ozone concentrations and titration effects in and around the Boulder, Jonah, and Warbonnet sites and, to a lesser extent, the Daniel site.

Inspection of the spatial and time series plots of ozone concentrations on the 1.33-km domain reveals that with the enhanced snow albedo algorithm, the revised CMAQ version can produce more ozone and a modestly better diurnal response than CAMx, which assumed a constant albedo value of 0.5 over snow covered grid cells. **Figure 3-19** shows that both models predict elevated ozone over southwestern Sublette County during the IOPs, but overall CMAQ systematically predicts higher ozone than CAMx in this area. When available, the airplane transects from the 2008 UGWOS campaign (e.g., **Figure 3-32**) do show some elevated ozone (75 to 105 ppb) in the area near LaBarge during the IOPs. In particular, comparison of CMAQ ozone concentrations with observations at the LaBarge site (**Figures 3-16** and **3-19**) shows very good performance during all IOPs. At this point it is unclear why the ozone CMAQ performance is good at LaBarge and not at other sites in the UGRB.

Additional analyses of the base case modeling at both the surface and aloft were conducted to further characterize model performance at the Boulder, Jonah and Daniel sites. These analyses focused on the model performance for precursor emissions, pollutant transport within the UGRB and an assessment of the vertical distribution of emissions and resultant concentration profiles. It was found that, when compared to available observations, the models generally underpredicted NO_X concentrations and significantly underpredicted concentrations for paraffin VOC and reactive VOCs such as xylene (see **Figures 3-20** to **3-23**). The surface-level spatial plots of ozone precursors seem to be reasonable provided the emissions inventory and meteorology, but the model performance in unmonitored areas cannot be assessed.

Modeled performance in the vertical direction was also analyzed using spatial plots for specific layers and well as vertical transects across the 1.33-km domain. With fewer observations available above the surface, the model results were reviewed for insight into the transport, modeled chemistry and the ultimate fate of ozone and its precursors. It was found that the emissions were placed at their expected locations and levels (see **Figures 3-24** to **3-26** and **Figure 4-11**) based on source type and knowledge of the emissions inventory. It was found that within the mixed layer the winds are light and variable and should keep most of the precursor emissions within the UGRB (see **Figure 3-22** and the surface or layer 7 plots in **Figures 3-31** to **3-34**). At higher levels during the night and early morning, there is a tendency for a strong northwest flow to develop, which may transport precursor emissions out of the basin (see the layer 7 or layer 10 plots in **Figures 3-31** and **3-34**), however most emissions are emitted below these levels nor does this occur during typical ozone production times. An assessment of the vertical mixing in the model showed model mixing heights within the range of those observed at the SODAR during the 2008 UGWS campaign, which indicates reasonable vertical mixing of precursor emissions within the model (see **Figure 3-30** and supporting text). The analysis of vertical cross-sections of several precursor emissions further demonstrated the expected placement and retainment of the emissions within the mixed layer and also indicated strong titration of ozone in the presence of the NO_X sources at the Jonah monitor as shown in **Figure 3-29** despite collocated VOC sources. Finally, ozone values above the surface layer do not match the observations in magnitude, spatial locations or vertical profiles (see **Figure 3-27**, **Figure 3-32**, and **Figure 3-33**).

As a result of the generally poor performance for ozone at the areas-of-concern, a model sensitivity run was conducted to include an additional HONO area source. Based on the high HONO observations found during the midday in 2011 during elevated ozone events, as well as emerging information about the importance of snow pack chemistry, a test was conducted to assess model response to increased HONO emissions. The resulting ozone concentrations increased, but not significantly (see **Figure 4-6**) at Boulder or Jonah. Systematically higher ozone concentrations were modeled at Daniel and the majority of the 1.33-km domain (see **Figures 4-6** and **4-9**). The level of HONO observed in 2011 was also unable to be sustained during the day due to its rapid destruction (see **Figure 4-8**), indicating the potential need for a new pathway to be included in the chemical mechanism or a larger HONO emission source.

Another test that was conducted was to collapse the entire emissions inventory into the first layer of the model into an area source. This would force the precursor emissions to mix, thus providing information about the model response to plume rise and subsequent mixing of the NO_X and VOC sources. The results show that across the domain, there are slightly higher ozone values as the result of the test, but in the vicinity of Boulder and Jonah the model response is complex (see **Figure 4-15**). In this area, near the large NO_X sources, the ozone concentrations can change dramatically over a very small distance. Although most of the 1.33-km domain shows no change or a slight increase in ozone concentrations as a result of the plume rise treatment, Boulder and Jonah are near large NO_X sources and show substantial ozone reductions (decreases up to 30 ppb from the base case) due to titration. This titration, also seen in the base case runs, further demonstrates that NO_X emissions around Boulder, Jonah and Daniel frequently destroy the modeled ozone. It also demonstrates the spatial heterogeneity of NO_X and VOC emissions in the area as there is also some ozone enhancement near the Boulder and Jonah sites.

When the model results are evaluated with respect to the conceptual model (summarized in Section 1.2), many aspects of the conceptual model seem to be in place. As detailed above, the results indicate that the models have:

- Reasonable placement of precursor emissions within the mixed layer;
- The expected pollutant recirculation within the mixed layer;
- Reasonable (minimal) vertical mixing with attendant low mixing heights; and
- Sufficient snow cover in the UGRB and the revised CMAQ code has enhanced albedo/photolysis over snow cover.

In spite of the above factors, the models perform poorly when evaluated for ozone and precursor concentrations at the observation sites of Boulder, Jonah and Daniel. High concentrations of ozone precursors are an important component of the conceptual model, but were not replicated by the models. The inclusion of an additional HONO source to account for snow pack chemistry did not significantly improve the model's ozone performance. All "off-the-shelf" modeling options were explored, and any future steps for attempting to improve model performance should include model and/or chemical mechanism development, which were options beyond the scope of this project.

6.0 References

Amorosa, A., H. Beinea, R. Sparapania, M. Nardinoc, and I. Allegrinia. 2006. Observation of coinciding arctic boundary layer ozone depletion and snowsurface emissions of nitrous acid. Atmos. Env., 40, 1949-1956.

Argonne. 2007. Process-scale Modeling of Elevated Wintertime Ozone in Wyoming, Prepared for Division of Environmental Quality, Air Quality Division, December

Baek, B. H. and A. DenBleyker. 2010. User's guide for the SMOKE-MOVES integration tool. User's guide prepared for the U.S. Environmental Protection Agency by UNC Institute for the Environment, Chapel Hill, NC, and ENVIRON, Novato, CA, July. Available on the Internet at http://www.smoke-model.org/smoke_moves_tool/SMOKE-MOVES_Tool_Users_Guide.htm.

Byun, D., J. Ching. 1999. Science Algorithms of the USEPA Models-3 Community Multiscale Air Quality (CMAQ) Modeling System, USEPA Tech. Rep. USEPA-600/R-99/030.

Carter, W. P. L., J. H. Seinfeld. 2011. Estimation of VOC Incremental Reactivities in Winter Ozone Episodes in the Upper Green River Basin of Western Wyoming, Prepared for Division of Environmental Quality, Air Quality Division, June.

Community Modeling and Analysis System (CMAS). 2012. CMAQ version 5.0 Technical Documentation. February 2012

ENVIRON and Alpine Geophysics. 2011. Winter 2008 WRF Modeling of the Upper Green River Basin, Prepared for Division of Environmental Quality, Air Quality Division, November.

ENVIRON, T&B Systems Incorporated, Meteorological Solutions. 2011. Final Report 2011 Upper Green River Winter Ozone Study. Prepared for the Division of Environmental Quality, Air Quality Division, October.

ENVIRON. 2010a. A Conceptual Model of Winter Ozone Episodes in Southwest Wyoming. Prepared for Division of Environmental Quality, Air Quality Division, January.

ENVIRON. 2010b. User's Guide: Comprehensive Air Quality Model with Extensions, Version 5.30, ENVIRON International Corporation, 773 San Marin Drive, Suite 2115, Navato, California, 94998

ENVIRON. 2008. Winter Ozone Box Model Study, Prepared for Division of Environmental Quality, Air Quality Division, January 2010.

GEOS-Chem tropopause. 2014. Internet website: http://wiki.seas.harvard.edu/geos-chem/index.php/Dynamic_tropopause.

Guenther, A. and T. Sakulyanontvittaya. 2011. Improved Biogenic Emission Inventories across the West. Prepared for the Western Governors' Association, August.

Guenther, A., T. Karl, P. Harley, C. Wiedinmyer, P. I. Palmer, and C. Geron. 2006. Estimates of global terrestrial isoprene emissions using MEGAN (Model of Emissions of Gases and Aerosols from Nature. Atmos. Chem. Phys., 6, ed., 3181-3210. doi: 10.5194/acp-6-3181-2006. Available on the Internet at http://www.atmos-chem-phys.net/6/3181/2006/acp-6-3181-2006.pdf.

Honrath, R. E., Y. Lu, M. C. Peterson, J. E. Dibb, M. A. Arsenault, N. J. Cullen, and K. Steffen. 2002. Vertical fluxes of NO_X, HONO, and HNO3 above the snowpack at Summit, Greenland. Atmos. Env., 36, 2629-2640.

McVehil-Monnett Associates, Inc. 2011. Ground-Level Ozone and Meteorological Parameter Correlation Analysis for the Upper Green River Basin, Prepared for Division of Environmental Quality, Air Quality Division, October.

Meteorological Solutions. 2011. Comparison of Weather Conditions During the 2011Upper Green Winter Ozone Study to Past Study Seasons Prepared for Division of Environmental Quality, Air Quality Division, October.

National Center for Atmospheric Research (NCAR). 2009. Mesoscale and Microscale Meteorology Division, ARW Version 3 Modeling System User's Guide. Internet website: http://www.mmm.ucar.edu/wrf/ users/docs/user_guide_V3.1/ARWUsersGuideV3.pdf. July 2009.

Pollard E. K., Y. Du, and S. B. Reid. 2011. Preparation of wildland and agricultural fire emissions inventories for 2008. Technical memorandum prepared for the U.S. Environmental Protection Agency, Research Triangle Park, NC, by Sonoma Technology, Inc., Petaluma, CA, STI-910221-4159, June.

Reed, J. 2013. Modeling Background Ozone Concentrations in the UGRB During February 2008. Presented at 2013 Western Air Quality Modeling Workshop – Technical Methods and Applications, July 10.

Reid, S. B., E. K. Pollard, Y. Du, J. Reed, and C. Taylor. 2013. Development and quality assurance of air quality model-ready emissions inputs for winter ozone modeling in southwestern Wyoming. Technical memorandum prepared for Josh Nall, Wyoming Department of Environmental Quality, STI-911064-5470-TM, March.

Seinfeld, J.H. and Pandis, S. N. 1998. Atmospheric Chemistry and Physics. From Air Pollution to Climate Change. 1st edition, J. Wiley, New York.

Sonoma Technology, Inc. (STI). 2010 Wyoming Statewide Air Monitoring Network Assessment Optional Task 2: Emissions Inventory Assessment, Prepared for the Wyoming Department of Environmental Quality, Air Quality Division, September.

State of Wyoming. 2009. Technical Support Document I For Recommended 8-hour Ozone Designation for the Upper Green River Basin, Wyoming, March.

Sullivan, D. C., S. M. Raffuse, D. A. Pryden, K. Craig, N. J. M. Wheeler, L. R. Chinkin, N. K. Larkin, T. Strand, and R. Solomon. 2009. Enhancements to the BlueSky emissions assessment and air quality prediction system. Draft report prepared for the National Aeronautics and Space Administration, Washington, DC, by Sonoma Technology, Inc., Petaluma, CA, and the AirFire Team, Pacific Northwest Research Lab, US Forest Service, Seattle, WA, STI-905028-3753-DR, November.

Tonnesen, G. 2013. Preliminary Winter Time Modeling of Elevated PM2.5 and Ozone in the Intermountain West, Presented at 2013 Western Air Quality Modeling Workshop – Technical Methods and Applications, July 10.

TRC. 2010. Summary Report for the Assessment of Winter Ozone in the Upper Green River Basin Using the CALGRID Photochemical Grid Model for the February 18-24, 2008 Period, Prepared for the Wyoming Department of Environmental Quality, Air Quality Division, June.

Upper Green River Winter Ozone Studies (UGWOS). 2011. Upper Green River Winter Ozone Study Reports. Internet website http://deq.state.wy.us/aqd/Upper%20Green%20 Winter%20Ozone%20Study.asp.

Upper Green River Winter Ozone Studies (UGWOS). 2010. Upper Green Winter Ozone Study Reports. Internet website http://deq.state.wy.us/aqd/Upper%20Green%20 Winter%20Ozone%20Study.asp.

Upper Green River Winter Ozone Studies (UGWOS). 2009. Upper Green River Winter Ozone Study Reports. Internet website http://deq.state.wy.us/aqd/Upper%20Green%20 Winter%20Ozone%20Study.asp.

Upper Green River Winter Ozone Studies (UGWOS). 2008. Upper Green River Winter Ozone Study Reports. Internet website http://deq.state.wy.us/aqd/Upper%20Green%20 Winter%20Ozone%20Study.asp.

Upper Green River Winter Ozone Studies (UGWOS). 2007. Upper Green River Winter Ozone Study Reports. Internet website http://deq.state.wy.us/aqd/Upper%20Green%20 Winter%20Ozone%20Study.asp.

U.S. Environmental Protection Agency (USEPA). 2012. Air Quality System Data Mart. Internet website: http://www.epa.gov/airdata/. Accessed January 4, 2012

U.S. Environmental Protection Agency (USEPA). 2007. Guidance on the Use of Models and Other Analyses for Demonstrating Attainment of Air Quality Goals for Ozone, $PM_{2.5}$, and Regional Haze. EPA-454/B-07-002, April.

Whitten, G., G. S. Yarwood, Rao, and M. Yocke. 2005. Updates to the Carbon Bond Chemical Mechanism: CB05, Final Report to the USEPA, RT-0400675.

Whitten, G. Z., H. Gookyoung, K. Yosuke, E. McDonald-Buller, D. T. Allen, W. P. L. Carter, G. Yarwood, A new condensed toluene mechanism for Carbon Bond: CB05-TU, Atmospheric Environment, Volume 44, Issue 40, December 2010, Pages 5346-5355.